Proactive Integrated Control for Relieving Freeway Congestion

by

Xu Wang

A thesis submitted in partial fulfillment of the requirements for the degree of

Doctor of Philosophy

in

Transportation Engineering

Department of Civil and Environmental Engineering
University of Alberta

ABSTRACT

Active bottlenecks limit traffic flow on freeway corridors. To relieve bottleneck severity, ramp metering (RM), variable speed limit (VSL) and their integration are often implemented to control the on-ramp and mainline input flow. Currently, freeway operation has become proactive based on short-term prediction. Macroscopic traffic flow models are often applied as prediction models in proactive traffic control strategies. Prior to field implementation, the models need to be calibrated and validated carefully to ensure that they represent real-life traffic situations. This study proposes modifications for METANET model to adapt it to the unpredictability of bottleneck activation during peak hours. The modified model is calibrated and verified its improvement of model prediction accuracy from segment-specific parameters. The modified model is validated that it can replicate traffic state evolutions during peak hours and be applicable in proactive traffic control practice.

Weaving maneuvers (i.e., intensive lane changes) are a major cause of bottlenecks during high-demand periods. To consider weaving impacts in RM, this study introduces a proactive optimal RM algorithm that uses dynamic weaving capacity at weaving segments. Sensitivities of capacity and capacity drop are applied to dynamically estimate weaving capacity within a macroscopic traffic flow model. The proposed traffic flow model conducts estimation in a model predictive control (MPC) frame-work. The proposed RM

algorithm is evaluated in macro-simulation and its effectiveness is enhanced by real-time estimated weaving capacity.

The RM control research reveals a need of theoretical methods for weaving capacity estimation. This study then defines a linear optimization problem to solve weaving capacity and then establishes a lane-changing model to constrain the weaving flows. The proposed method is evaluated and analyzed for sensitivity with field data from two weaving segments. The capacity estimates from the proposed model are consistent with those from the HCM 2010 model and with field observations. Moreover, the weaving capacity is sensitive to weaving maneuvers. The proposed method is finally applied to estimate the real-time maximum discharge flow rate; the estimates match field measurements.

Next, this study presents a proactive integrated control of RM and VSL, with goals to improve network-wide travel time and traffic flow. By decoupling the traffic prediction and simulation models, the possible control error sources are analyzed. The evaluation reveals the proactive integrated control achieves an amelioration in total time spent (TTS) up to 13.65% and an increase in total travel distance (TTD) up to 3.41%. The isolated and integrated controls benefit the traffic network in different extent under different demand scenarios. In addition, control rate profiles are analyzed in detail and found that RM is activated during slight congestion and the most congested situation to assist VSL. Through the integration, the infrastructure utility is maximized.

Speed transition zones are complex when dynamically created and shifted by VSL. This study then attempts to represent speed limit effect and estimate real-time driver compliance at speed transition zones. The field data from two speed transition zones are investigated for temporal and spatial variations of speed and driver compliance using statistical tests. After selecting several key factors from statistical tests, a linear regression is established to rank the contributions of the selected factors and other general factors proposed by previous research. The regression results confirm speed limit value, surrounding traffic speed and existence of activated speed enforcement or education devices contribute more to driver compliance.

Finally, this study reports the preliminary VSL test and details its implementation procedure on Whitemud Drive, Edmonton, Canada. DynaTAM-VSL software is designed to realize all necessary functions for VSL filed implementation. The preliminary test is conducted, and the VSL control performance and reliability are evaluated. The results for before-and-after VSL control are finally analyzed in depth. The analysis compares average traffic speed, standard deviation of speed, total travel time and total travel distance. The results from this study confirm that VSL can relieve recurrent traffic congestion.

PREFACE

a. Articles published in refereed journals

1. **Xu Wang**, Md. Hadiuzzaman, Jie Fang, Tony Z. Qiu, and Xinping Yan (2014). Optimal Ramp Metering Control for Weaving Segments Considering Dynamic Capacity Estimation, *Journal of Transportation Engineering (ASCE)*, 140 (11), 04014057.

2. **Xu Wang**, Ying Luo, Tony Z. Qiu, and Xinping Yan (2014). Capacity Estimation for Weaving Segments Using a Lane Changing Model. *Transportation Research Record: Journal of Transportation Research Board*, 2461, pp. 94-102.

b. Articles submitted to refereed journals

1. **Xu Wang**, Mudasser Seraj, Yuwei Bie, Tony Z. Qiu and Xinping Yan. Implementation of Variable Speed Limits: Preliminary Test on Whitemud Drive, Edmonton, Canada. Under Review.

2. **Xu Wang**, Tony Z. Qiu and Xinping Yan. Mainline and Ramp Flow Interaction under Proactive Integrated Freeway Control. Under Review.

3. **Xu Wang**, Yuwei Bie, Tony Z. Qiu and Xinping Yan. Effect of Speed Limits at Speed Transition Zones. Under Review.

4. **Xu Wang**, Derek Yin, Tony Z. Qiu and Xinping Yan. Applicability Analysis of a Macroscopic Traffic Flow Model in Traffic State Prediction. Under Review.

.

ACKNOWLEDGEMENTS

My first and deepest appreciation goes to my supervisor, Dr. Tony Z. Qiu, for his continuous support, patient guidance and infinite encouragement throughout my PhD study at the University of Alberta. Without him, I could not have made it here. I enjoyed working at his research group and look forward to cooperate with him in future.

Special thanks to other committee members, Dr. Karim El-Basouny, Dr. Amy Kim, Dr. Wei Victor Liu and Dr. Behrouz Far for their insightful comments and suggestions.

I would like to thank my research teammates, Dr. Jie Fang, Dr. Md Hadiuzzaman, Ying Luo, Mudasser Seraj and Yuwei Bie, for their valuable suggestions and help to my research. Besides, I would like to express my gratitude to Rochelle Borchman and Aalyssa Atley for their patient guidance in writing academic papers.

Last but not the least, I would like to express my deepest love to my family members for always being by my side all these years. Their endless supports and understanding helped me to stay focused during my graduation study.

TABLE OF CONTENTS

LIST OF TABLES

LIST OF FIGURES

LIST OF ABBREVIATIONS

Acronym	Definition
AADT	Annual Average Daily Traffic
ALINEA	Asservissement Linéaire d’Entrée Autoroutière
ATDM	Active Traffic and Demand Management
CTM	Cell Transition Model
DOT	Department of Transportation
DSDS	Dynamic Speed Display Sign
DynaTAM	Dynamic Analysis Tool for Active Traffic And Demand Management
FD	Fundamental Diagram
FOT	Field Operational Test
HCM	Highway Capacity Manual
HERO	Heuristic Ramp-Metering Coordination
ITS	Intelligent Transportation Systems
LOS	Level of Service
MH Model	Multilane Hybrid Model
MPC	Model Predictive Control
MTFC	Mainline Traffic Flow Control
NTCIP	National Transportation Communications for Intelligent Transportation System Protocol
O-D	Origin-Destination
RG	Route Guidance
RM	Ramp Metering
RMSE	Root Mean Square Error
SDS	Standard Deviation of Speed
SPECIALIST	Speed Controlling Algorithm using Shockwave Theory
SQP	Sequential Quadratic Programming

Acronym	Definition
STL	Standard Template Library
SWARM	System Wide Adaptive Ramp Metering
TF	Total Flow
TMC	Transportation Management Center
TOD	Time-of-Day
TTD	Total Travel Distance
TTS	Total Time Spent
TTT	Total Travel Time
TWT	Total Waiting Time
V-D	Volume-Density
VDS	Vehicle Detection Station
VMS	Variable Message Sign
VR	Volume Ratio
VSL	Variable Speed Limit
WMD	Whitemud Drive

LIST OF NOTATIONS

Symbol	Definition	Unit
i	segment index	
L	length of segment	kilometer (km)
λ	lane number of segment	
ρ	traffic density	vehicles per kilometer per lane (veh/km/ln)
v	traffic speed	kilometers per hour (km/h)
t	time index	
T	discrete time step length	second (s)
k	time step presently in the calculation	
q	boundary flow between segments	veh/h/ln
r	on-ramp flow rate	vehicles per hour (veh/h)
s	off-ramp flow rate	veh/h
τ	reaction term parameter	hours (h)
η	anticipation parameter	km^2 per hour (km^2/h)
κ	positive constant	veh/km/ln
ρ_{cr}	critical density	veh/km/ln
v_f	free flow speed	km/h
α	a link specific fundamental diagram parameter	
Q	link flow	veh/h/ln
μ	the ratio of actual boundary flow to flow measurement	
$Q_{\max}$	possible maximum discharge flow	veh/h/ln
Q_{BN}	bottleneck flow when downstream bottleneck is activated	veh/h/ln

Symbol	Definition	Unit
N_p	prediction horizon	
N_c	control horizon	
r^*	optimal RM values	veh/h
k_c	control sampling time index	
$\boldsymbol{x}$	traffic measurements	
$\boldsymbol{x}$	predicted future traffic state	
J	objective function	
$Q'_{\max}$	bottleneck capacity	veh/h/ln
$Q_d\%$	percentage of capacity drop	
ω	shockwave speed	km/h
ρ_{Jam}	jam density	veh/km/ln
ω'	shockwave speed related to FDs with capacity drop	km/h
α_{TTT}	weighting factor for TTT	
α_{TWT}	weighting factor for TWT	
α_{TTD}	weighting factor for TTD	
R^2	R Square	
$L_{\max}$	maximum length of a weaving segment	km
VR	volume ratio	
N_{WL}	number of weaving lanes	
L_s	segment length	km
c_{BF}	basic freeway capacity	veh/h/ln

Symbol	Definition	Unit
c_{BR}	basic ramp capacity	veh/h/ln
N_F	number of lanes on freeway	
N_{ONR}	number of lanes on on-ramps	
N_{OFR}	number of lanes on off-ramps	
q_{FF}	through traffic flow from freeway to freeway, at capacity	veh/h
q_{FR}	traffic flow from freeway to off-ramp, at capacity	veh/h
q_{RF}	traffic flow from the on-ramp to freeway, at capacity	veh/h
q_{RR}	the traffic flow from the on-ramp to off-ramp, at capacity	veh/h
D_{FF}	traffic demand from freeway to freeway	veh/h
D_{FR}	traffic demand from freeway to off-ramp	veh/h
D_{RF}	traffic demand from on-ramp to freeway	veh/h
D_{RR}	traffic demand from on-ramp to off-ramp	veh/h
τ_{LC}	actual time for a vehicle to change its lane	s
λ	demand (sending) function	veh/h/ln
μ	supply (receiving) function	veh/h/ln
π	fraction of decision-makers per unit time	s^{-1}

Symbol	Definition	Unit
W	ratio of weaving vehicles	
u	control variable for VSL	km/h
$u*$	optimal control variable for VSL	km/h
$V_{\max}$	maximum speed limit value	km/h
$V_{\min}$	minimum speed limit value	km/h
$V_{\max,\text{diff}}$	maximum speed limit difference	km/h
$q_{o,in}$	flow measurements at the entrance of a ramp	veh/h/ln
$q_{o,out}$	flow measurements at the exit of a ramp	veh/h/ln
K_{est}	gain parameter of the filter	
N^{BB}	bumper-to-bumper capacity of the ramp	veh
L_{ph}	average physical length of the vehicles	m
o_{mid}	occupancy measurement at the middle of the ramp	
ε_{el}	electrical length of detectors placed at the middle of the ramp	m
H_o	null hypotheses	
H_a	alternative hypotheses	
y	dependent variable	
x	independent variable	
b	coefficients for independent variable	

CHAPTER 1. INTRODUCTION AND RESEARCH OBJECTIVES

1.1 Introduction

Around the world, as traffic demand steadily increases, so too does congestion, which is a major traffic problem that lowers mobility on freeways. Fundamentally, congestion is related to the ratio of the demand arrival rate to the supply service rate [1]. Active traffic and demand management (ATDM) strategies, including Ramp Metering (RM), Variable Speed Limit (VSL) and Route Guidance (RG), can help to delay or avoid congestion and to reduce its adverse impact. Over the last decade, driven by rapid development of Intelligent Transportation Systems (ITS), several ATDM strategies have been implemented with real-time data collection and facility spatial coordination and integration. These strategies effectively and efficiently alleviate freeway congestion.

RM uses traffic lights together with a signal controller to regulate the ramp entering flow, and is the most investigated and applied freeway traffic control method. RM can be operated in two modes: 1) the traffic spreading mode, in which reduction in ramp flow is caused by spreading peak demand; and 2) the traffic restricting mode, which sets a metering rate below the non-metered ramp volume [2]. However, RM regulates only the input flow from on-ramps;

therefore, it is insufficient for controlling heavily congested freeways. VSL is regarded as an appropriate supplement to RM.

VSL control changes posted speed limits based on real-time road, traffic and weather conditions, thereby improving traffic safety and mobility by restricting speed in adverse environmental conditions. VSL influences the collective mainline vehicle speed and driver behavior. Basically, there are two effects of VSL: 1) the homogenization effect; and 2) prevention of traffic breakdown by reducing flow [2].

RG distributes traffic flow into various routes to reduce travel time and improve the utilization of existing network infrastructure [3]. Specifically, it aims at establishing either user equilibrium or system optimal conditions within a freeway network. Previous studies have revealed that RG is helpful mostly for non-recurrent events that make traffic conditions unpredictable [4].

Over the past several decades, many papers and reports have documented the development of ATDM strategies. The reported control algorithms generally fall into three categories: fixed-time, reactive and proactive. Fixed-time strategies are derived offline and control variables are predetermined based on historical data. They are only effective for recurrent congestion and cannot be automatically adjusted because of the absence of real-time measurements. Reactive strategies apply control variables to maintain traffic conditions closed to predefined values in response to real-time measurements. They cannot forecast traffic flow evolutions nor take proactive countermeasures.

Thus, proactive control strategies are generally preferred: they use traffic flow models and optimal control variables to predict future traffic states and achieve pre-specified objectives. Much research has been devoted to describe the relationship between traffic dynamics and control variables. With the help of existing traffic models, several proactive control strategies have been designed and implemented in simulation, where RM and VSL are commonly integrated as ramp and mainline traffic flow control methods, respectively; however, these simulations do not address important questions: how does mainline flow interact with ramp flow? How do ramp flow control and mainline flow control influence each other? How can ramp and mainline control be integrated to achieve the optimal network flow? This research intends to address these questions.

1.2 Issues Related to the Previous Research

For proactive, integrated freeway control, several model-based strategies have been derived; for example, the model predictive control (MPC)-based control with the extended METANET traffic flow model. The MPC-based control features a prediction module and optimizes control variables based on prediction in every control horizon. MPC works in a closed loop, while a controller updates and considers real-time traffic states so that prediction errors bear low sensitivity. Previous studies [2, 5-10] revealed MPC's great potential for freeway control and METANET's accuracy for traffic state estimation. However, throughout the related literature, several elements that affect the control performance of traffic state prediction and strategy integration have not been clearly studied:

1. Macroscopic traffic flow models are often applied as prediction models in proactive traffic control strategies. Prior to field implementation, the models need to be calibrated and validated carefully to ensure that they represent real-life traffic situations. However, existing tests have been conducted on relatively simple freeway corridors, so the model performance is still unknown for complicated corridors with multiple potential bottlenecks.

2. During peak hours, traffic flow is limited by bottleneck flow. Previous observations showed bottlenecks can be activated by complicated weaving maneuvers and cause capacity drop. ATDM is designed to relieve or avoid bottleneck activation through adjusting bottleneck flow and flow proportions. Hence, ATDM design should consider weaving impacts; however, it has received no attention in the published literature. In addition, capacity is one of the main inputs of macroscopic traffic flow models. One major impact of weaving is a reduction in segment capacity. An accurate and applicable model for weaving capacity estimation is required to include weaving impact in proactive control strategies. Whereas, no research has coupled weaving capacity estimation with macroscopic traffic flow models.

3. Weaving capacity is estimated in two ways: empirical and theoretical models. Empirical models require large amounts of field data and have weak transferability. Theoretical models were not designed for traffic operation,

because certain parameters are difficult to measure with basic traffic operation facilities and microscopic driver behaviors are site-specific. There is no weaving capacity model established for traffic operation.

4. RM and VSL adjust traffic flow from on-ramps and mainline, respectively. On-ramp and mainline flows interact at merging, diverging and weaving segments. No existing research has insight into the impact of these complex interactions on traffic operation. RM and VSL perform differently on different demand levels; however, no previous studies have explicitly studied their relationship and applicable conditions.

5. RM control is mandatory, while most VSL is advisory. To evaluate VSL control, compliance rates are often assumed because of the lack of field data. These assumptions may lead to control designs that do not meet the needs of practical applications, because real-world disturbances influence traffic control performance. Hence, it is essential to investigate into the driver compliance and disturbances from real-world scenarios.

6. Currently, VSLs have become proactive based on short-term prediction. Proactive VSLs succeed in simulation evaluations, but few have been deployed in the field and their real-world effectiveness has not been proved.

1.3 Research Objectives and Scope

To address the research gap, this study adopts a proactive integrated control in an MPC framework. The overall goal of the proposed research is to gain insight into the interaction between ramp and mainline flow control. There are 6 specific objectives:

1. Modify the METANET model to adapt it to the unpredictability of bottleneck activation during peak hours, calibrate and validate the modified model using field data to confirm its applicability in real life conditions. The validated model can present traffic dynamics and reproduce specific phenomena;

2. Analyze weaving impact on traffic flow and traffic control by developing a capacity estimation method, modifying boundary conditions in traffic dynamics and applying the traffic dynamics in traffic control;

3. Develop and evaluate a weaving capacity estimation method, which is potentially applicable for traffic operation, and estimate real-time maximum discharge flow rate in peak hours;

4. Design an integrated control strategy to improve traffic mobility considering traffic characteristics at bottlenecks, and update the RM rates and speed limits based on real-time traffic prediction; then investigate the impact of traffic demand and demand proportions on not only integrated control, but also the relationship between RM and VSL and their applicable conditions;

5. Analyze the complex driver speed behaviors at speed transition zones by statistical tests and linear regression, and propose some suggestions and guidelines for VSL algorithm design and implementations;

6. Capture and analyze the effect of real driving behaviors on traffic control through field operational tests (FOT), and evaluate real-life performance of proactive traffic control;

The research scope will be restricted to proactive control for freeway corridors, including on-ramps, off-ramps and weaving segments. The research scope can be divided into three key components: macroscopic traffic flow model, traffic control optimization, and control implementation. The outline of this research is presented schematically in FIGURE 1.1.

1.4 Research Contributions

This research provides several state-of-the-art knowledge contributions to freeway ATDM:

1. This research will modify, calibrate and validate the macroscopic traffic flow model METANET at a complicated corridor, where multiple bottlenecks exist. The modification of METANET accommodates the unpredictability of bottleneck activation and is applicable as a prediction module in proactive traffic control implementation,

2. After the prediction performance of METANET is confirmed, this research will develop a proactive approach for freeway control considering weaving capacity, with goals to reduce network-wide travel time and improve traffic flow. Cell transmission model (CTM) and a weaving estimation model will be adopted to enhance the boundary condition. Real-time estimated

weaving capacity can enhance the effectiveness of freeway operation and can be applied to mitigate or avoid active bottlenecks.

3. Weaving capacity estimation can enhance freeway operation effectiveness so there is a need for a theoretical estimation method. This research will develop a weaving capacity estimation method by combining a lane-changing model with linear optimization. The proposed method is capable of real-time weaving capacity estimation and enhancing traffic state prediction by improving the accuracy of boundary flow estimation in CTM.

4. This research will investigate the interaction between RM and VSL, and their applicable conditions, through a sensitivity analysis between traffic demand and control performance. These results can help traffic engineers decide on ATDM strategies.

5. As a part of integrated control, the driver response for VSL is complex. This research will represent speed limit effect and estimate real-time driver compliance at speed transition zones. The proposed driver compliance estimation model can be incorporated into VSL algorithms. The obtained conclusions will suggest and guide future VSL algorithm design and implementations.

6. The real-life benefit of VSL needs to be discovered. This research will investigate the effect of freeway control on driving behaviors from the field operational tests. The results will help modify and improve future proactive control implementation.

1.5 Organization of the Dissertation

As shown in FIGURE 1.1, the focus of this research is proactive freeway control. Six major areas of studies were conducted and presented in the remainder of this dissertation: applicability analysis of METANET model in traffic state prediction (CHAPTER 3); optimal RM control for weaving segments considering dynamic weaving capacity estimation (CHAPTER 4); capacity estimation for weaving segments using a lane changing model (CHAPTER 5); mainline and ramp flow interaction under proactive integrated freeway control (CHAPTER 6); effect of speed limits at speed transition zones (CHAPTER 7); preliminary test for VSL implementation (CHAPTER 8). In addition, CHAPTER 2 gives a detailed review of previous relevant studies and CHAPTER 9 summarizes the main conclusions and recommendations for future research.

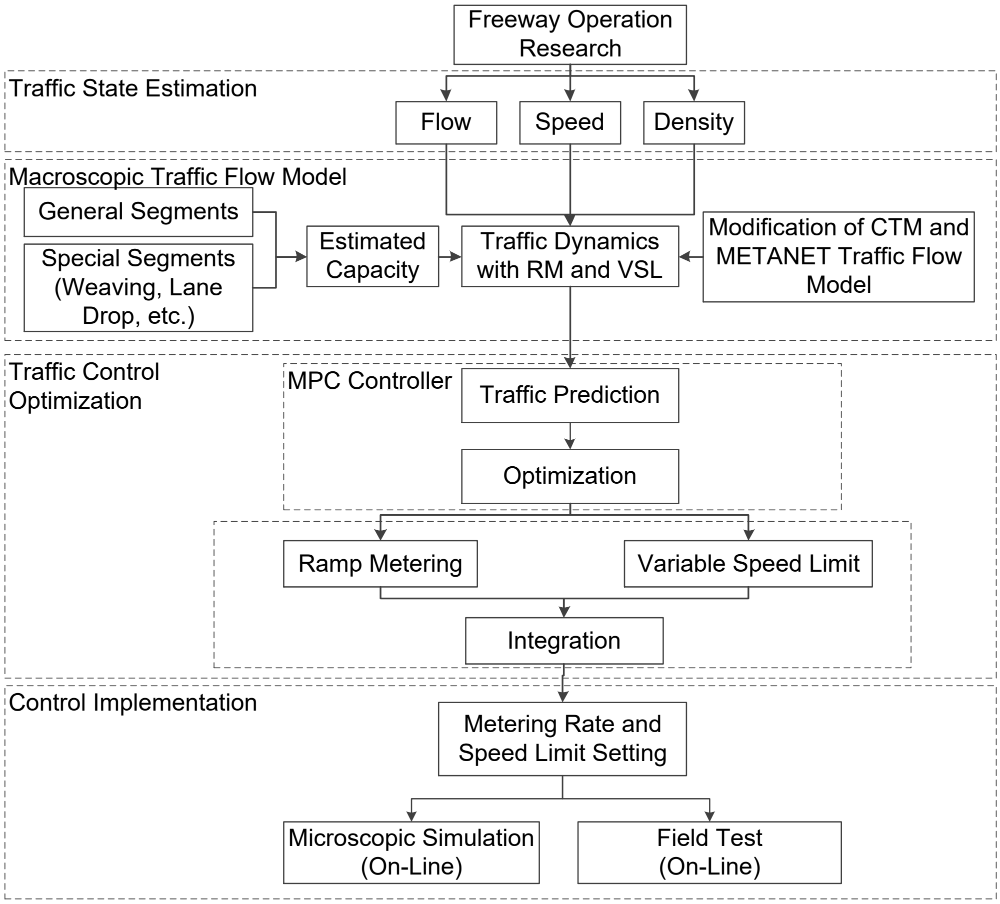

FIGURE 1.1. Research Flowchart.

CHAPTER 2. LITERATURE REVIEW

This research will design a proactive integrated control of RM and VSL using a Model Predictive Control (MPC) approach. This chapter gives a review of macroscopic traffic flow model calibration and validation, a brief summary of existing RM and VSL implementations, an introduction of previous weaving capacity estimation methods as well as an overview of studies on driver compliance with speed limits. For the sake of explicitness, this chapter categorizes and presents them in sections. In addition, this chapter also reviews some earlier results on RM and VSL control implementation, including both field tests and simulations.

2.1 Macroscopic Traffic Flow Model Calibration and Validation

Macroscopic traffic flow models discretize traffic flow spatially and temporally, and describe traffic dynamics by aggregated variables, i.e., flow, density and speed. They generally include physical or non-physical parameters to represent traffic characteristics accurately. Macroscopic models are categorized as first-order, second-order or higher-order models, according to the number of differential equations they include [11]. Second-order models, such as Payne's model [12], are essentially speed dynamics coupled with density dynamics. The density dynamics states the conservation of vehicle number in a section of roadway. In the related literature, macroscopic traffic flow models, which are often considered in proactive control strategies , are either the cell transmission model (CTM) [13] or the METANET model [14].

The METANET model is a modified version of Payne's model [12]. Cremer and Papageorgiou [15] modified Payne's model to a nonlinear time-discrete traffic dynamics model. They also presented the parameter identification process, or in other words, model calibration. Parameters were optimized on the basis of field-collected data in a no-speed-limit scenario, and were analyzed for their sensitivity. Then the constructed model demonstrated its accuracy in traffic estimation. However, the results may be inapplicable on freeways with speed limits. Papageorgiou et al. [16] demonstrated the derivation procedure of each equation in METANET. Moreover, they tested various combinations of mathematical models, which all had the conservation law and fundamental relationship. Field traffic data verified the model performance and parameter sensitivity. They chose the equation combination with the best model performance and called it the METANET model. Furthermore, some model parameters were simplified by a sensitivity analysis. Then, Papageorgiou et al. [17] extended the model by adding a lane drop term. With the results of all the above studies in hand, Messmer and Papageorgiou [14] summarized the application of METANET as a macroscopic simulation tool with relatively low computational complexity.

Since the METANET model was established, many efforts have been made to adapt the model in various scenarios by calibrating and validating the model parameters with field measurements, comparing model performance with other traffic flow models, or proposing possible modifications. Yin and Qiu [18] tested the compatibility of METANET with micro-simulation data under three different demand levels and seven time step lengths. They concluded from the results that the optimum time step length is 20 seconds (s). Another finding is that excessive traffic demand leads to stop-and-go conditions and therefore larger prediction errors. After METANET was demonstrated as an accurate traffic flow model in many studies, Spiliopoulou et al. [11] compared it with the first-order model CTM. Both models were calibrated and validated using the same data source. They were revealed to be able to replicate real traffic evolutions, but METANET is slightly more accurate. In addition, other studies have tried to improve METANET by adding modifications. Lu et al. [19] modified the original METANET model from a density-speed dynamics to a flow-speed dynamics model. This modification was expected to overcome the limitation of point sensors in density estimation. Frejo et al. [20] proposed a stepwise parameter calibration approach in order to achieve the global optimum of model performance. They also replaced the typical fundamental diagram (FD) in METANET with two new forms. The modified FDs showed better model estimation.

2.2 Ramp Metering

As the most applied freeway operation method, RM regulates input flow based on traffic state estimation or prediction. With appropriate metering rates, RM can balance freeway demand and capacity, maintain optimum freeway operation and improve safety on adjacent freeways and arterial streets [21].

2.2.1 Classifications of RM Algorithms

Generally, RM algorithms can be classified into three categories: fixed-time, reactive and proactive. Fixed-time RM strategies apply static models and control ramp flows offline, according to historical traffic demand [22]. Their objective criterion is to maximize total discharge flow with ramp queue and capacity constraints [23]. However, their metering rates cannot be automatically adjusted to temporal and spatial changes of active bottlenecks, especially for non-recurrent bottlenecks. Without real-time traffic information, fixed-time strategies may either over- or under-utilize freeway infrastructure. Therefore, reactive RM strategies are derived online to analyze and prevent traffic conditions beyond preset values. Demand-Capacity [24], Occupancy [24] and Asservissement Linéaire d'Entrée Autoroutière (ALINEA) [25] are typical local reactive strategies. These strategies rely on real-time measurements of flow or occupancy to alter metering rates and to maintain desired traffic conditions. Comparative field tests have exhibited the effectiveness of these reactive strategies [25, 26]; however, their effectiveness is debatable once multiple bottlenecks are activated or ramp storage space is restricted [27]. In contrast to local reactive methods, coordinated methods consider traffic conditions over a freeway corridor or a whole network. Typical coordinated methods include BOTTLENECK [28], METALINE [29], ZONE [30], System Wide Adaptive Ramp Metering (SWARM) [31], HEuristic Ramp-metering Coordination (HERO) [27], and optimal control strategies [32, 33]. In addition, other studies describe artificial intelligence approaches, such as fuzzy logic control [34], neural network [35], and iterative learning control [36].

As the third category, proactive RM control strategies take current traffic measurements and forecast their control consequences, coordinating and specifying optimal system-level status based on traffic state prediction over a sufficient time horizon. Papamichail et al. [37] proposed a model-predictive hierarchical control. Another common class is MPC. In the last decade, several researchers presented MPC-based traffic control strategies [5-7, 38-40]. This kind of dynamic optimal control problem adapts to feedback from new traffic measurements and disturbances. Its optimization provides a sequence of optimal control; only the first control variable is applied. In other words, due to its receding horizon control, MPC can handle the prediction errors caused by disturbances or model mismatch [41]. Therefore, MPC has succeeded in macro-simulation applications with non-linear models to solve multi-objective problems, which have constraints and high-level uncertainty.

2.2.2 *Field Tests*

The initial field implementation of RM dates back to the 1960s in Chicago, U.S. Since then, the installation and operation of RM has continually grown as Intelligent Transportation System (ITS) technologies have been deployed in North America and Europe. Many reports and papers have documented these installation and operation. Chicago area freeway RM control system [42, 43]was evaluated . The application of the system resulted in 60% reduction of peak-period congestion and 18% reduction of accident rate. Papageorgiou et al. [26] conducted a field evaluation of the RM algorithm ALINEA, in Boulevard Périphérique, Paris, and A10 West motorway, Amsterdam. Seven typical days were selected for both no-control and control scenarios. In the context of that studied corridor, the reduction in total time spent (TTS) for recurrent congestions amounted to 5.9%. In terms of non-recurrent congestions, ALINEA decreased total travel time (TTT) by 10.8% and increased total travel distance (TTD) by 6%. In Los Angeles County, U.S., SWARM was under a three-month evaluation in 2000 [31]. Three types of SWARM (SWARM 1, SWARM 2a and SWARM 2b) were assessed with the existing fix-time control system. All types of SWARM improved the traffic conditions generally, e.g. increased mainline speed by 6%-39%, reduced travel time by 3%-40%, decreased delay by 8%-79%, but SWARM 1 mode unfortunately decreased mainline traffic volume by 2%. In 2000, the Minnesota Department of Transportation [44] evaluated and reported the impacts of RM on traffic mobility and safety in the Twin Cities metropolitan area. The study focused on particular sections of I-494, I-94, I-35W and I-35E considering cases with and without control over a five-week period. Peak-period data showed that RM increased mainline throughput by 14%, saved annual travel time by 25,121 hours and reduced crashes by 26%. RM was indicated as a cost-effective investment of public funds in Twin Cities. Their follow-up evaluation showed that traffic mobility and safety was continually improved by ramp meters. Also, observed through market research, the support for the meter was stronger than before [45]. In Wisconsin, comparative traffic data taken over two months showed that RM improved traffic speed by 4%, reduced TTT by 2% and decreased crash rates by 13% corridor wide [46]. Besides the above performance criteria, Xie et.al [47] introduced delay volume and average vehicle delay to quantify the performance of RM along US 95, Las Vegas. By these two measures, the segments, which were lightly congested in the no-control case, experience almost no congestion in the controlled scenario.

Overall, field tests provide direct means to measure congestion magnitude for before and after control cases; however, field tests require large scale construction of transportation infrastructure. Also, they generally cannot generate various traffic scenarios and maximize control performance. To the author's knowledge, few proactive control methods have been deployed in the field due to the massive construction and facility requirements, which incur vast cost. Therefore, simulations are required to assess system performance, especially at the planning stage, and predict traffic behaviors in the operational level.

2.2.3 Simulation Evaluations

To execute proactive control in simulation, an accurate traffic flow model should be implemented in a predictive control framework to represent all the major traffic dynamics, including free flow, congestion and their transitions. A macroscopic traffic flow model, METANET [14], has been developed and applied in the testing of several proactive strategies as both a simulator and a traffic predictor.

Papamichail et al. [27] proposed a nonlinear model-predictive hierarchical control approach, and tested it in an extended METANET model. To optimize RM control, their algorithm contained a three-layer hierarchical structure. By coordinated RM, the hierarchical control led to a 47.8% amelioration of network TTS. Hegyi et al. [6] considered optimal coordination and combined VSL with RM by MPC. The original METANET was extended to incorporate speed limits and driver compliance in the prediction horizon of MPC. The nonlinear optimization problem was solved by a sequential quadratic programming (SQP) algorithm. In the authors' subsequent study [7], the same control strategy was used, but for RM control only. Simulations compared traffic situations between an ALINEA-based controller and an MPC-based controller. In the results, although MPC featured greater computational complexity, it yielded smoother control signals and traffic states. Moreover, MPC rendered a lower TTS. Furthermore, in one of their most recent studies, Zegeye et al. [39] proposed a receding-horizon parameterized control approach based on MPC and state feedback control. A multi-start SQP algorithm was used to solve the optimal control inputs. Due to its much shorter computation time, this algorithm more efficiently performed than the conventional SQP algorithm. The above-mentioned MPC applications all deploy SQP algorithms to solve nonlinear optimization problems; however, for real-life applications, these solution algorithms may not guarantee a reasonable computation time. To this end, Ghods et al. [38] introduced a game theory to obtain optimal control inputs for the integration of VSL and RM. Each controller optimizes its objective function by SQP, assuming other controllers keep their optimizations from the previous time step. This algorithm repeats until each controller reaches a convergence. The proposed algorithm was verified in METANET; its computation time was significantly reduced.

2.3 Variable Speed Limit

In the literature, numerous VSL control algorithms can be found which are designed to improve traffic safety. However, this research specifically aims to relieve traffic congestion and improve mobility. Basically, congestion is degradation in service quality resulting from an increase in usage (demand driven congestion) or a decrease in capacity (supply driven congestion including geometric and incident-induced restrictions). VSL are established to encourage uniform driving behavior and to delay or avoid demand driven congestion, and to reduce supply driven congestion, given that there is some remaining capacity on the roadway.

2.3.1 VSL Control Algorithms

VSL control algorithms can be categorized broadly into rule-based and model-based control. Rule-based VSL switching base their real-time decisions on preselected thresholds of traffic flow, occupancy or mean speed. Park and Yadlpati [48] proposed a VSL logic considering both safety and mobility measures. Its basic idea is to increase speed limit when very few vehicles are passing a work zone, while to reduce speed limits during a high traffic. The authors evaluated the method in a micro-simulation with two other VSL logics under varying compliance rates and demand conditions. Through simulation-based experiments, the proposed logic was found to outperform other logics for either mobility or safety in most scenarios. For locations where lack detectors, a time-of-day (TOD) speed limit control was proposed to maximize the use of available data by Kang and Chang [49]. Its core logic is to divide the entire day into a number of control periods and to accommodate the time-varying traffic conditions by implementing VSL within each control period. A real-life case, the work zone on I-80 SB, confirmed the effectiveness of the proposed control in a micro-simulation. It is notable that the proposed TOD speed limit control also features its robustness in contending with inevitable variations in the actual volume during each time-of-day period without the extensive use of traffic sensors. In addition, a tree logic-based algorithm was designed to deploy VSL by Hellinga et al. [50]. Based on traffic data received from loops, appropriate speed limit was determined by some predefined trigger conditions. A VSL decision corresponds to a combination of volume, occupancy and speed data so that the proposed algorithm is applicable for real life implementation. Its impact on travel time and safety was evaluated by varying levels of congestion in a microscopic simulation combined with a categorical crash potential model. Simulations exhibited that the proposed control could improve safety but at the cost of increased travel time. Moreover, notable safety improvements were achieved in heavy and moderate congestions while safety reductions were found in uncongested conditions. To sum up, rule-based strategies apply predefined trigger conditions to adjust VSL but they cannot adapt to temporal and spatial variance of congestion. Thus, recent research focuses on model-based VSL strategies.

Model-based control obtains optimal control variables through the optimization of a pre-established model with traffic measurements. There are generally four categories of research in model-based VSL control, i.e. linear optimization, non-linear optimization, fuzzy logic, and MPC approach. Firstly, Lin et al. [51] implemented two linear optimization VSL algorithms in simulation and explored their effectiveness. Both two methods approximate traffic dynamics by certain laws and calculate the target speed by linear optimization. With VSL, they aim to minimize queue length and maximize the throughput respectively. Simulation results demonstrated that the proposed models can increase traffic throughput, and reduce average delay as well as speed variance using appropriate parameters. For the non-linear optimization approach [52-54], it models a traffic system using the extended METANET and optimizes a cost criterion function using a solution algorithm. Their cost criteria include TTS, TTT, queue length and penalty terms. To solve the non-linear optimization problem, Kalman filter and feasible-direction algorithm are commonly applied. They were tested to be efficient even for large-scale networks. Applications of fuzzy control in freeway control [55, 56] were reported. An adaptive fuzzy control was proposed by Ghods et al. [56] to deal with VSL control with reasonable computation effort. A fuzzy controller is composed of three major components: 1) fuzzification, which transforms crisp input values into grades of membership for linguistic terms of fuzzy sets; 2) inference, which combines the facts obtained from the fuzzification with the rule base, and conducts the fuzzy reasoning process; and 3) defuzzification, which converts a fuzzy set into a single number.

Another branch of VSL methods is MPC-based control. All methods above are based on real-time traffic state estimation, but prediction is also necessary for an effective control strategy. If the formation or arrival of a shockwave in the controlled area is predictable, then preventive measures can be taken in advance. Furthermore, by using predictive control, the disturbance can be anticipated, which may prevent these kinds of instabilities. Hegyi et al.

[6] adopted MPC-based VSL control to optimally coordinate series of VSL signs upstream of an isolated bottleneck. The proposed MPC-based VSL control included a METANET-based prediction of the freeway evolution as a function of the current traffic state and a given control input. Specifically, in the speed dynamics, desired speed was modified to incorporate speed limits. The desired speed is to be taken as the minimum of the desired speed and the speed limit. The controller aimed at minimizing TTT only. Similar research [57-59] has been conducted while they were all evaluated in macro-simulation. Recently, Hadiuzzaman and Qiu [60] proposed a CTM-based MPC approach, resulting in a 10-15% travel time reduction and a 5-7% flow improvement. In their following research [10], they implemented an extended METANET model to the MPC approach. The controller updated the speed limit according to the optimization of TTT and total flow (TF). A conclusion can be drawn that real-time traffic state prediction had a remarkable impact on feedback controls.

2.3.2 Field Tests

A number of empirical studies have been conducted mostly for improving traffic safety at work zones. The general consensus emerged from those implementation results is that VSL control has positive impact on safety. In 1995, the UK Highways Agency introduced mandatory VSL signs between Junctions 11 and 15 at one mile intervals on the M25 motorway. UK Highways Agency [61] reported a 10% decrease in injury collisions, a 9% reduction in the amount of flow breakdown, and 6% reduction of start-stop driving conditions.

VSL implementation resulted traffic headways more uniformly distributed within a short range of 0.8-1.5 sec. In a German study [62], an empirical approach was adopted to investigate the impact of VSL control in reducing congestion. To improve driver safety, feedback was given to the driver with advisory speed limit and road condition. Safety benefit (20%-30%) was more significant than mobility. In addition, the Dutch experiment [63] intended to homogenize the traffic flow along a stretch of highway using enforced VSL. Only two speed limits (70 and 90 kilometer per hour, kph) were used, with 1-min update rate. Test results showed speed control was effective in reducing speed, speed variation, and the number of shock waves. Besides, an empirical evaluation of the implemented VSL control strategies was conducted by Papageorgiou et al. [64]. That study concluded that there was no clear evidence of positive impact of VSL on improving traffic flow. However, the authors also observed that their study was limited due to implemented VSL control algorithm. The authors suggested that a more robust and efficient VSL control strategy could be developed and implemented to investigate its mobility benefit.

Most model-based VSL approaches incorporate control systems that have a high computational complexity or contain parameters without direct physical interpretation, which may make real-life applications difficult. To the author's knowledge, the only model-based VSL method applied in real-world tests was SPEed Controlling ALgorithm using Shockwave Theory (SPECIALIST) on the Dutch A12 freeway [65]. It translates the shockwave theory to a practically applicable algorithm. The general steps of SPECIALIST are shockwave detection, solvability assessment, control scheme generation and control scheme application [66]. Quantitative results showed that about 80% of the shock waves were resolved in practice by the algorithm, and the average gain of TTT per resolved shockwave was 35 vehicle hours (veh*h).

2.4 Integrated Freeway Control

Ramp metering is a ramp control and has no control after vehicles enter the freeway. The benefit of RM may be limited if congestion is not caused by excessive on-ramp demand. Also, RM sometimes needs to be switched off once the on-ramp queue spills back to surface streets. Thus ramp metering alone might be insufficient for freeway control. VSL control is a mainline traffic flow control (MTFC) and a good supplement to RM. Much recent research has focused on integrated control.

There are several possible ways to combine VSL and RM depending on what model is adopted and how the control strategy is designed: 1) RM is determined before VSL; 2) VSL is determined before RM; and 3) an approach based on a tightly coupled second order model involving both density dynamics and speed dynamics without priority. Lu et al. [57] designed RM before VSL and used the second approach to design a combined traffic control strategy in [67]. Hegyi et al. [6] applied coupled traffic dynamics (the third approach) to consider optimal coordination and combined VSL with RM by MPC. The original METANET was extended to incorporate speed limits and driver compliance in the prediction horizon of MPC. The objective function in MPC takes the TTS on both mainline and ramps, with a term that penalizes abrupt variations in RM and VSL signals. The nonlinear optimization problem was solved by an SQP algorithm. Furthermore, one of their most recent studies proposed a receding-horizon parameterized control approach based on MPC and state feedback control. A multi-start SQP algorithm was used to solve the optimal control inputs. Due to a much shorter computation time, the modified SQP algorithm performed more efficiently than conventional SQP [39].

The above-mentioned MPC applications all deploy SQP algorithms to solve nonlinear optimization problems; however, for real-life applications, these solution algorithms may not guarantee a reasonable computation time. To this end, Ghods et al. [38] introduced a game theory to obtain optimal control inputs for the integration of VSL and RM. Each controller optimizes its objective function by SQP, assuming other controllers keep their optimal decisions in the previous time step. This algorithm repeats unless each controller reaches a convergence. The proposed algorithm was verified in a macro-simulation and found its computation time was significantly reduced.

2.5 Weaving Capacity Estimation

During peak hours, a weaving segment may be activated as a recurrent bottleneck. To be specific, a weaving segment is formed where a merging segment is closely followed by a diverging segment, and two traffic streams may cross and conflict [68]. Weaving, or intensive lane changes, may result in capacity drop, which has been observed in the field [69, 70]. An important point to note is that, capacity is one of the main inputs in traffic operation strategies which aim to relieve bottleneck severity. Obtaining more knowledge for weaving maneuvers and weaving impact will enhance freeway design and operation.

Weaving segments have long been investigated, including estimating capacity, evaluating level of service (LOS) and analyzing safety impact. A methodology for weaving segment design and analysis was first presented in the Highway Capacity Manual (HCM) 1950. Since then, a number of approaches have been developed and made efforts to improve procedures in HCMs. HCM 2000 presented procedures for determining prevailing or expected LOS by converting predicted speed to an overall density [71]; however, this requires classifications of segment configurations and operation types. To address this issue, Roess and Ulerio [72] developed a model to replace configuration types with lane changing activity and intensity, which performed better in field tests. This direct methodology has been developed for inclusion in HCM 2010. For safety research, a crash prediction model was built for a one-lane exit to identify influential factors, and to explain that left-side off-ramps potentially cause a higher number of severe injury and fatal crashes [73].

In the last decade, capacity estimation at weaving segments has been a major focus of transportation researchers. Several direct methodologies have been developed either by empirical or theoretical means. In empirical methods, the HCM 2000 provides detailed procedures and multipage tables for capacity determination [71]. Later, a regression-based equation in HCM 2010 substituted the cumbersome tables in HCM 2000. In the latest HCM model [74], volume ratio, short length and number of lanes for weaving movements constitute the difference between the capacity of a basic freeway and a weaving segment. This method is statistically significant. Moreover, a capacity estimation approach was proposed by Kwon et al. based on a Kalman filter [69]. This method estimates origin-destination (O-D) flows at a weaving segment depending on the collected data from the upstream mainline and on-ramps. However, in addition to the parameters involved in the aforementioned empirical models, complex driver behaviors also determine the capacity at weaving segments. As a result, capacity can also be estimated from a theoretical point of view.

Throughout the literature, the only theoretical model for capacity estimation at weaving segments was developed by Lertworawanich and Elefteriadou [70, 75]. This capacity estimation method is a linear optimization problem with gap acceptance theory to constrain weaving flows. The results indicated that an increase in complex weaving maneuvers has a notable impact on weaving capacity. This model works well in tests, whereas it was not designed for traffic operation; thus, its parameters are difficult to directly measure with basic traffic operation facilities. Furthermore, the driver behavior parameters in this model may be site-specific. For traffic operation purposes, this study replaced the gap acceptance theory by a lane changing model. The applied lane changing model was proposed by Laval and Daganzo to model vehicle's latitudinal interactions [76, 77]. It categorizes lane changes into mandatory and discretionary actions, and ensures consistency between microscopic and macroscopic measurements. To achieve this objective, it converts lane-specific macroscopic variables to a lane changing rate, and discretizes it into a time-space point. In general, this model requires less input and is more applicable in flow estimation.

2.6 Driver Compliance with Speed Limits

Effect of speed limit enforcement or education tools on driver compliance has attracted researchers' attention. Soole et al. [78] conducted a thorough review on effectiveness studies of speed enforcement. The common indexes, such as 85th percentile speeds, average speeds and proportion of speeding vehicles, indicated the effectiveness of speed enforcement. Evaluation methods are usually the before-and-after method using statistical indexes. For example, Lee et al. [79] compared short-term and long-term performance of speed-monitoring displays at school zones. These devices reduced vehicular speed significantly in both short term and long term, but level of driver attention was slightly reduced in long-term applications. Similar observations were obtained by Woo et al. [80], who also found the speed-monitoring display exerted an influence on speeding even they were turned off. Furthermore, Santiago-Chaparro et al. [81] extracted vehicle trajectories to examine spatial variations of speed. They concluded that vehicles with greater speeding have higher probability to reduce speed in front of speed feedback signs, and the effectiveness is lost only 300 feet after the signs.

Apart from indexes mentioned above, driver compliance with speed limits was explored spatially and temporally. Wasson et al. [82] measured space mean speed using vehicle probe data and showed temporal and spatial driver compliance with or without enforcement techniques. The temporal elasticity of speed limit compliance was found to be significant. However, in VSL scenario, Soriguera et al. [83] reported a very limited driver compliance even speed enforcement radars were applied in their test bed. They observed a surprising point that at sections with high compliance, discharge flows under low speeds and high densities are stably near the capacity value. This phenomenon is opposite to the finding by Papageorgiou et al [64]. Moreover, a further study by Ardeshiri and Jeihani [84] looked into potential factors that contribute to speed compliance. Upstream speed limit compliance, time of day and day of week were found to affect speed compliance using regression techniques. Another study by Fang et al. [85] intended to predict driver response by traffic characteristics. Driver response was formulated as a linear regression of speed, density and speed limit value. Field tests proved the statistical significance of the regression model. In conclusion, various factors may influence driver compliance and their extent of influence is site specific.

As discovered by Soriguera et al. [83], driver compliance with VSLs may be limited and hence results in unsatisfactory control performance. Hellinga and Mandelzys [86] proved in micro-simulation that driver compliance is positive correlated with VSL safety performance but negative correlated with operational performance. They also pointed out settings of VSL strategy should depend on driver compliance. A similar approach was performed by Habtemichael and de Picado Santos [87]. Unlike the conclusions obtained by Hellinga and Mandelzys [86], the authors summarized the safety benefits of VSLs are not at the expense of an increase in travel time. Put simply, higher driver compliance with VSLs improves both mobility and safety. Although previous research cannot reach a consensus, driver compliance correlates and influences VSL mobility and safety performance. In addition, micro-simulation by Lu et al. [67] obtained similar mobility benefits with compliance rates at 100% and 30%. However, from another VSL algorithm they proposed [88], they claimed VSL benefits are not sensitive if a compliance rate is higher than 10%. Hence, the effect of compliance on VSL performance greatly depends on the VSL algorithm itself. Despites the tight correlation between driver compliance and VSL algorithms, existing VSL algorithm design mostly assumes full compliance, especially in traffic prediction model for proactive VSL algorithms. Throughout the literature, only several recent researches undertook VSL algorithm design considering the impact of driver compliance. Heygi [89] introduced a non-compliance factor in the speed equation of METANET model. The author predefined a fixed proportion value to present the non-compliance rate. In contrast, Fang et al. [85] considered dynamic driver response by modifying the speed equation of METANET with a regression model.

2.7 Summary

Overall, several research areas related to proactive integrated control strategies have been studied for a long time. In the literature, various traffic control strategies have been proposed. The traffic control strategies were reviewed by categories, i.e. isolated or integrated control of RM and VSL, and fixed-time, reactive or proactive strategies, respectively. By either simulation or field tests, they have been confirmed their effectiveness and efficiency for relieving traffic mobility and safety issues. Different categories have their own strength and weakness. Most existing control strategies implemented in practice belong to fixed-time or reactive strategies. Proactive control strategies forecast future traffic condition by traffic flow prediction models and optimize traffic control variables by optimization of certain objectives. Well-established proactive strategies can come up countermeasures in advance and hence prevent or relieve traffic congestion.

To enhance the performance of proactive control strategies, many studies have been devoted. Through: prediction model establishment, calibration and validation studies, macroscopic traffic flow models have been revealed to be applicable for representation and prediction of traffic evolutions. Next, capacity at weaving segments is sensitive to weaving maneuvers so that weaving capacity estimation can help in accurate capacity calculation. Furthermore, driver responses and compliance to speed control are complicated. Previous research indicated that driver compliance can be estimated to replicate driver response to speed limit control.

CHAPTER 3. APPLICABILITY ANALYSIS OF A MACROSCOPIC TRAFFIC FLOW MODEL IN TRAFFIC STATE PREDICTION

3.1 Introduction

As traffic demand steadily increases around the world, so does congestion, which is a major traffic problem that lowers mobility on freeways. Over the past several decades, transportation agencies have turned to traffic operation strategies to improve the utilization of existing freeway infrastructure. In the meantime, transportation professionals have been seeking more efficient and less costly solutions to manage ever increasing traffic demand. Recently, proactive control strategies have become popular in the literature; they use traffic flow models with control variables to predict future traffic states and achieve pre-specified objectives. Although many papers [2, 37, 90] have documented the development of proactive control strategies, the real-life benefits of their applications are still unknown. The main factors that hinder proactive strategies from being implemented in the field are the following: (a) high computational complexity, and (b) the accuracy and reliability of the traffic flow prediction models. Proactive strategies are characterized by their traffic flow prediction models. However, the prediction models generally contain parameters with no intuitive physical interpretation. Without optimal assignment of calibrated parameters, traffic flow models can hardly perform well as prediction models in real-life applications. Therefore, prior to field applications, traffic flow models have to be carefully calibrated and validated, and the sources of potential prediction errors must be traced. In fact, existing studies in the literature have seldom investigated the applicability and error sources of traffic flow models in traffic prediction.

This study chose a macroscopic traffic flow model METANET [14], which is often used in proactive control strategies. The METANET calibration and validation studies mentioned in the literature review were carried out on simple traffic corridors (nearly straight roadways with no complex recurrent traffic situation). METANET divides a corridor into several segments. Some of the parameters to be calibrated in METANET reflect driver behavior characteristics. If the corridor is nearly straight and traffic conditions are simple, the established model with global parameter values can replicate traffic evolutions on the whole corridor. Otherwise, a complex corridor with complicated geometric and traffic conditions may require segment-specific parameter values to reflect segment-specific behaviors. Also, METANET requires modifications to accommodate complex traffic conditions, especially for congestion periods. Therefore, it is necessary to test the model on complicated traffic corridors and potentially make modifications before real-world implementation. The following three questions need to be answered: (a) How does each term in METANET work in traffic prediction? (b) Can

METANET replicate complex traffic states, e.g. driver behavior changes in a complex geometric or traffic environment? (c) How does each parameter to be calibrated affect the prediction performance? Consequently, this study aims to bridge these gaps: with field measurements, METANET was modified, tested and analyzed for its applicability on a complicated traffic corridor.

In this research, the METANET model was modified to accommodate multiple bottleneck situations, and then calibrated and validated using geometric and traffic data from an urban freeway corridor, called Whitemud Drive, in Edmonton, Canada. The resulting model prediction performances were compared according to constructed models with segment-specific and global parameters. Subsequently, prediction profiles for the validation dataset were compared with measurement profiles to uncover potential prediction error sources. The results improved the understanding of each term in the METANET model, and could lead to more reliable implementation of proactive control strategies in the future.

The remainder of this chapter is organized into sections: Section 3.2 specifies the methodology, which includes an introduction of the METANET model, proposed modifications, and model calibration and validation procedure; and Section 3.3 is devoted to model calibration and validation result analysis.

The remainder of this chapter is organized into sections: Section 3.2 specifies the main methodologies, including introduction of METANET model, proposed modifications, and procedure of model calibration and validation;

Section 3.3 is devoted to model calibration and validation result analysis; Section 3.4 is the concluding remarks.

3.2 Methodology

3.2.1 Macroscopic Traffic Flow Model METANET

To apply the dynamic traffic model METANET [14], the freeway corridor was divided into several segments ($i=1, 2,..., N$) of length L_i and lanes λ_i (as shown in FIGURE 3.1). The aggregated traffic state variables were defined for each segment and updated for each time step. Based on spatial and temporal discretization, the evolutions of traffic density $\rho_i(k)$ in vehicles per kilometer per lane (veh/km/ln) and traffic speed $v_i(k)$ in kilometers per hour (km/h) at each time index t ($t = kT$, T is the discrete time step length, k is the time step presently in the calculation) were calculated by Equations (3.2) and (3.3). The details were well documented by Messmer and Papageorgiou [14].

$$\rho_i(k+1) = \rho_i(k)+\frac{T}{L_i\lambda_i}\left[\lambda_{i-1}q_{i-1}(k)-\lambda_i q_i(k)+r_i(k)-s_i(k)\right] \tag{3.1}$$

where, q is the boundary flow between segments in vehicles per hour per lane (veh/h/ln); r and s are on-ramp and off-ramp flow rates in vehicles per hour (veh/h) respectively.

$$v_i(k+1) = v_i(k)+\underbrace{\frac{T}{\tau}\left\{V\left[\rho_i(k)\right]-v_i(k)\right\}}_{\text{relaxation term}} + \underbrace{\frac{T}{L_i}v_i(k)\left[v_{i-1}(k)-v_i(k)\right]}_{\text{convection term}} - \underbrace{\frac{\eta T\left[\rho_{i+1}(k)-\rho_i(k)\right]}{\tau L_i\left[\rho_i(k)+\kappa\right]}}_{\text{anticipation term}} \tag{3.2}$$

where, τ is the reaction time parameter response to the perception of traffic states in hours (h); η is the anticipation parameter (km^2 per hour, km^2/h); κ is a positive constant (veh/km/ln). These global parameters need to be identified in model calibration using traffic measurements.

In Equation (3.2), $V\left[\rho_i(k)\right]$ expresses the fundamental density-speed relationship, which is usually calculated by the following equation:

$$V\left[\rho_i(k)\right] = v_{f,i}\exp\left[-\frac{1}{\alpha_i}\left(\frac{\rho_i(k)}{\rho_{cr,i}}\right)^{\alpha_i}\right] \tag{3.3}$$

where, ρ_{cr} is the critical density (veh/km/ln); v_f is the free flow speed (km/h); and α is a link specific model parameter that determines the shape of the FD.

It is important to note that, considering the impacts from on-ramps and lane drops, two additional terms can be added to Equation (3.2) [14]. However, this study excluded those two terms. The detailed reasons were explained in our previous research [18] and are not repeated here. The main reason is that some previous studies [16, 17] included these terms but no visible amelioration was achieved. Thus, so far, most previous studies [11, 15] ignore these additional terms.

The density dynamics (Equation (3.1)) is derived from flow conservation law. It is the space-time-discretized form of the fundamental equation for conservation of matter $\partial\rho/\partial t + \partial q/\partial x = r - s$. On the other hand, the speed dynamics (Equation (3.2)) describes the mean speed adjustment caused by traffic density change after time delay τ. Constant parameters η and κ are introduced in space-time discretization of the speed dynamics. Parameter η indicates the importance of the anticipation term, while parameter κ is introduced in case ρ is too small.

With the values of these parameters obtained from calibration, the performance of METANET can be evaluated. If τ reaches an extremely large value after calibration, it means the error from other variables in the relaxation term is so large that τ has to be large to eliminate the prediction error. Suppose the prediction in the last time step $v_i(k)$ is accurate, the error should be from the estimation of $V\left[\rho_i\left(k\right)\right]$. Similarly, when η keeps rising or κ keeps dropping during calibration, some error may exist in the estimation of $\rho(k)$ in the anticipation term. In the worst scenario, when the calibrated parameters τ, η and κ all get unreasonably high or low values, the prediction of $v_i(k+1)$ approaches $v_i(k)$. In this case, the prediction model performs poorly, as it cannot capture the temporal variations in traffic states. In conclusion, the parameters to be calibrated (τ, η and κ) work simultaneously to minimize the prediction error; meanwhile, their values also reflect the performance of each term in the prediction model.

3.2.2 Boundary Flow Estimation in Density Dynamics

The constitutive condition in METANET is that time step length T is supposed to meet physical constraint $T \leq L/v_f$. If this condition is violated, some vehicles may skip one segment in one time step. This "jumping" effect will lead to model instability and inaccuracy. Furthermore, the boundary flow q in Equation (3.1) is considered as the transition flow between segments, while v and ρ are regarded as space-mean speed and density measurements over a segment. Papageorgiou et al. [16] applied a weighted sum of the successive segment flow to estimate boundary flow. The basic idea is that discharge flow is set as the flow on the current segment if the downstream segment is free flow, or set as the flow on the downstream segment if downstream is congested. To simplify this boundary flow estimation rule, this study checks speed contour maps or flow-density diagrams to identify which segment flow ($Q = \rho v$) will be chosen in boundary flow estimation. Based on the above analysis, the following equation was proposed.

$$q_i(k) = \begin{cases} \mu_i Q_i(k) & \text{if downstream is free-flow in peak hour} \\ \mu_i Q_{i+1}(k) & \text{if downstream is congested in peak hour} \end{cases} \tag{3.4}$$

where, μ is the ratio of actual boundary flow to flow measurement, which reflects origin-destination (O-D) distribution of a segment, in case some ramp data are missing.

3.2.3 Segment-Specific Fundamental Diagram

Fundamental diagrams model the bivariate relationships between traffic flow, density and speed. In the following discussion, FDs are specified as flow-density relationships unless otherwise noted. FDs may vary across links, and they are empirically confirmed and theoretically derived from microscopic behaviour models in previous studies. Equation (3.3) models the shape of the speed-density relationship, which can also be derived from the flow-density relationship. Although discharge flow can be estimated from FDs based on density measurements, the discharge flow may not match the estimation result. FIGURE 3.2 presents three extreme cases that have different discharge flow vs. density relationships. In the figures, FDs are simplified as triangular FDs. Different from traditional FDs, the x-axis indicates density (veh/km/ln) and the y-axis indicates total flow on all lanes (veh/h) to show the flow variation across segments.

Case (a): Although the number of mainline lanes decreases on the connection from Segment 2 to Segment 3, some O-D distributions may not trigger a bottleneck. In Case (a), the discharge flow from Segment 2 to Segment 3 does not exceed the capacity of Segment 3. Neither Segment 3 nor the connection between the two segments is activated as a bottleneck. Whereas, due to special O-D distributions on Segment 2, Segment 2 carries critical weaving manoeuvers and generates a bottleneck, but the bottleneck does not propagate to upstream segments. Thus, the bottleneck on Segment 2 does not affect other segments, and discharge flows from all segments follow their own FDs (see FIGURE 3.2 (a)).

Case (b): O-D distributions on Segment 2 change so that weaving manoeuvers are not too heavy to activate the bottleneck in Case (a). However, the exiting flow from Segment 2 is larger than the capacity of Segment 3, so another bottleneck is triggered at the connection of the two successive segments.

The discharge flows from upstream segments are restricted by bottleneck flow when the shockwave propagates to them. In this case, the discharge flow vs. density relationship (as shown in FIGURE 3.2 (b)) does not follow its FD.

Case (c): O-D distributions are the same as those in Case (b), yet a bottleneck also exists downstream because of special reasons, such as sharp curves or weaving manoeuvers. If this congestion keeps spreading to upstream segments, the bottleneck flow limits upstream discharge flow. FIGURE 3.2 (c) illustrates the discharge flow vs. density relationship for all the segments.

In summary, discharge flow on a segment follows not only its FD but also downstream bottleneck flow. Discharge flow is limited by downstream bottleneck flow until the bottleneck is resolved, and then it returns to its FD. This conclusion also matches the concept built in CTM [13]. Equation (3.3) ignores the limited bottleneck flow and overestimates $V\left[\rho_i(k)\right]$ once an activated downstream bottleneck spreads to the current segment. Solely considering the current segment state neglects the uncertainty of bottleneck activation. With this conclusion in mind, FIGURE 3.3 plots the FDs without or with downstream bottleneck. Likewise, Equation (3.3) can be replaced by Equation (3.5) below to take limited bottleneck flow into account. This modification improves the applicability of METANET to a complex corridor with multiple bottlenecks.

$$V\left[\rho_i(k)\right]=\min\left\{v_{f,i}\exp\left[-\frac{1}{\alpha_i}\left(\frac{\rho_i(k)}{\rho_{cr,i}}\right)^{\alpha_i}\right],\frac{Q_{\max,i}}{\rho_i(k)}\right\} \tag{3.5}$$

where, $Q_{\max,i} = \begin{cases} v_{f,i}\rho_{cr,i} \exp\left[-\dfrac{1}{\alpha_i} \right] & \text{if downstream is free-flow} \\ Q_{BN,i} & \text{if downstream is congested} \end{cases}$, $Q_{\max}$ is the possible maximum discharge flow, and Q_{BN} is the bottleneck flow when downstream bottleneck is activated.

3.2.4 METANET Calibration Procedure

The model calibration process strives to achieve the highest model accuracy by adjusting unknown parameters so that the model can replicate real-world traffic evolutions. The following initial and boundary conditions were proposed to calibrate the model so that the modified METANET model can be used in proactive control strategies.

(a) The initial traffic conditions ($k = 0$) at each segment are taken from measurements. METANET predicts traffic states for the remaining time steps ($k = 1,...,K$).

(b) At each prediction step ($k = 1,...,K$), $\rho_i(k)$ and $v_i(k)$ in Equations (3.1) and (3.2) are aggregated, smoothed and converted into space-mean data from point-based loop detector data.

(c) Equation (3.1) is derived from flow conservation law where boundary flows (q_{i-1} and q_i) at the segment ends are required. Since loop detectors were located in the middle of segments for better measurement of speed and density (as shown in FIGURE 3.1), boundary flow is estimated by Equation (3.4).

Calibration of METANET is a nonlinear optimization problem, which involves multiple parameters. To reduce its complexity, the calibration process in this study consists of three steps: (a) estimate boundary flow-related parameters through minimizing the prediction error of density; (b) estimate FD-related parameters using the fundamental relationship between speed and density; and (c) optimize other parameters by minimizing the prediction error of speed dynamics. This stepwise calibration approach helps the calibration results obtain global optimum. Before introducing the calibration process, several assumptions are proposed as follows:

(a) This analysis focuses on two cases, i.e., the segment-specific parameter case and global parameter case. In the segment-specific parameter case, parameters τ, η and κ from different segments are given different values. They stay the same during the total simulation length. Likewise, ρ_{cr}, v_f and α are specific for one specific segment (as claimed by Messmer and Papageorgiou [14]). On the contrary, the global parameter case applies the same parameter values across all segments.

(b) A previous validation practice [11] reported that the value of κ has a minor impact on the entire model performance. Thus, κ is given a fixed value (10 veh/km/ln), which can reduce the dimension of the calibration parameter vector.

Based on the above assumptions, the three-step calibration process is summarized in FIGURE 3.4. Step 1 optimizes the total prediction error D of density dynamics from field measurements (Equation (3.6)). Given the fundamental relationship in Equation (3.5), Step 2 compares the estimated speed with measurements. Then the total error F (Equation (3.7)) is minimized and the optimal FD-related parameter set (β) is obtained. Using β and pre-determined κ, Step 3 minimizes the total speed difference between METANET prediction and measurements (Equation (3.8)). This three-step optimization is performed using a specific optimization technique, for example, sequential quadratic programming (SQP) in this study. Eventually, the METANET model together with the calibrated $\left[\tau,\eta,\kappa,\rho_{cr},v_f,\alpha,Q_{BN},\mu\right]$ can represent traffic dynamics for the studied corridor after these three steps.

$$D(\delta)=\sqrt{\sum_{i=1}^{N}\sum_{k=1}^{K}\left[\rho_i^m(k)-\rho_i(k|\delta)\right]^2} \tag{3.6}$$

where, $\delta=[\mu]$

$$F(\beta)=\sqrt{\sum_{i=1}^{N}\sum_{k=1}^{K}\left[V_i^m(k)-V_i(k|\beta)\right]^2} \tag{3.7}$$

where $\beta=\left[v_f,\rho_{cr},\alpha\right]$

$$S(\gamma)=\sqrt{\sum_{i=1}^{N}\sum_{k=1}^{K}\left[v_i^m(k)-v_i(k|\gamma)\right]^2} \tag{3.8}$$

where $\gamma=[\tau,\eta]$

3.2.5 METANET Validation Procedure

The model validation procedure ensures that the model with calibrated parameters can reliably represent or predict real-world traffic dynamics, including free flow and congestion as well as their transitions. Thus, the calibrated model must be applied to the same traffic corridor with different datasets, other than the one used in calibration. Existing validation practice [11] reported that accurate estimation or prediction of flow is not a major problem, while that of speed is more challenging. Moreover, as density can hardly be measured from basic detection techniques, this study calculates density with the aid of relationship between flow and speed. To sum up, the validation process is carried out by assessing the root mean square error (RMSE) between model output (ρ and v) and field measurement (ρ^m and v^m). The performance index is calculated according to Equation (3.9).

$$\mathrm{MOE} = \sqrt{\sum_{i=1}^{N}\sum_{k=1}^{K}\left\{\left[\rho_i^m(k) - \rho_i(k)\right]^2 + \left[v_i^m(k) - v_i(k)\right]^2\right\}} \tag{3.9}$$

3.3 METANET Calibration and Validation Results

3.3.1 Study Site and Data Collection

The eastbound section (from 170th Street to 122nd Street) of an urban freeway corridor, called Whitemud Drive (WMD), in Edmonton, Canada, was studied (FIGURE 3.5). There are six on-ramps and five off-ramps on the studied section. The posted speed limit is 80 km/h. The City of Edmonton has installed vehicle detection stations (VDSs) and traffic video cameras along this corridor. The VDSs are placed on the mainline and ramps. They collect traffic data, such as volume, speed and occupancy, every 20 s, and send this data to the city's central computer system for archival. The cameras record real-time vehicle movements. Since loop detectors on VDSs provide measurements over a short distance, speed and occupancy measurements should be converted into space-mean speed and density before being taken in the prediction model. FIGURE 3.5 shows the VDSs and camera locations. To implement the prediction model, the studied corridor was divided into nine segments, each of which is approximately 800 meters (m). The dashed lines in FIGURE 3.5 represent the start and end of each segment.

3.3.2 Field Data Analysis

Complete datasets from the VDSs were available from 2011 to 2014. FIGURE 3.6 presents speed contour maps for two typical days in November, 2013. As Edmonton often bears adverse weather conditions in winter, the weather records were checked to ensure enough visibility for driving. Also, the traffic incident records of this corridor were checked to eliminate the impact of incidents.

As observed in FIGURE 3.6, different O-D distributions during AM and PM peaks lead to three recurrent bottlenecks along this urban freeway. In the AM peak (6AM-9AM), one area of congestion originates close to the on-ramp of Terwillegar Drive, where vehicles pass a sharp curve. It is triggered due to the curve and weaving manoeuvers on Segment 9, and it propagates far upstream to 147th Street. In the PM peak (4PM-7PM), another area of congestion begins at a segment adjacent to 53rd Avenue, where the mainline lane number reduces from three to two, while most vehicles during peak hours take the mainline instead of the off-ramp. The third area of congestion starts from the sharp curve around 147th Street and propagates upstream. When downstream bottlenecks are activated and spread upstream, discharge flows from upstream are restricted, as explained in the methodology section. This phenomenon is demonstrated by the flow-density plots in FIGURE 3.7. Due to no adverse weather or incidents during the two days, the reason why congestion happens can be inferred as high traffic demand. As a result, traffic data on November 5, 2013, were used in the following calibration test, while those in November 25, 2013, were considered in the validation test.

3.3.3 Parameter Calibration

METANET model parameters $\left[\tau,\eta,\kappa,\rho_{cr},v_f,\alpha,Q_{BN},\mu\right]$ were identified from the whole day of data for November 5, 2013. The optimization of minimizing the total errors (Equations (3.6)-(3.8)) was completed using the SQP technique in the MATLAB Optimization Toolbox. The multi-start SQP searched continuously and picked the optimized objective function value from multiple local minima. The parameters that constitute METANET are listed in TABLE 3.1.

From the performance indexes F and S, it was revealed that the calibrated segment-specific parameters can improve estimation/prediction accuracy of traffic states. For instance, with segment-specific FD parameters, the speed estimation error by FDs decreased from 305.9 km/h to 261 km/h. Meanwhile, the speed prediction error was reduced from 1608 km/h to 1020.5 km/h. However, the calibrated FDs using segment-specific parameters on uncongested or slightly congested segments may misestimate the real fundamental relationships, as not much congestion data are used in the calibration (Segment 4 and 8 in TABLE 3.1 (c) and FIGURE 3.7). When these segments encounter congestion in the validation, the calibrated parameters will cause prediction errors. Moreover, segment-specific parameters are so sensitive to the traffic characteristics on a segment that they can easily hit the constraint boundaries during the optimization process (τ value of Segment 8 in TABLE 3.1 (e)). In short, segment-specific parameters are beneficial for traffic prediction accuracy, although they may bring prediction errors to their application.

The varying values of calibrated τ and η in TABLE 3.1 (e) indicate not only best fit for each segment in mathematics but also the difference in driver behaviors. As explained in the last section, τ in the speed dynamics possesses a physical meaning, i.e., reaction time. Segments 2-7 had τ values within a normal range (11.6-39.7 s), but Segment 8 obtained an extremely high value (239.9 s) that almost hit the constraint boundary. This high value of τ shows its speed evolutions seldom depend on its FD. To reduce the impact of FD (estimation error of 99.3 km/h in TABLE 3.1 (c)) on speed prediction, τ achieved a high value in the calibration. Furthermore, except for the FD relationship, external traffic factors also contribute to driver speed changes. The external factors include downstream density in the anticipation term and upstream speed in the convection term. Parameter η quantifies the importance of downstream density in the anticipation term. For example, vehicles on

Segment 8 pass the bottleneck and start to accelerate depending on the downstream traffic state. At this time, downstream density is the most critical impact factor for vehicle speed. This is why segments that carry acceleration behaviors all generate high η values, e.g. Segment 3, 4 and 8. In turn, for vehicles that are still stuck in congestion and will continue at low speed, downstream density does not allow them to speed up greatly. In other words, if both the current segment and its downstream segment are congested during peak hours, the model calibration generates low η values, e.g. Segment 2, 5, 6 and 7. When analyzing those segments combined with flow-density plots in FIGURE 3.7, we noticed that Segments 2, 5, 6 and 7 and their downstream segments yielded congestion during peak hours. Their η values were low, ranging from 5 km^2/h to 13.7 km^2/h. The low η values reflect that the anticipation term is less important for these segments. Driver speed is not much affected by the density of a congested downstream segment. The main contributing factors are their previous speed and upstream speed in the relaxation and convection terms. This can also explain why Segments 5-8 all have relatively large prediction errors in both $F_i(\beta)$ and $S_i(\beta)$, and why only Segment 8 obtained an extremely high value of τ. Speeds on Segments 5-7 are influenced more by other terms other than the anticipation term. Both their FD relationships and upstream speeds determine their speed transitions. Despite high FD estimation errors, the relaxation term is still required and τ values are low. However, the speed on Segment 8 is influenced mostly by downstream density, i.e., the anticipation term. Thus, Segment 8 does not need the relaxation term to describe its speed change so that is why its τ value is very high. In summary, the calibration results for the model parameters can describe the primary driver behaviors on segments: if speed transitions mainly depend on FD relationships, the calibrated τ is small; if the speed transition mainly depends on downstream density, the calibrated η is large; the tuning of τ and η also corrects the possible errors considering upstream speed, as there is no parameter to be tuned in the convection term.

The largest calibration errors ($F_i(\beta)$ and $S_i(\beta)$) from segment-specific parameters happened on Segment 5 in both the FD estimation of TABLE 3.1 (c) and speed dynamics of TABLE 3.1 (e). Segment 5 is the most complicated segment with an intricate flow-density relationship (see FIGURE 3.7). The complicated traffic conditions and the unpredictability of bottleneck activation disturb the speed transition prediction. Overall, in the calibration stage, the model performance by global parameters is acceptable, but that by segment-specific parameters is better. In the following validation tests, segment-specific parameter values were applied.

3.3.4 Model Validation

The constituted models were validated subsequently using the dataset from November 25, 2013. The performance index of prediction error was evaluated by Equation (3.9). FIGURE 3.8 displays the peak-hour density and speed evolutions of field measurements and the METANET prediction for model validation. Overall, METANET can replicate free flow, congested flow and the transitions between them. According to Equation (3.9), the performance index achieved 568.4 in the AM peak and 563 in the PM peak. These index values indicate the prediction is accurate. As density dynamics is the estimation based on flow conservations law, the density prediction is more accurate. In terms of speed dynamics, it can also capture speed drops and increases. However, it can be summarized from FIGURE 3.8 that the shapes of density or speed evolutions between successive segments are similar. Speed prediction results adapt to upstream segment speed, downstream segment density and the calibrated FD relationship. Thus, the speed or density of a segment is affected by upstream or downstream traffic states so that prediction errors come from the aforementioned factors. If the traffic states on successive segments are triggered by different reasons, the predicted states may not match real traffic conditions. Moreover, in the calibration case, Segment 4 does not experience any congestion but the validation case does. The calibrated FD by segment-specific parameters, which has little congestion data, may not reflect the real speed-density relationship. The speed drop cannot be predicted promptly. Thus there is a lag between prediction and measurements in speed drop and the lag may spread to the downstream (speed prediction at Segment 4 in FIGURE 3.8 (d)).

In this validation test, the prediction horizon N_p was three hours. Traffic measurements were input into the prediction model at the time step index $k = 0$. The following three hours regarded prediction results from previous steps as the measurements and also model input. Whereas, in real-life applications of METANET in proactive control strategies, such as model predictive control (MPC)–based strategies, the prediction horizon N_p and control horizon N_c together need to be tuned. There are tuning rules that make trade-offs for the length of N_p and N_c between lower computational complexity and more control freedom [2]. Generally, the prediction horizon is 10-15 minutes and the control horizon is 5 minutes, while the data collection interval is much shorter (e.g. 20 s) than the prediction horizon. It means that during the real-life application of METANET in traffic control, the prediction horizon (e.g. 10 minutes) is much shorter than the one used in this validation test (i.e. three hours). Meanwhile, during one prediction horizon, the detectors keep collecting traffic data and providing the data to the controller. It follows that the field-measured traffic data can correct the prediction error made in previous prediction steps. In contrast, the prediction error accumulated during the three-hour prediction in this validation test. Consequently, the modified METANET is accurate enough for control purposes, e.g., VSL or ramp metering (RM) field tests for the study site.

3.4 Summary

This chapter calibrated and validated a modified METANET model for a complicated corridor, where multiple bottlenecks exist. According to the calibration and validation results, the following main conclusions were obtained:

(1) The METANET model with modifications can generally reflect and predict real traffic states under complex traffic conditions with multiple bottleneck locations. The modification of METANET accommodates the unpredictability of bottleneck activation. METANET is applicable as a prediction module in proactive traffic control implementation, such as the VSL or RM field test on the study site.

(2) The speed dynamics in METANET is a weighted summation of traffic state change inducements: speed at the last time step acts as a baseline for prediction; the relaxation term makes the predicted speed follow the fundamental speed-density relationship; and the convection term and anticipation term consider the impact of upstream speed and downstream density respectively. All terms collaborate and contribute to model prediction accuracy, but they may cause prediction errors as well.

(3) The obtained values for parameters τ, η, and κ from calibration give the feedback for the model prediction performance. The values of segment-specific parameters show the driver behavior characteristics.

(4) The prediction performance by segment-specific parameters surpasses that by global parameters, despite the potential problems produced by the segment-specific parameters.

TABLE 3.1. Calibrated Parameter Values for METANET Model

(a) Boundary Flow Adjustment Parameter Values

Parameter \ Segment No.	2	3	4	5	6	7	8	$D(\delta)$ (veh/km/ln)
$\mu_\cdot$	1.0054	1.0055	1.0062	0.9996	0.9718	1.0032	0.9992	649.5

(b) Global Parameter Values for FD

Parameter	Value	$F(\beta)$ (km/h)
ρ_{cr} (veh/km/ln)	31.1	305.9
v_f (km/h)	84.5	
α	2.9	
Q_{BN} (veh/h/ln)	1200	

(c) Segment-Specific Parameter Values for FD

Parameter \ Segment No.	2	3	4	5	6	7	8	$F(\beta)=\sum_{i=2}^{N-1} F_i(\beta)$ (km/h)
ρ_{cr} (veh/km/ln)	33.9	33.2	22.2	33.3	27.7	30.1	32	261
v_f (km/h)	84.2	83.9	84.6	84.4	85	84.9	85	
α	2.6	2.6	2.3	2.6	3.1	3.2	3.2	
Q_{BN} (veh/h/ln)	990	990	NA	1230	1120	1440	NA	
$F_i(\beta)$ (km/h)	86.6	84.3	59.6	131.8	113.7	99	99.3	

(d) Global Parameter Values for Speed Dynamics

Parameter	Value	$S(\gamma)$ (km/h)
τ (s)	33.0035	
η (km^2/h)	21.2672	1608
κ (veh/km/ln)	10	

(e) Segment-Specific Parameter Values for Speed Dynamics

Segment No. / Parameter	2	3	4	5	6	7	8	$S(\gamma)=\sum_{2}^{N-1} S_i(\gamma)$ (km/h)
τ (s)	38.7	12.6	11.6	14.2	21.1	39.7	239.9	
η (km^2/h)	5	23.9	35.1	13.7	5.1	5	27.7	
κ (veh/km/ln)				10				1020.5
$S_i(\gamma)$ (km/h)	147.2	181.2	129.7	731.7	362.7	401.6	377.2	

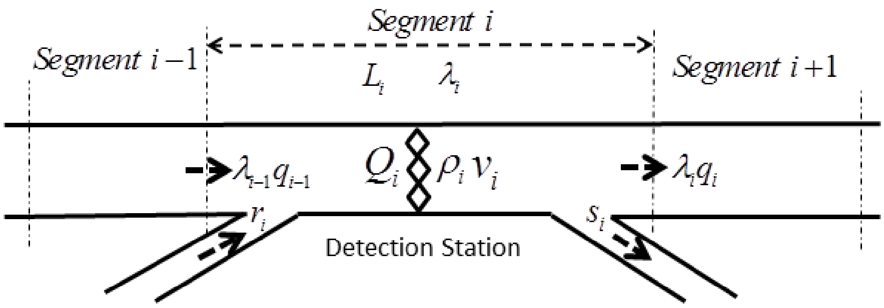

FIGURE 3.1. Freeway Segmentation.

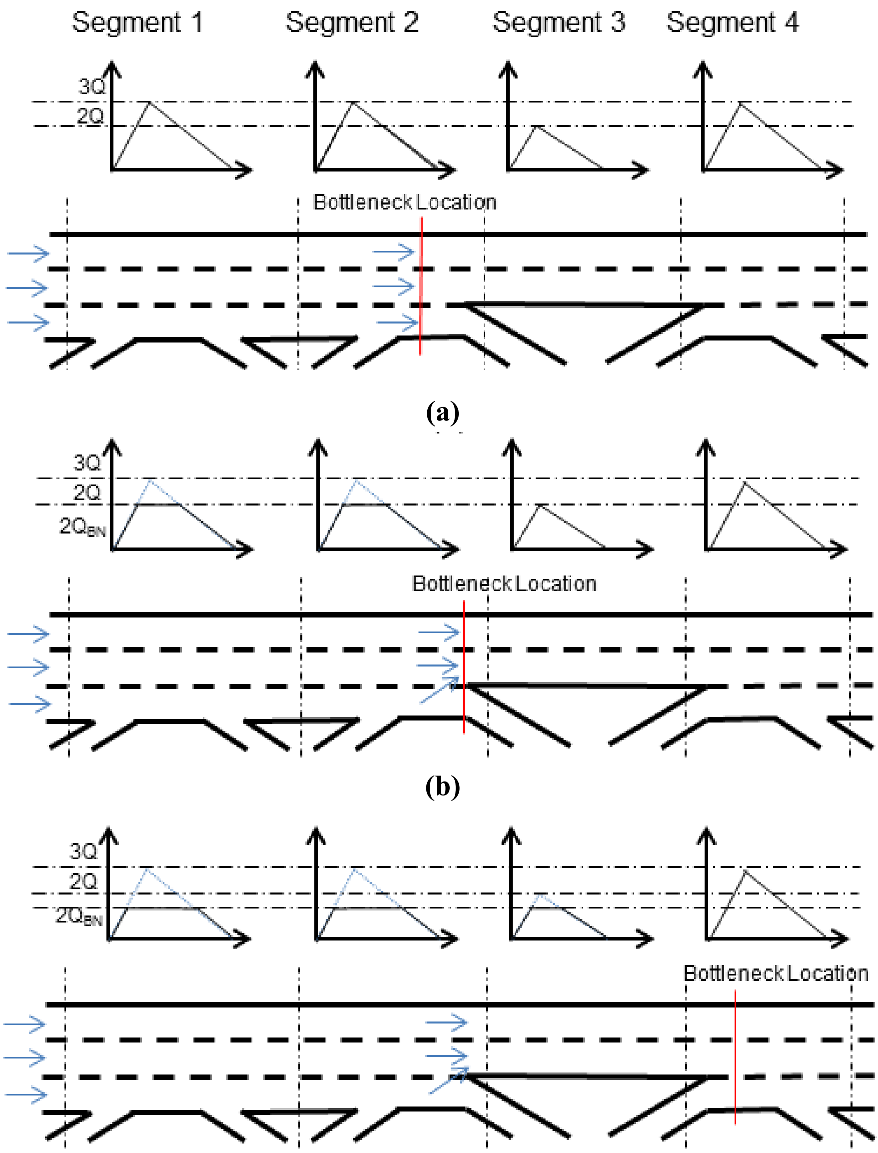

(c)

FIGURE 3.2. Segment-Specific Discharge Flow vs. Density Relationships: (a) Case (a); (b) Case (b); and (c) Case (c).

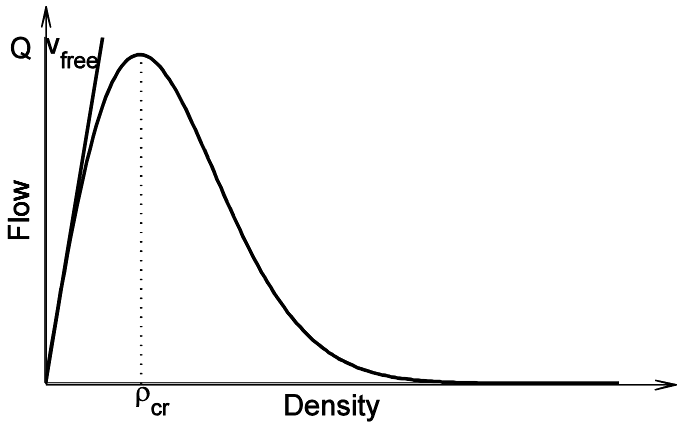

(a)

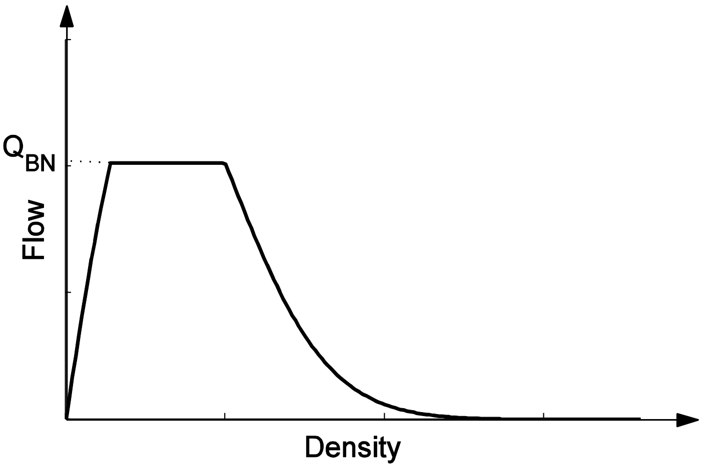

(b)

FIGURE 3.3. Discharge Flow vs. Density Relationships:

(a) downstream is free flow; (b) downstream bottleneck exists.

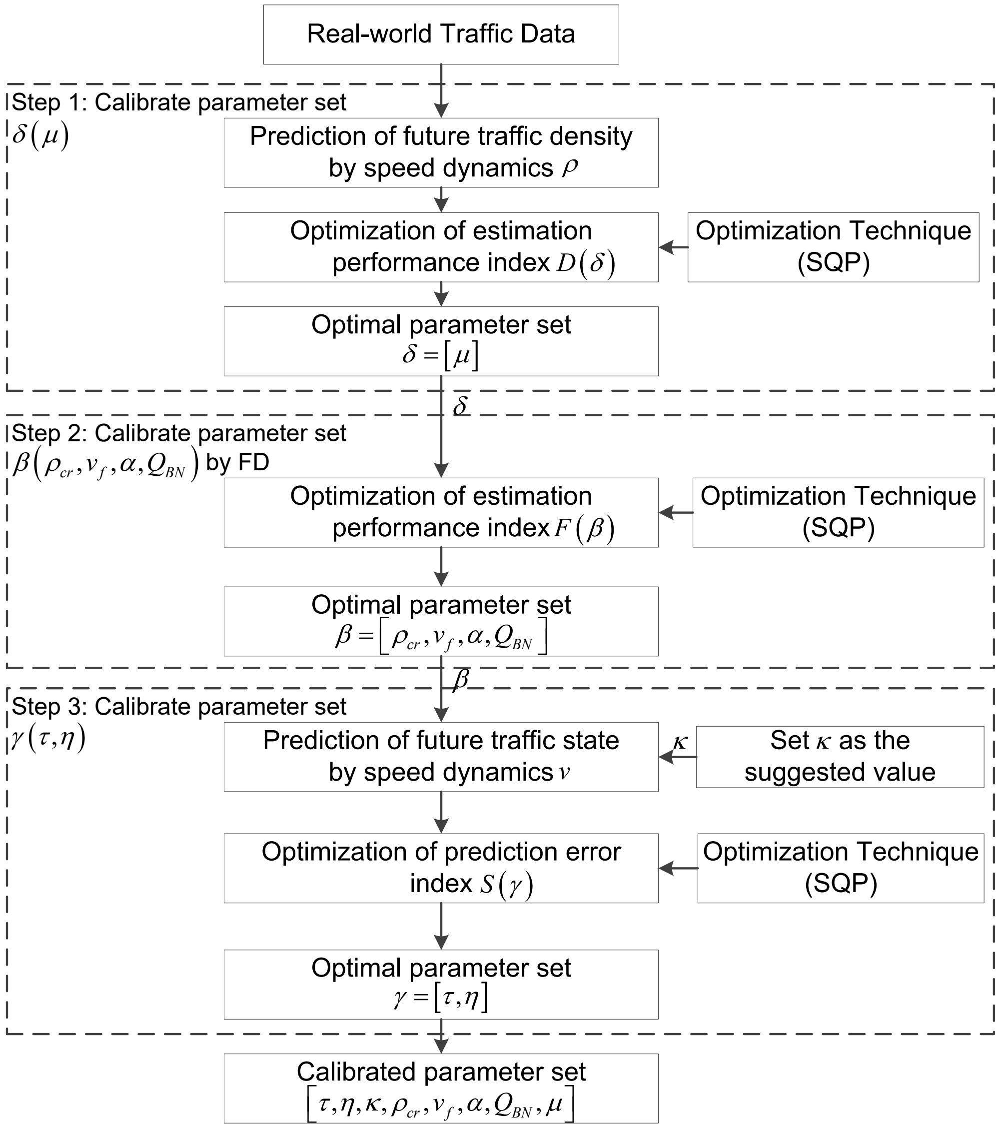

FIGURE 3.4. METANET Calibration Procedure.

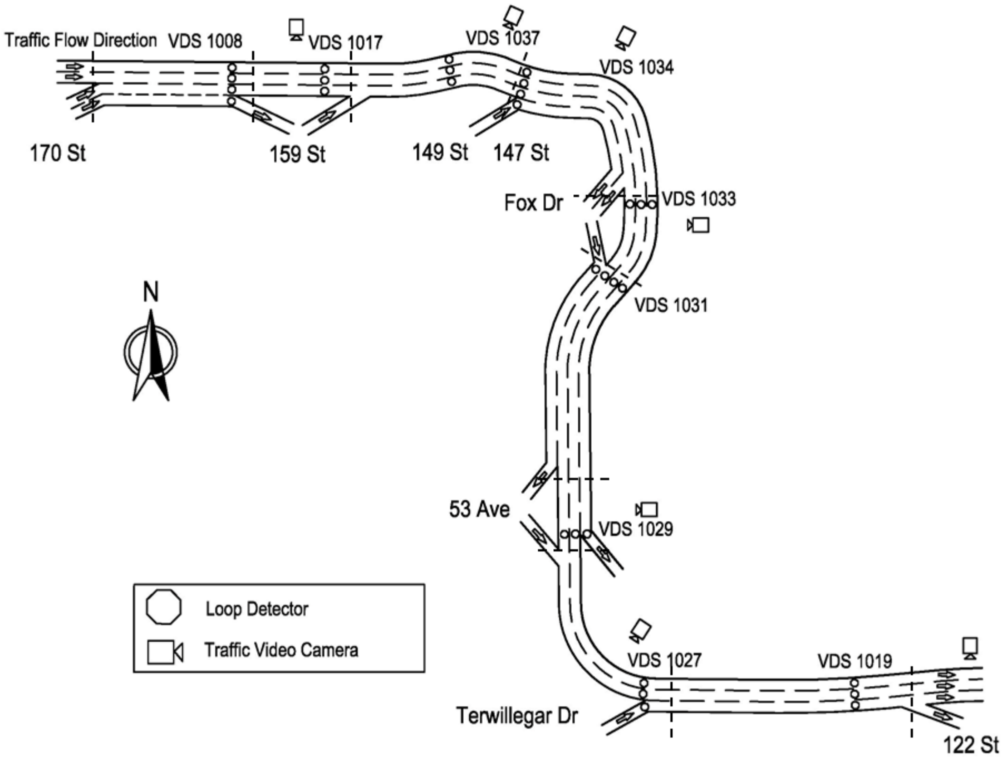

FIGURE 3.5. Study Site and Segmentation.

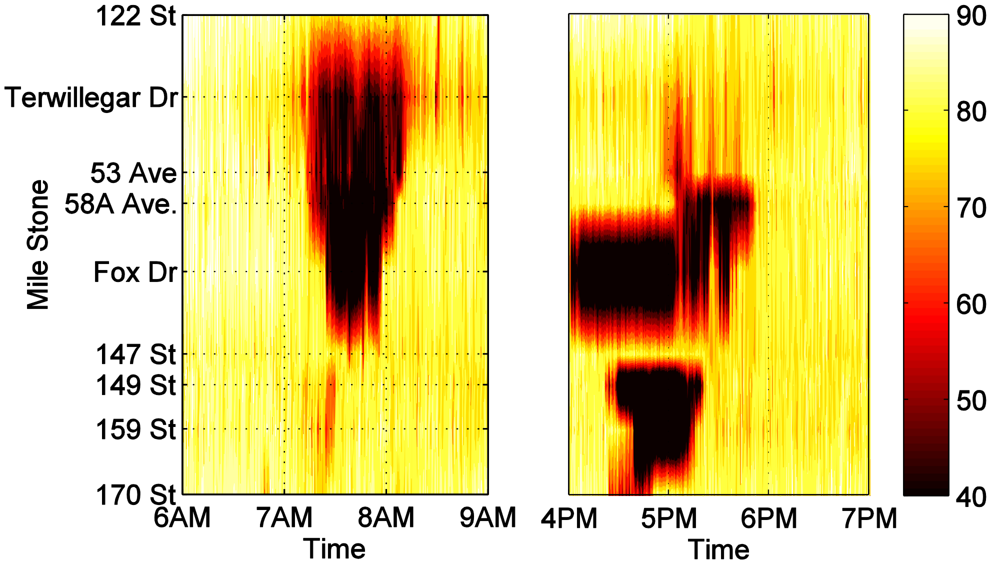

(a) Nov 5, 2013

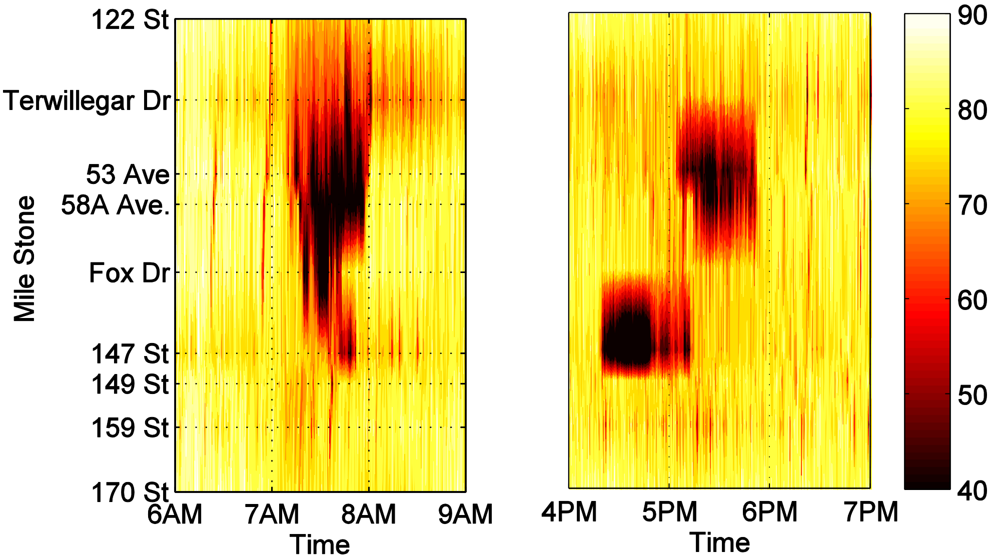

(b) Nov 25, 2013

FIGURE 3.6. Speed Contour Maps.

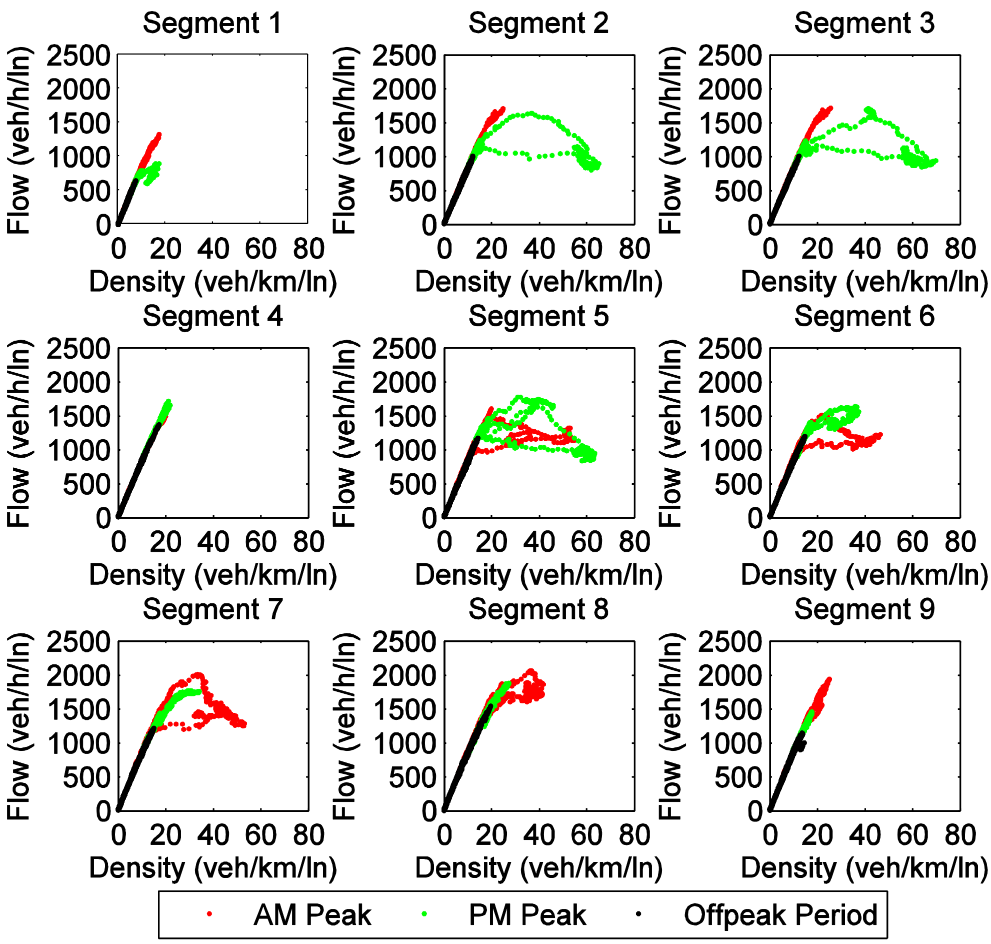

FIGURE 3.7. Discharge Flow vs. Density Plots, Nov 5, 2013.

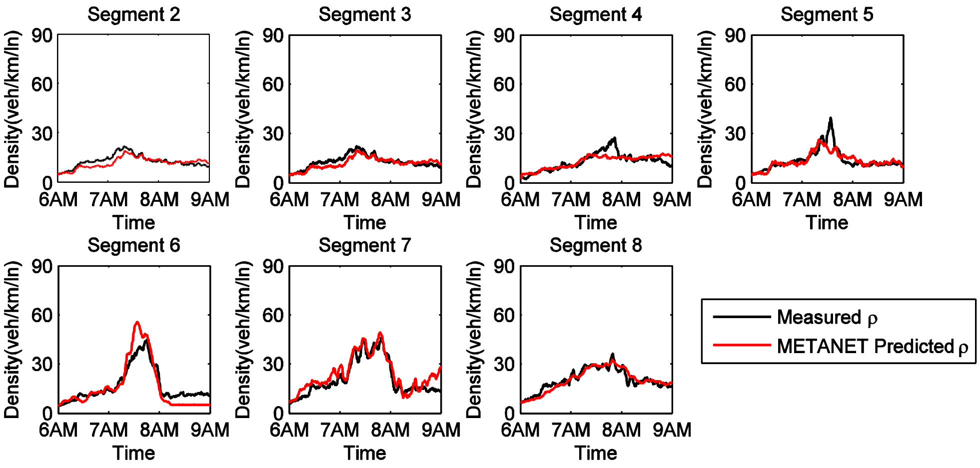

(a) Density Prediction for the AM Peak

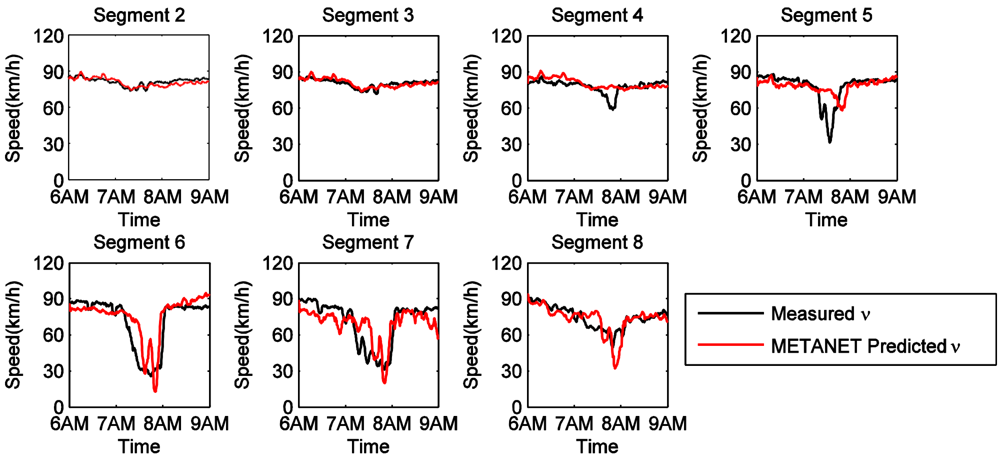

(b) Speed Prediction for the AM Peak

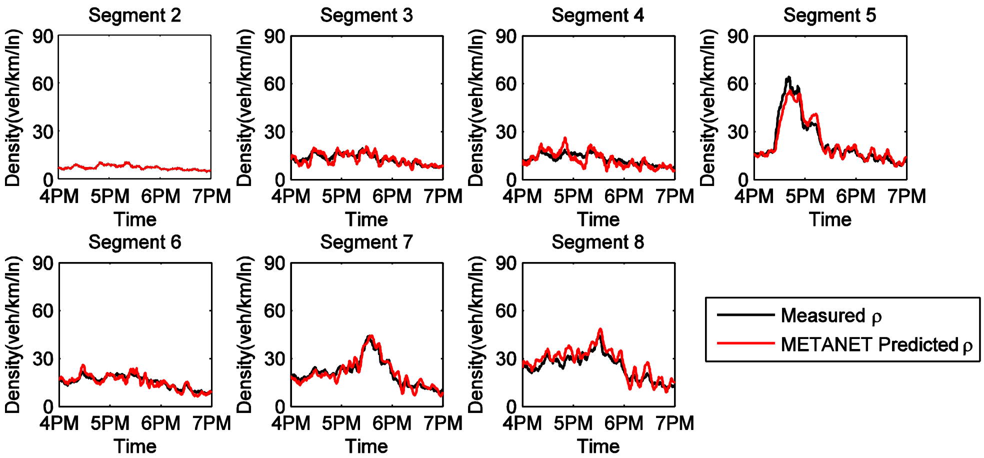

(c) Density Prediction for the PM Peak

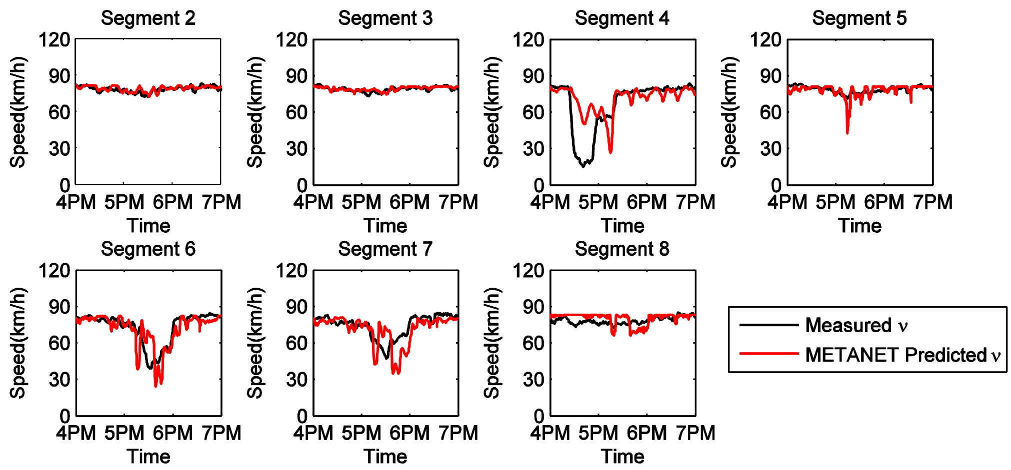

(d) Speed Prediction for the PM Peak

FIGURE 3.8. Density and Speed Prediction, Nov 25, 2013.

CHAPTER 4. OPTIMAL RAMP METERING CONTROL FOR WEAVING SEGMENTS CONSIDERING DYNAMIC WEAVING CAPACITY ESTIMATION[1]

4.1 Introduction

On freeway corridors, traffic flow is limited by active bottlenecks. Weaving maneuvers (i.e., intensive lane changes) are a major cause of bottlenecks during high demand periods. To relieve bottleneck severity, ramp metering (RM) is implemented as an active traffic control method. Ample research has been devoted to developing RM control algorithms and to exploring weaving impacts; however, RM control that is considerate of dynamic weaving impact and its evaluation has received little attention in the published literature.

4.1.1 Proactive RM Control Algorithms

Proactive RM control algorithms take current traffic measurements, forecast their control consequences and coordinate and specify optimal system-level updates based on traffic state prediction over a sufficient time horizon. Their implementation requires a control framework and an accurate traffic flow model to represent or predict all of the critical traffic dynamics, including free flow

[1] A version of this chapter has been published. Xu Wang, Md. Hadiuzzaman, Jie Fang, Tony Z. Qiu, and Xinping Yan (2014). Optimal Ramp Metering Control for Weaving Segments Considering Dynamic Weaving Capacity Estimation. Journal of Transportation Engineering (ASCE), 140 (11), 04014057.

and congestion and their transitions. Recent research applied optimal control using a macroscopic traffic flow model, METANET [14] and model predictive control (MPC) [6, 7, 38, 39, 67]. In these studies, the optimal control problem adapted to feedback from real-time traffic measurements and disturbances. Because of the MPC's receding horizon control, it can handle the prediction errors caused by disturbances or model mismatches [41]. Therefore, MPC is successful in simulations with non-linear models that solve multi-objective problems, which have constraints and a high level of uncertainty. The advantages of MPC over the traditional optimal control were described by Hegyi et al. [6]. Bellemans et al. [7] considered optimal RM coordination using MPC. Simulations compared control outcomes between an ALINEA-based controller and an MPC-based controller. Results showed that, although MPC requires greater computational complexity, it yields smoother control signals and traffic states. Hegyi et al. [6] applied a modified METANET model to optimally integrate VSL with RM by MPC. The nonlinear optimization problem was solved by a sequential quadratic programming (SQP) algorithm. Furthermore, a recent study proposed a receding horizon parameterized control approach based on MPC and state feedback control [39]. A multi-start SQP algorithm was implemented to solve the optimal control inputs. Because of its much shorter computation time, the modified SQP algorithm performed more efficiently than the conventional SQP algorithm. The aforementioned MPC applications all deployed SQP algorithms to solve nonlinear optimization problems in simulation; however, for real-life applications, these solution algorithms may not guarantee a reasonable computation time. To this end, Ghods et al. [38] introduced a game theory to obtain optimal control inputs for the integration of VSL and RM. Each controller optimized its objective function by SQP, assuming that the other controllers maintained their optimal decisions from the previous time step. This algorithm repeated until each controller reached a convergence. Their algorithm was verified in macro-simulation; its computation time was significantly lower than previous algorithms.

4.1.2 Weaving Capacity Estimation

Weaving is defined as the crossing of two or more traffic streams traveling in the same general direction along a significant length of highway without the aid of traffic control devices. Weaving segments are formed when merging segments are closely followed by diverging segments [68]. Many studies have investigated weaving segments; most of these studies focused on capacity estimation. In the original METANET model, there is a specific term for a speed reduction due to weaving at a lane drop area; however, there is no modification for ramp weaves. Several direct methodologies were developed theoretically or empirically. Based on the gap acceptance theory and linear optimization, Lertworawanich and Elefteriadou [70, 75] developed a capacity estimation method for Type A and Type B weaving segments. This methodology estimated capacity at weaving areas as a function of volume ratio, speed and traffic flow rate. Volume ratio is defined as the ratio of weaving flow over total flow. To estimate weaving segment capacity, Roess and Ulerio [74] substituted a regression-based equation for the HCM 2000 multipage tables. In this model, volume ratio, short length and the number of lanes for weaving movements constituted the difference between the capacity of a basic freeway segment and a weaving segment with the same free-flow speed. This method became the weaving methodology in the HCM 2010.

Capacity estimation research often covers analysis of capacity sensitivity to traffic or geometric parameters. Lertworawanich and Elefteriadou [75] found that ramp weave capacity is an increasing function of the basic freeway segment capacity, but that the rate of increase on a ramp weave is less than the rate of increase on a corresponding basic freeway segment. Zhang [91] presented an analysis of weaving ratio and weaving segment length, both of which are parameters that may potentially influence weaving capacity. [92] empirically explored bottleneck activations and discharge flow variations through studying vehicle counts and vehicle trajectories. Their study found that both the spatial distribution and amount of lane changes influenced weaving bottleneck discharge flow. [74] performed another sensitivity analysis and illustrated that capacity is generally linearly sensitive to volume ratio, short length, number of weaving lanes and free-flow speed. These results all indicate that sensitivity can potentially be applied in optimized RM strategies to increase capacity estimation accuracy.

4.1.3 Research Objectives

Overall, bottlenecks may be activated by lane drops or weaving maneuvers when demand is excessive or driving maneuvers are complicated. Weaving capacity is sensitive to traffic and geometric parameters. Field data indicates that intensive lane changes at weaving segments significantly affect capacity and may result in capacity drops [69, 70]. Theoretically, RM is designed to relieve or even prevent bottleneck activation through limiting the upstream input flow. Thus, RM strategy design should consider weaving impacts. However, capacity was predefined and fixed in most preceding RM strategies. To the author’s knowledge, the design and implementation of an RM algorithm with dynamic weaving capacity estimation has received little attention in the published literature. To this end, this chapter aims to bridge that gap: with real-time data, the proposed RM control algorithm dynamically estimates weaving capacity, which renders more accurate results than models that use fixed capacity. There are three objectives: 1) quantify weaving capacity sensitivity to on-ramp and mainline demand; 2) design an RM strategy with real-time weaving capacity estimations; and 3) evaluate the proposed method by measures of effectiveness (MOEs).

The remainder of this chapter is organized into sections: Section 4.2 introduces the proposed method, including capacity estimation, capacity sensitivity analysis and the prediction model; Section 4.3 calibrates and validates the proposed model to represent an authentic freeway corridor; and Section 4.4 is devoted to the analysis and comparisons of the simulation results.

4.2 Methodology

The proposed RM control strategy aims for optimal network performance according to real-time predicted traffic states and dynamically estimated weaving capacity. The proposed strategy was implemented within an MPC approach. To be specific, the strategy has a multi-module structure to collect field traffic information, predict traffic conditions and optimize and apply control variables (see FIGURE 4.1). A METANET-based traffic flow model, DynaTAM-RM (Dynamic Analysis Tool for Active Traffic and Demand Management-Ramp Metering), was used to perform traffic state predictions according to coordinated RM.

In the proposed MPC-based RM strategy, the optimal RM values, r^*, were calculated at each control sampling time index, k_c. Based on the traffic measurements, $\boldsymbol{x}$, and initial r values, the controller predicted future traffic states, $\hat{x}$, over a prediction horizon, N_P. The objective was then to find the future trend of RM values that resulted in optimal traffic states. The optimal RM values corresponded to the traffic states that resulted in the best performance with the chosen objective function, J, over the entire N_P. The optimization problem was solved in consideration of the constraints on RM values and traffic dynamics. It was assumed that after the control horizon, N_c (which corresponds to the control sampling time index, k_c), the same RM values, $\boldsymbol{r}^*(k+N_c-1)$, remained effective until N_P ($N_P \geq N_c$). However, only the control inputs, $\boldsymbol{r}^*(\mathrm{k,k+1,...,k+N_c\text{-}1|k_c})$, were implemented on the MPC cycle over the control horizon, N_c. After that, in a rolling horizon framework, the prediction and the control horizon were shifted forward one time index, k_c, and the whole process started over again. For the next control sampling time index, k_c+1, the optimal RM values, $\boldsymbol{r}^*(\mathrm{k+N}_c\mathrm{,...,k+N_p\text{-}1})$, which were calculated at k_c but were not implemented, were used as initial guesses for the RM values in the optimization process.

4.2.1 Capacity Estimation

Triangular fundamental diagrams (FDs) (see FIGURE 4.2) were plotted to estimate weaving segment capacity. The FDs were based on flow vs. density scatterplots [93]. First, free-flow capacity ($Q_{\max}$) was estimated by taking the average of the largest five flows across a segment in a simulated period. Second, free-flow speed was determined as the slope in a regression line of points with speed values that were greater than the speed limit. Next, the vertically projected value of the intersection was defined as the critical density, beyond which the traffic state was congested. However, when the bottleneck was activated, actual capacity could be reduced to different levels according to the severity of the bottleneck. Thus, the bottleneck capacity, $Q'_{\max}$, was the flow value at critical density along the least-square regression line of points greater than the critical density. The difference between $Q_{\max}$ and $Q'_{\max}$ was the capacity drop caused by an active bottleneck, which was converted to percentage in this analysis.

4.2.2 *Capacity Sensitivity Analysis*

To identify the sensitivity of capacity to traffic demand, a nominal range sensitivity method was used [94]. In the sensitivity analysis, one traffic parameter was individually varied across its entire range of plausible values, while all of the other parameters were held at their base-case values.

Weaving segment capacity is sensitive to various factors, such as volume ratio, short length, number of weaving lanes and free-flow speed [74, 91]. For RM control, the only parameters that can be considered are the on-ramp and mainline input flows. In the present study, the Origin-Destination (O-D) distribution for each input flow was fixed during the peak periods. Through controlling the on-ramp flows, the volume ratio was adjusted, which may affect weaving segment capacity. Thus, for the sensitivity analysis, the capacity estimation model was developed as a function of traffic demand. The recommended model (Equations (4.1) and (4.2)) contains both capacity and capacity drop estimation; the estimation model is detailed later.

$$Q_{\max} = f\left(r_i, q_{i-1}\right) \tag{4.1}$$

$$Q_d\% = f\left(r_i, q_{i-1}\right) \tag{4.2}$$

where, i is the link index; $Q_{\max}$ is the capacity, in vehicles per hour per lane (vphpl); $Q_d\%$ is the percentage of capacity drop, $\left(Q_{\max} - Q'_{\max}\right) \big/ Q_{\max} \times 100\%$;

r is the on-ramp flow, vehicles per hour (vph); and q is the mainline flow from segment upstream, vph.

4.2.3 Prediction Model

Within the prediction horizon of the MPC framework, the DynaTAM-RM model was developed for traffic flow prediction. Using METANET [14] as the base model, several physical constraints were applied to estimate link boundary flows. The estimated capacity drops were introduced to represent active bottlenecks caused by weaving maneuvers.

To apply the traffic flow model, the freeway corridor was divided into several links ($i = 1, 2, ..., N$) of length, L_i, and lanes, λ_i, as shown in FIGURE 4.3. In the basic METANET model, a freeway section is divided into several links. Each link can be discretized into a number of smaller segments. In the proposed model, each link was considered a segment. The evolutions of traffic speed, $v(k)$ in kilometers per hour (km/h), traffic density, $\rho(k)$ in vehicles per kilometer per lane (vpkpl), and traffic flow, $q(k)$ (vph), at each time instant, t ($t = kT$; T is the discrete time step; and k is the time index present in the calculation), were calculated by Equations (4.3) to (4.7).

Equation (4.3) was adopted from the original METANET model to calculate the speed evolution in a segment. Traffic speed is a summation of four terms, which are traffic speed in the last control horizon, relaxation, convection and anticipation terms, respectively:

$$v_i(k+1) = v_i(k)+\frac{T}{\tau}\{V[\rho_i(k)]\text{-}v_i(k)\} \\ +\frac{T}{L_i}v_i(k)[v_{i\text{-}1}(k)\text{-}v_i(k)]\text{-}\frac{\upsilon T[\rho_{i+1}(k)\text{-}\rho_i(k)]}{\tau L_i[\rho_i(k)+\kappa]} \tag{4.3}$$

The model's global parameters were calibrated from the measured data, where, τ is the reaction term parameter in hours (hr), υ is the anticipation parameter (km2/h); and κ is the positive constant (vpkpl).

In Equation (4.3), $V[\rho_i(k)]$ was calculated as:

$$V[\rho_i(k)] = v_{f,i}\exp\left[-\frac{1}{\alpha_i}\left(\frac{\rho_i(k)}{\rho_{cr,i}}\right)^{\alpha_i}\right] \tag{4.4}$$

where, ρ_{cr} is the critical density (vpkpl); and α is a model parameter that determined the shape of an FD.

The relaxation term ensures that with a lag time, τ, the mean speed, v, is relaxed to the desired speed, $V[\rho_i(k)]$. The selection of the desired speed is critical in reflecting driver behaviors. The convection term ensures that vehicles entering from the upstream segment, i-1, onto the current segment, i, adapt their speed gradually, rather than instantaneously,. The anticipation term dictates how drivers react to upcoming scenarios. If a driver notices a high traffic density in the downstream segment $i+1$, he or she will slow down, while if a driver notices a low traffic density in the downstream segment $i+1$, he or she will speed up. Parameter κ was added to avoid the singularity or sensitivity of the term to the model in low density situations.

The modified density dynamics considered the on-ramp flow (r) and off-ramp flow (s). Several segment-specific constraints with capacity drop were introduced, while the boundary flows were calculated among the successive segments. The boundary flows were inputs to density dynamics (Equation (4.5)). The segment-specific constraints originated from the cell transmission model (CTM) [13], which uses the local demand-supply approach and is a discretized version of the Lighthill, Whitham and Richards (LWR) model. Thus, the following equations were applied:

$$\rho_i(k+1) = \rho_i(k) + \frac{T}{L_i\lambda_i}(q_{i-1}(k) - q_i(k) + r_i(k) - s_i(k)) \tag{4.5}$$

$$q_i(k) = \min\begin{Bmatrix} v_i(k)\rho_i(k)\lambda_i + r_{i+1}(k) - s_{i+1}(k), \\ Q_{\max,i+1}\lambda_{i+1}, \omega_{i+1}\left(\rho_{Jam,i+1} - \rho_{i+1}(k)\right)\lambda_{i+1} \end{Bmatrix} \tag{4.6}$$

where, ω is the shockwave speed, km/h; and ρ_{Jam} is the jam density, vpkpl.

For weaving segments, when a bottleneck was triggered, the actual capacity decreased, which resulted in a capacity drop (see FIGURE 4.2). Thus, that constraint was modified as:

$$q_i(k) = min\begin{Bmatrix} v_i(k)\rho_i(k)\lambda_i + r_{i+1}(k) - s_{i+1}(k), \\ Q'_{\max,i+1}\lambda_{i+1}, \omega'_{i+1}\left(\rho'_{Jam,i+1} - \rho_{i+1}(k)\right)\lambda_{i+1} \end{Bmatrix} \tag{4.7}$$

where, $\omega'\left(\rho'_{Jam} - \rho(k)\right) = \frac{\rho'_{Jam} - \rho(k)}{\rho'_{Jam} - \rho_{cr}(k)}Q'_{\max}$; ω' is the shockwave speed related to FDs with capacity drop, km/h; $Q'_{\max} = Q_{\max}\left(1 - Q_d\%\right)$; and $\rho_{cr}(k) = \frac{Q_{\max}}{v_f}$.

The proposed methodology also included two inequality constraints: 1) Equation (4.8) enables an applicable flow rate lower than the difference between the mainline capacity and current flow rate; and 2) Equation (4.9) considers the limited storage space to avoid spillback from on-ramps to surface streets. Equation (4.10) models on-ramp queue length.

$$q_{i-1}(k)+r_i(k)\leq Q_{\max,i} \tag{4.8}$$

$$r_i(k)\geq r_{\max,i}(k) \text{ (when } w_{o,i}(k)>95\%w_{cap}) \tag{4.9}$$

$$w_{o,i}(k+1)=w_{o,i}(k)+T\left(d_o(k)-r_{m,i}(k)\right) \tag{4.10}$$

4.2.4 Objective Function

The objective function in the control framework is a weighted summation of total travel time (TTT) and total travel distance (TTD) on the mainline, as well as the total waiting time (TWT) on ramps. This optimization problem simultaneously balances traffic mobility, infrastructure utility and the temporal equity of mainline and on-ramp vehicles. Thus, the optimization is a challenge of finding an optimal control value to achieve the minimum value of the objective function, J (Equation (4.11)), over a prediction horizon, N_P. The weighting factors (α_{TTT}, α_{TWT} and α_{TTD}) were selected in simulation. The nonlinear optimization problem was solved by SQP using iterative comparisons of model behavior to measured traffic data.

$$J=T\sum_{j=1}^{N_p-1}\sum_{i=1}^{N}\begin{Bmatrix}\alpha_{TTT}\lambda_i L_i\rho_i(k+j)+\alpha_{TWT}w_{0,i}(k+j)\\ -\alpha_{TTD}\lambda_i L_i\rho_i(k+j)v_i(k+j)\end{Bmatrix} \tag{4.11}$$

4.3 Model Calibration and Validation

4.3.1 Study Site

To carry out and evaluate the proposed RM control algorithm, the westbound direction of Whitemud Drive (WMD) (between 122 St. and 159 St.), an urban freeway in Edmonton, Canada, was simulated (as shown in FIGURE 4.4). To implement the prediction model, WMD was divided into 13 segments. WMD has six on-ramps, six off-ramps and three weaving segments: Segments 3, 7 and 11. Due to the high proportion of lane-changing behaviors, recurrent bottlenecks are often triggered along WMD at Segments 3 and 7. The following analysis will take Segment 3 as an example.

Flow on each segment was measured as the average value of loop counts from merging and diverging areas, speed was estimated as space mean speed and density was determined from the fundamental relationship of traffic variables, $q = \rho v$. In addition, based on the HCM 2010 definitions, the short length (L_s) of Segment 3 is 0.821 km, and three lanes are used by weaving vehicles. The studied area is classified as a two-sided weaving segment with a right-hand on-ramp onto WMD from 122 St. followed by a left-hand off-ramp from WMD onto Terwillegar Drive. Only the ramp-to-ramp flow was considered weaving, whereas the through movement was not, because through vehicles do not need to change lanes, and generally do not shift lane position in response to a desired exit leg.

4.3.2 Prediction Model Calibration and Validation

To prepare the data for DynaTAM-RM calibration, a micro-simulation model (VISSIM v5.4) was used during evening peak hours (t=4:00-6:30 PM). There were 5 model construction steps: 1) identification of important geometric features (number of lanes on the mainline, on-ramps and off-ramps of freeway, etc.); 2) traffic data collection and processing; 3) analysis of the mainline data to identify bottlenecks; 4) VISSIM network model coding; and 5) model calibration based on the observations from step 3 [95]. The field data, used as inputs to calibrate the VISSIM model, was compiled from two separate sources: loop detectors deployed on the mainline and video recordings of the studied on-ramps and off-ramps. The micro-simulation model was run 10 times with random seed numbers; simulation data was taken at 20-second (s) intervals and then averaged. Several parameters were calibrated: $Q_{\max}$ (or $Q'_{\max}$); v_f; ω (or ω'); ρ_{cr}; and ρ_{Jam}. The segment-specific parameters were extracted from the FDs. Segments 3 and 5 were chosen to show the calibration and validation results for bottleneck (weaving) segments and non-bottleneck segments, respectively. Thus, the FDs for Segments 3 and 5 are exhibited in FIGURE 4.5. These traffic parameters have been used in the constraints of Equation (4.6) to Equation (4.8).

ALINEA with queue control [25] was implemented on each on-ramp to collect traffic data for calibrating the global parameters [τ, υ, κ] of the speed equation (Equation (4.3)) for the control scenario. Traffic flow, speed and occupancy measurements taken at 20-s intervals were collected from detectors deployed on each segment. To optimize the global parameters, Equation (4.12) was applied to minimize the prediction errors by the SQP algorithm. For the proposed DynaTAM-RM with dynamic weaving capacity, the optimal value of

$f(\beta)$ was found to be 895.7 with the optimal global parameters of [0.028, 78.5, 180.0].

$$f(\beta)=\sqrt{\sum_{i=1}^{M}\sum_{k=1}^{K}\left[\left(\rho_i^m(k)-\rho_i\left(k|\beta\right)\right)^2-\gamma\left(v_i^m(k)-v_i\left(k|\beta\right)\right)^2\right]} \quad (4.12)$$

where, γ=0.8, and K=360

During model validation, three initial and boundary conditions were taken: 1) initial flow, density, and speed for all of the segments were taken as the measured values for the first time step only; 2) boundary flow, density and speed were taken as the measured values for all the time steps at Segments 1 and 13; and 3) ramp flows were assumed known and were directly used in Equation (4.5). The match between the measurements from the micro-simulation and the DynaTAM-RM simulation in the control situation for a typical segment is shown in FIGURE 4.6. Flow and density estimations from DynaTAM-RM are well matched with the observations, while speed estimation is reasonably matched. Similar findings were obtained for all of the other segments. Therefore, for the peak-hour simulation, DynaTAM-RM accurately and satisfactorily provided a replication of traffic flow under RM control.

4.4 Results and Analysis

4.4.1 Capacity Sensitivity

Through the calibrated micro-simulation model, on-ramp or mainline demand was individually varied across a range of plausible values, and all other traffic parameters were held at their base-case values. On-ramp demand ranged from

500-2000 vph, while mainline demand varied from 3500-5000 vph. Both varied at an interval of 100 vph. Each case was simulated 10 times with random seed numbers and results were averaged for analysis. Simulation results are summarized in FIGURE 4.7. As on-ramp or mainline demand increased, the capacity fluctuated in a small range without obvious trends, indicating that with fixed driver behavior parameters, the growing number of conflicts between weaving and non-weaving vehicles has little impact on capacity. As defined in the HCM 2010, weaving flow is only the ramp-to-ramp movement on the studied two-sided weaving segment. The variation in volume ratio ranges from 0.022-0.066 by changing the input flows separately within the defined ranges; when this is applied in the HCM 2010 capacity estimation method, the difference in capacity is only 32 vphpl. The present sensitivity results for capacity are in accordance with those from the HCM 2010.

Weaving impacts caused by increased demand was notable under congestion. FIGURE 4.7 (b) illustrates that the amount of capacity drop (%) increased with demand. A higher demand generated higher and more frequent interferences between weaving and non-weaving flow; thus, less flow was discharged under congestion. As shown in FIGURE 4.7 (b), only capacity drop was sensitive to the change in on-ramp and mainline demand. The proposed model (Equation (4.13) and FIGURE 4.7 (c)) results show that the R^2 value and the standard error (SE) were statistically significant. To predict dynamic weaving capacity, boundary flow estimations were also included in the DynaTAM-RM, q.

$$Q_d\% = 102.82\text{-}16.48\left(\frac{r_i}{1000}\right) + 9.33\left(\frac{r_i}{1000}\right)^2$$
$$\text{-}47.53\left(\frac{q_{i-1}}{1000}\right) + 6.33\left(\frac{q_{i-1}}{1000}\right)^2 \tag{4.13}$$
$$R^2 = 0.87051 \qquad SE = 1.42\%$$

where, $Q_d\%$ is the capacity drop; $\left(Q_{\max} \text{-} Q'_{\max}\right) / Q_{\max} \times 100\%$; r_i is the on-ramp flow, vph; and q_{i-1} is the mainline flow from segment upstream, vph.

4.4.2 Evaluation Scenarios

To test the proposed RM algorithm, three cases were compared: 1) a no-control case; 2) a control case that applied DynaTAM-RM with static weaving capacity; and 3) a control case that applied DynaTAM-RM with dynamic weaving capacity.

- ***No-Control Case***

In the no-control case, traffic state data for each 20-s interval was obtained from the original METANET model, which was considered the substitute for a real-world traffic scenario. The optimal global parameters [τ , υ , κ] in METANET were 0.023, 331.6, and 80.5, respectively. Currently, RM control is not implemented along WMD, on which the static speed limit is 80 km/h. The demand profiles for the mainline and on-ramps are plotted in FIGURE 4.8. The simulation was conducted in MATLAB software over a two-hour high-demand period and a 30-minute queue clear-up period. The first five minutes were considered a “warm-up.” Traffic data from the warm-up period and low demand period was excluded when evaluating the performance of the proposed RM algorithm.

- ***DynaTAM-RM with Static Weaving Capacity***

This case evaluated the control performance of DynaTAM-RM with static weaving capacity to show the direct impact of using dynamic weaving capacity while controlling ramp flows on the weaving segment. The calibrated segment-specific parameters [v_f , ρ_{cr} , $Q_{\max}$] were also adopted in the model to simulate flows. The global parameters [τ , υ , κ] were optimized at 0.007, 28.9, and 54.6, respectively. With the given demand inputs for mainline and on-ramps, the optimization problem was solved by SQP. In addition, the value for α_{TTD} of the objective function in MPC was set at 1. The values for α_{TTT} and α_{TWT} were related to mainline and on-ramp speed; both were set at 56 in simulation. The macro-simulation archived speed, flow and density of the 13 study segments at each 20-s interval. This data was used to calculate the selected MOEs of the proposed RM control. The achieved traffic state under this scenario is presented in TABLE 4. and TABLE 4.2.

- ***DynaTAM-RM with Dynamic Weaving Capacity***

This scenario deployed the proposed RM algorithm. As mentioned, the segment-specific parameters [v_f , ρ_{cr} , $Q_{\max}$] in DynaTAM-RM were calibrated for all of the segments; however, for the weaving segments, due to bottleneck activation, weaving capacity $Q'_{\max}$ was estimated according to

Equation (4.13). The weaving capacity was dynamically updated and applied in the control algorithm every 20 s. All other factors were the same as those in DynaTAM-RM with static weaving capacity.

4.4.3 Application Results and Analysis

Coordinated RM control optimizes the infrastructure utility on an entire traffic network, rather than just on an individual segment. The entire network performance is shown in FIGURE 4.9, which displays the density evolutions for all scenarios. Because of uncontrolled entrances into the mainline, two instances of congestion were caused along the studied corridor (FIGURE 4.9 (a)). One occurred shortly after demand increased at Segment 3, on which there are frequent weaving maneuvers. The other occurred at Segment 7 and propagated upstream during the PM peak hours. Compared with the no-control case, both applications of DynaTAM-RM result in improved traffic conditions (FIGURE 4.9 (b) and FIGURE 4.9 (c)). In the control cases, the density profiles are flatter than the no-control case, especially at weaving segments.

FIGURE 4.10 displays the evolutions of TTT, TWT and TTD, while TABLE 4.2 lists those results. For the no-control case, TTT stayed high during the first hour. After the first hour, TTT increased as the corridor became more congested, and travel time by each vehicle increased. The on-ramp demand decreased after one and a half hours of simulation, and then TTT declined. No ramps were metered in this case, so TWT remained 0 throughout the simulation. However, TTD slightly varied when on-ramp demand dropped.

In contrast, the network performance was improved by ramp meters. In the first ten minutes, only the on-ramps were metered as the demand was relatively low; therefore, the performance was nearly the same as in the no-control case. When the demand gradually increased, DynaTAM-RM applied RM rates from high to low. Because of its prediction module, DynaTAM-RM is capable of forecasting traffic states in the near future and applying corresponding control variables. After metering rates were applied at on-ramps, TTT and TTD increased as a result of increasing flow from the mainstream. The time consuming by stopped vehicles on ramps increased TWT.

After one hour of high demand, the corridor was congested and the queue of waiting vehicles behind the on-ramps continuously grew. The RMs were turned to a high rate to lessen the time spent in queue and to stop queued vehicles from spilling onto the surrounding surface streets. Notable drops occurred in TTT and TTD as the number of discharged vehicles decreased. TWT stayed high until on-ramp demand decreased at 5:30 PM. In the last 30 minutes, TTT, TWT and TTD in the control scenarios fluctuated before the mainline demand decreased.

Compared with the DynaTAM-RM with static weaving capacity, DynaTAM-RM with dynamic weaving capacity experienced improved travel time on ramps when mainline demand was high: when the proposed algorithm predicted bottleneck activation, the on-going ramp meter rates were lowered to ensure that the traffic flow did not reach weaving capacity. As the bottleneck warning was lifted, the model reset capacity and discharged more vehicles from the on-ramps; the static weaving capacity case cannot accommodate these capacity variations. Therefore, based on real-time weaving capacity estimation, DynaTAM-RM with dynamic weaving capacity outperforms that with static weaving capacity.

DynaTAM-RM with dynamic weaving capacity achieved TTT, TTD, and total flow (TF) amelioration; the amelioration amounted to -9.71%, 3.32%, and 8.40%, respectively (see TABLE 4.2). These improvements were higher than those made by DynaTAM-RM with static weaving capacity. Based on these MOE criteria, there are obvious benefits to applying dynamic weaving capacity estimation: mitigating bottleneck severity increased traffic mobility over the entire network.

4.5 Summary

Recurrent bottlenecks triggered by weaving maneuvers limit discharge flow at weaving segments and reduce traffic mobility on freeways. A severe bottleneck causes a major capacity drop. In the present research, a METANET-based traffic flow model, DynaTAM-RM, was proposed, which was considerate of dynamic weaving impacts. DynaTAM-RM was used within an MPC framework. DynaTAM-RM, providing real-time estimated weaving capacity, was evaluated and analyzed on the WMD test bed.

There are four major findings of this study: 1) weaving segment capacity drop was observed at bottleneck activation, which reveals the necessity of considering weaving capacity; 2) according to the weaving capacity estimation model and its sensitivity analysis, the proposed RM control is a promising congestion mitigation method; 3) the RM control variables were optimized in MPC by DynaTAM-RM considering dynamic weaving capacity; and 4) DynaTAM-RM with dynamic weaving capacity was simulated, evaluated and shown to be effective: the model provided a 9.71% decrease in TTT, a 3.32% increase in TTD and an 8.40% increase in TF, all of which were better improvements than those made with a static weaving capacity.

TABLE 4.1. Comparative Results for the Weaving Segment

Performance Criteria	Scenarios	No Control	DynaTAM-RM with Static Weaving Capacity	DynaTAM-RM with Dynamic Weaving Capacity
Mean Speed (kph)	Value	37.76	73.99	78.55
	%Change	-	95.95%	108.02%
Mean Density ($vpkpl$)	Value	29.9	17.82	18.06
	%Change	-	-40.40%	-39.60%
Congestion Duration (min)	Value	317	91	49
	%Change	-	-71.29%	-84.54%

TABLE 4.2. Comparative Results for the Corridor

Performance Criteria	Scenarios	No Control	DynaTAM-RM with Static Weaving Capacity	DynaTAM-RM with Dynamic Weaving Capacity
TTT ($veh \cdot h$)	Value	1008.2	910.3	896.5
	%Change	-	-9.71%	-11.08%
TWT ($veh \cdot h$)	Value	0	8.24	9.76
TTS ($veh \cdot h$)	Value	1008.2	918.54	906.26
	%Change	-	-8.89%	-10.11%
TTD ($veh \cdot km$)	Value	67244	69477	70451
	%Change	-	3.32%	4.77%
TF (veh)	Value	3808	4128	4234
	%Change	-	8.40%	11.19%

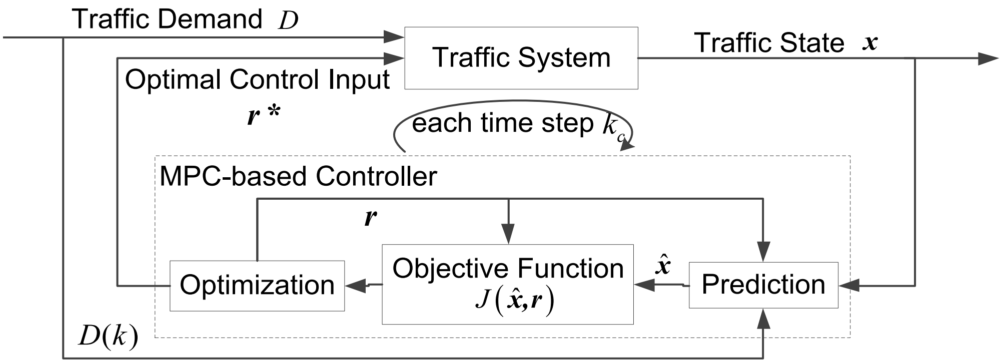

FIGURE 4.1. Proposed RM Control Framework.

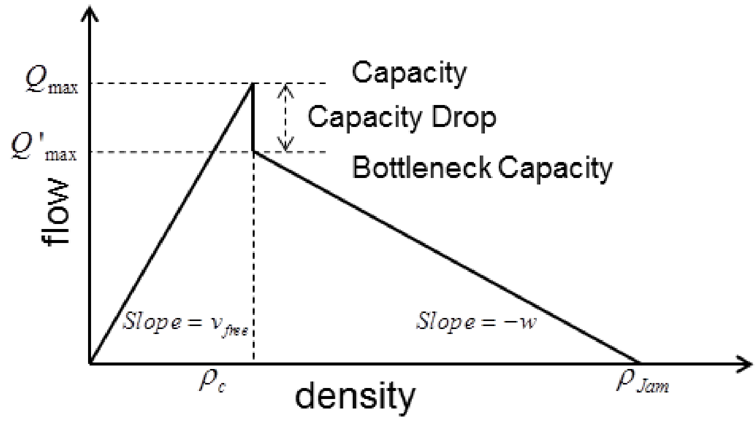

(a) With Capacity Drop

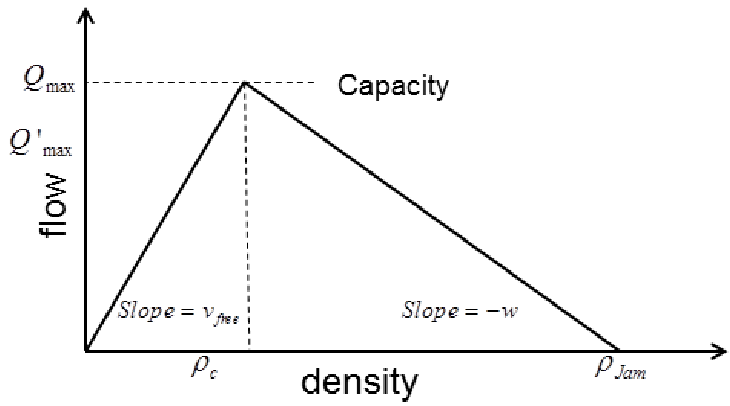

(b) Without Capacity Drop

FIGURE 4.2. Triangular FDs.

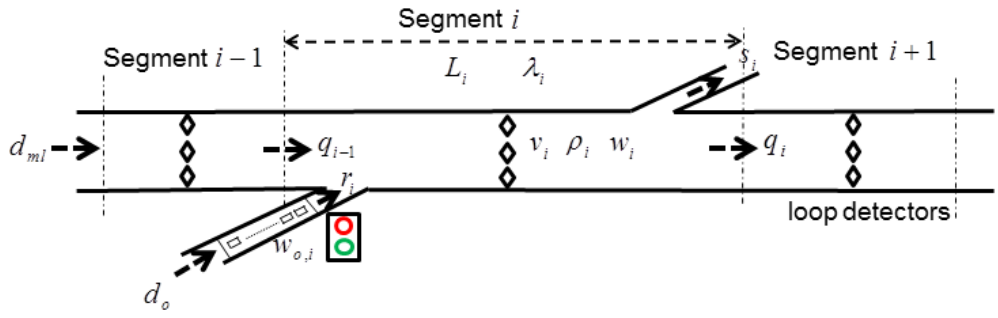

FIGURE 4.3. Segmentation of Freeway Segments.

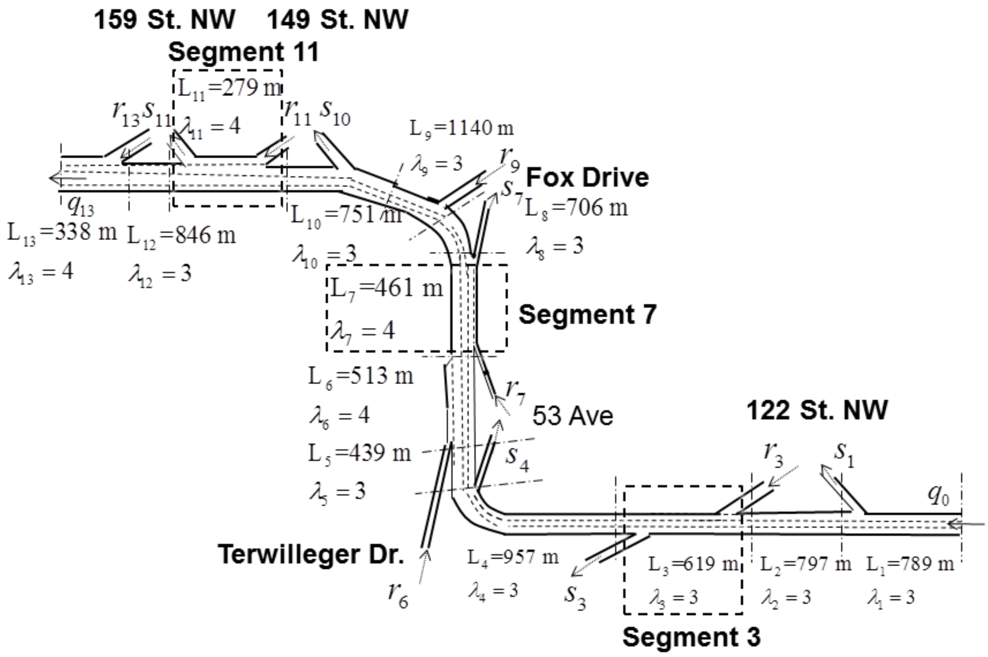

FIGURE 4.4. Studied Network.

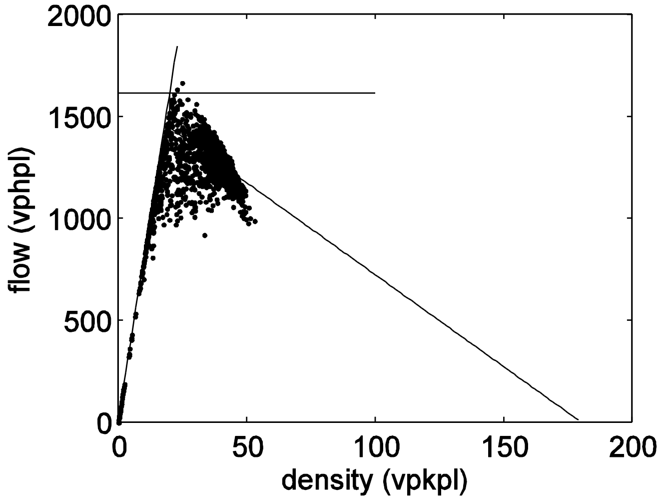

(a) Segment 3

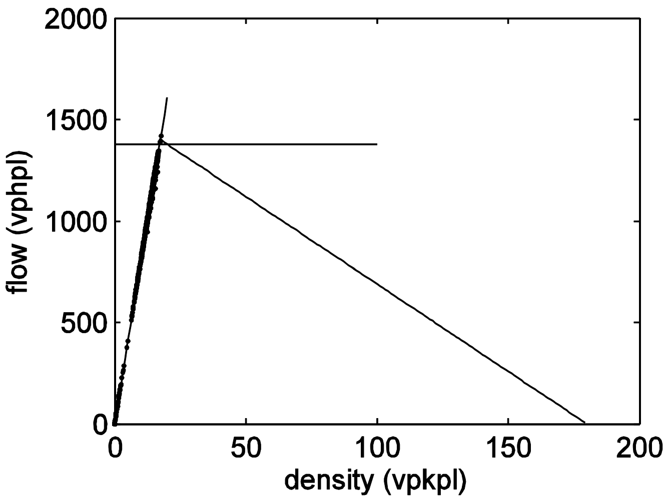

(b) Segment 5

FIGURE 4.5. Segment Specific FDs.

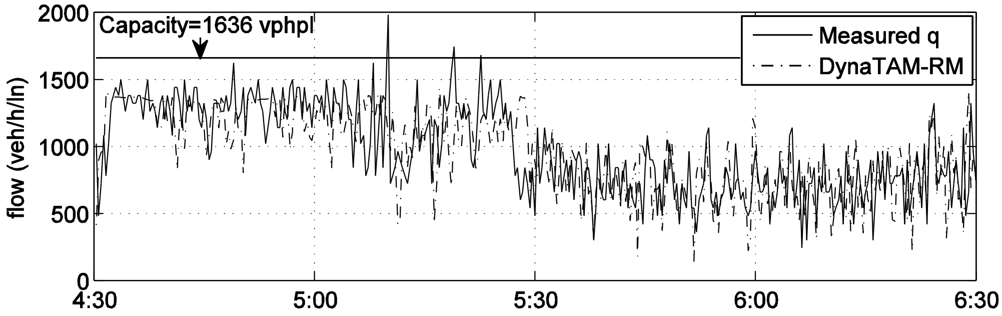

(a) Flow in Segment 3

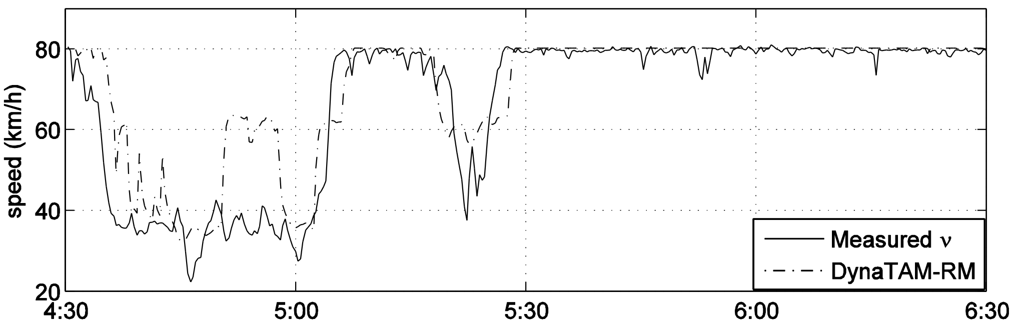

(b) Speed in Segment 3

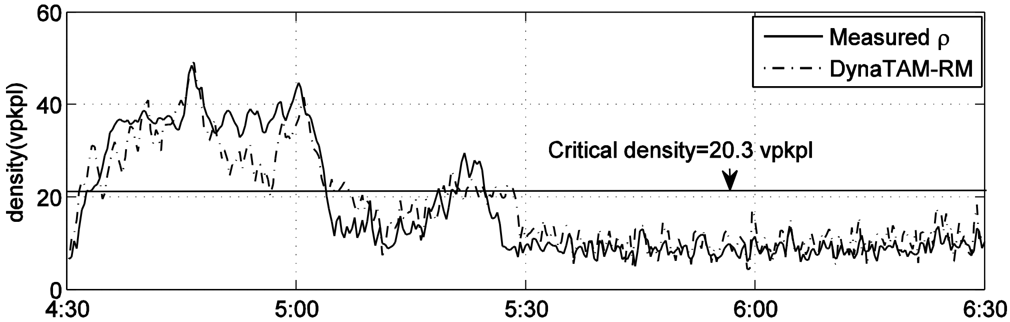

(c) Density in Segment 3

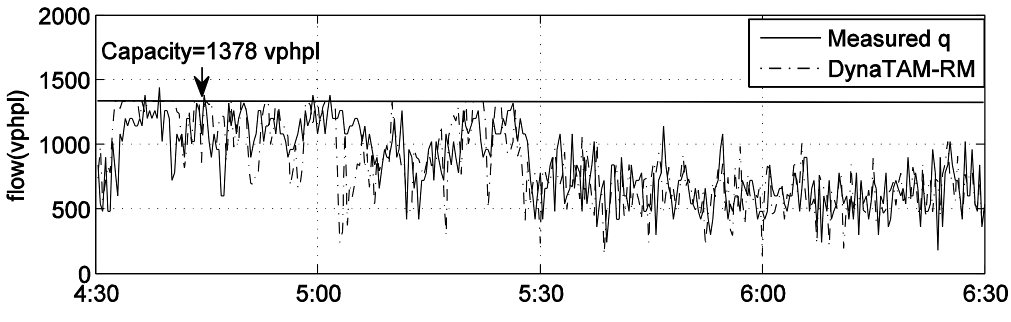

(d) Flow in Segment 5

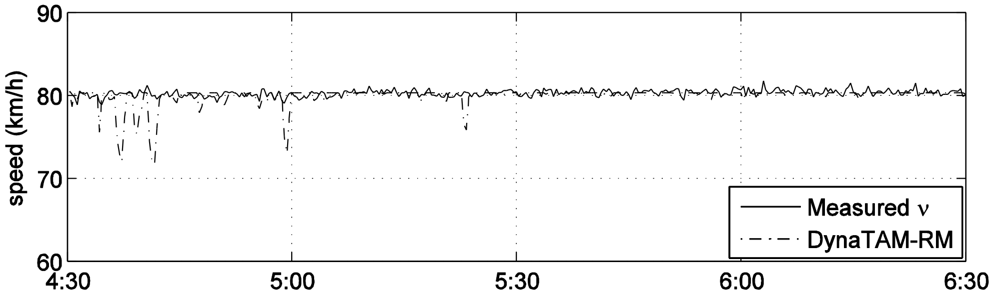

(e) Speed in Segment 5

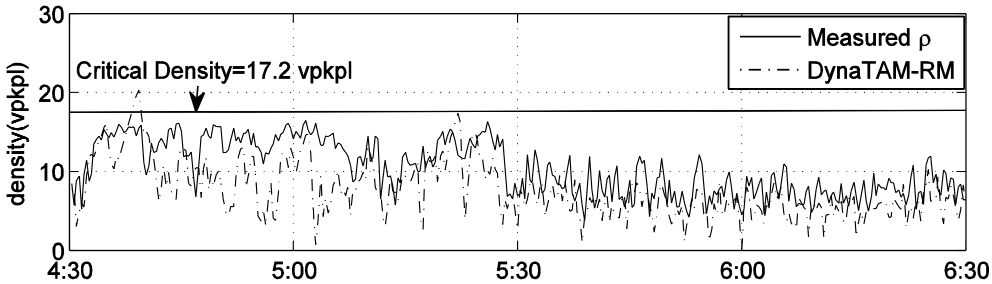

(f) Density in Segment 5

FIGURE 4.6. Comparisons between Measurements and DynaTAM-RM Simulation.

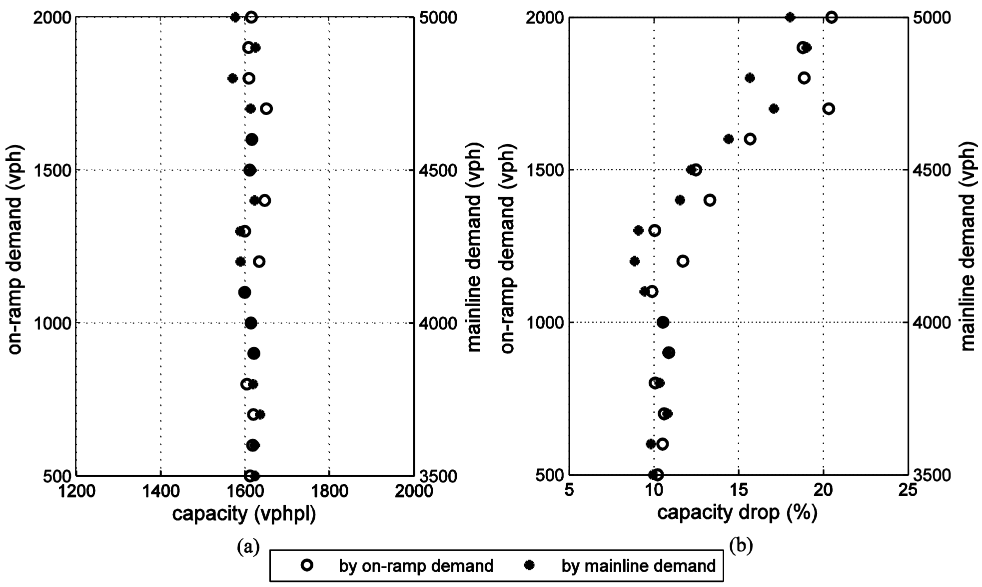

(a)

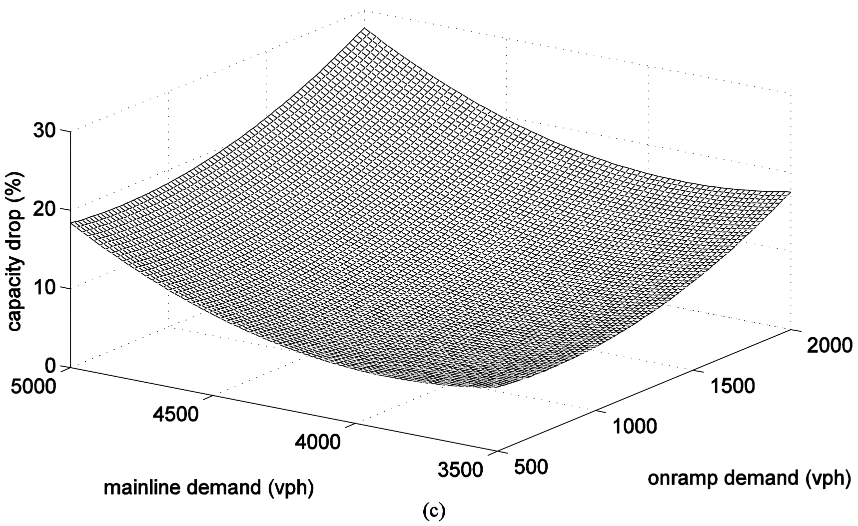

(b)

FIGURE 4.7. Capacity Sensitivity Analysis Results.

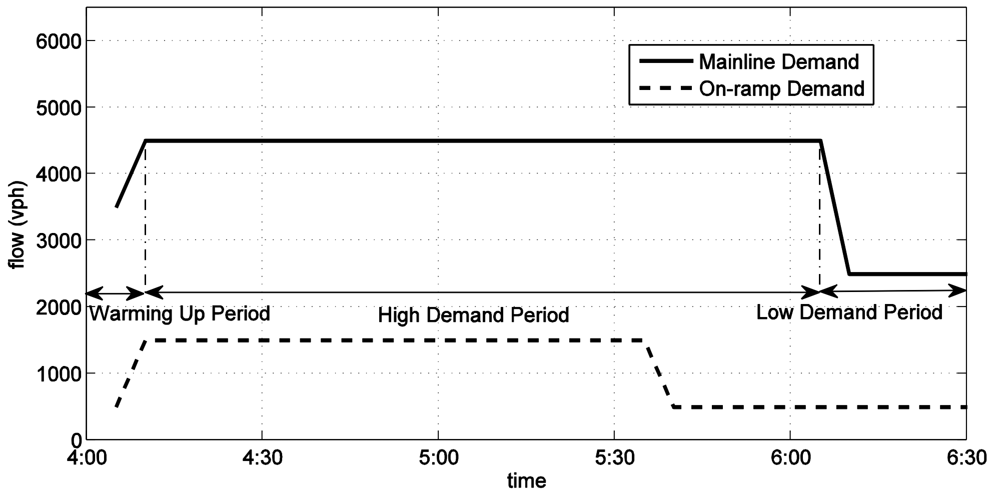

FIGURE 4.8. Demand Profile for Mainline and On-ramp.

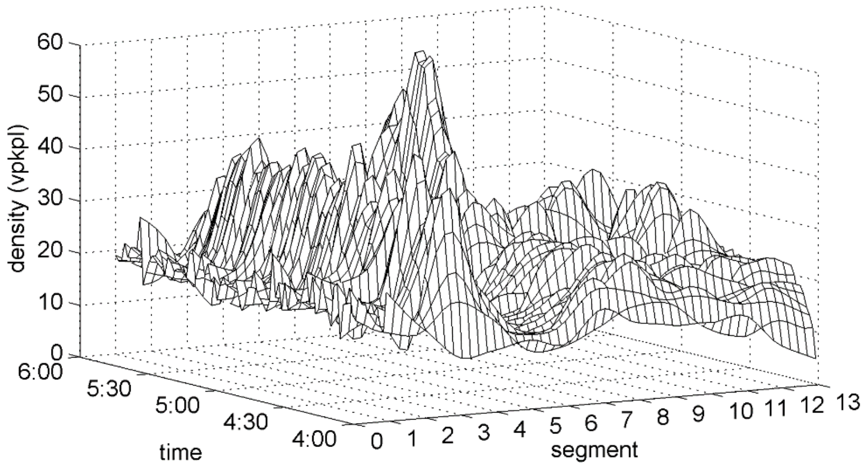

(a) No Control

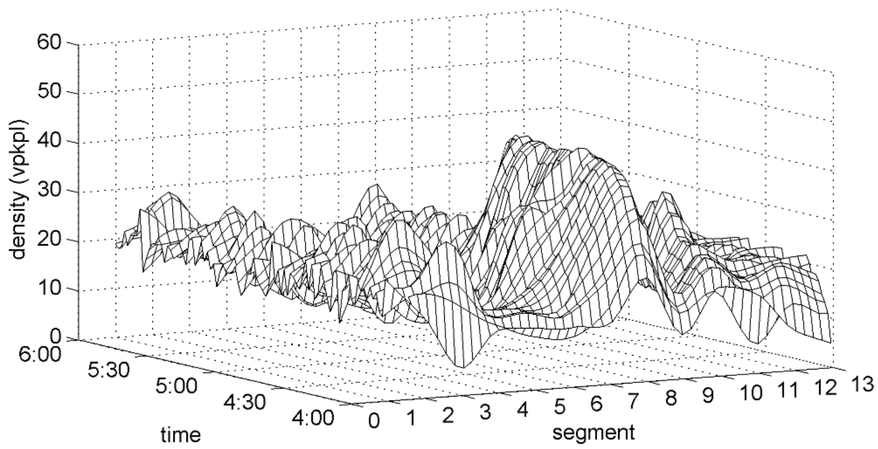

(b) DynaTAM-RM with Static Weaving Capacity

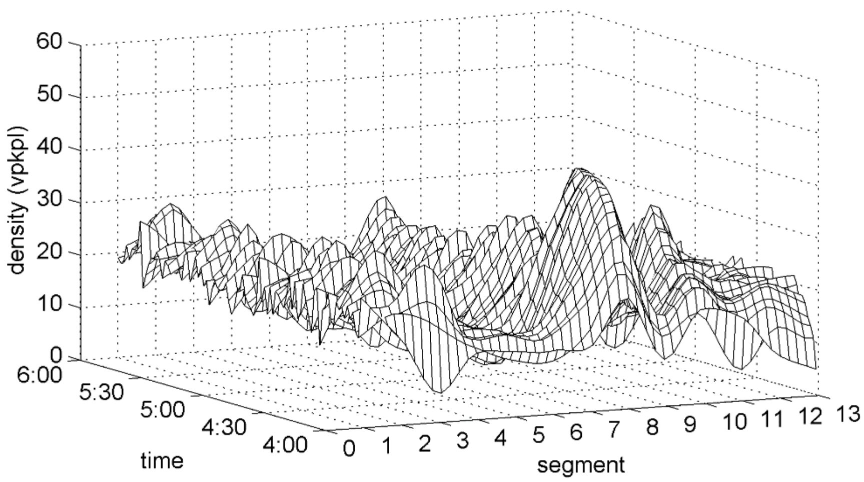

(c) DynaTAM-RM with Dynamic Weaving Capacity Estimation

FIGURE 4.9. Density Profile for Each Scenario.

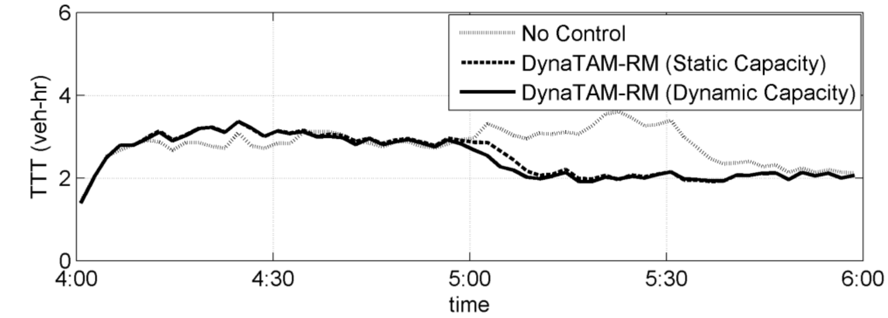

(a) TTT

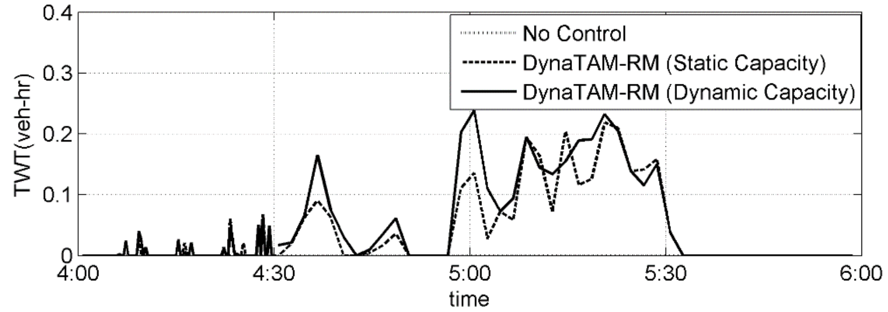

(b) TWT

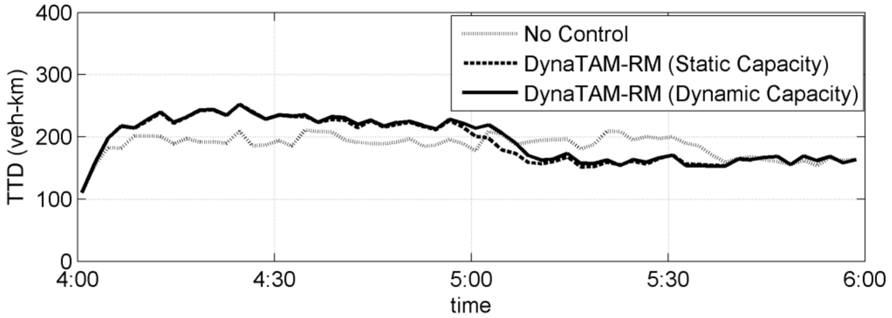

(c) TTD

FIGURE 4.10. Network TTT, TWT and TTD Profiles.

CHAPTER 5. CAPACITY ESTIMATION FOR WEAVING SEGMENTS USING A LANE CHANGING MODEL[2]

5.1 BACKGROUND

During peak periods, freeway bottlenecks can be activated by intensive lane changing at weaving segments, where merging and diverging areas are in close proximity. This weaving phenomenon has a major impact on capacity. Much research has been devoted to investigate capacity estimation models for weaving segments. However, due to the model parameters, they are difficult to directly adopt in active traffic management strategies to estimate real-time maximum discharge flow. To this end, this research defined a linear optimization problem to solve weaving capacity and then established a lane-changing model to constrain the weaving flows. The proposed method was evaluated and analyzed for sensitivity with field data from two weaving segments on the Whitemud Drive, Edmonton, Alberta, Canada. The capacity estimates from the proposed model were consistent with that from the HCM 2010 model and with field observations. Moreover, it was also observed that the weaving capacity is sensitive to weaving maneuvers. Finally, the proposed method was applied to

[2] A version of this chapter has been published. Xu Wang, Ying Luo, Tony Z. Qiu, and Xinping Yan (2014). Capacity Estimation for Weaving Segments Using a Lane Changing Model. Transportation Research Record: Journal of Transportation Research Board, 2461, pp. 94-102.

estimate the real-time maximum discharge flow rate; the estimates matched field measurements.

There are four objectives of this chapter: 1) develop a capacity estimation method using a lane changing model and linear optimization, which is potentially applicable for traffic operation; 2) evaluate the proposed capacity estimation method in two configurations of weaving segments; 3) investigate sensitivity and correlation between weaving capacity and flow proportions; and 4) estimate real-time maximum discharge flow rate in peak hours. The remainder of this chapter is organized into sections: Section 5.2 details the method in this work, including the linear optimization problem and the lane changing model; and Section 5.3 is devoted to analyzing the capacity estimates, as well as capacity sensitivity and estimating the real-time maximum discharge flow.

5.2 Proposed Capacity Estimation Methods

This part introduces the procedure and flowchart of the proposed capacity estimation method. This method is composed of two parts: 1) a linear optimization problem modified from the work by Lertworawanich and Elefteriadou [70, 75]; and 2) a lane changing model developed by Laval and Daganzo [76, 77], namely the multilane hybrid (MH) model. The linear optimization problem is constrained by the maximum lane changing number from the MH model, and the basic capacity of freeway and ramps.

5.2.1 Capacity Estimation Procedure

As mentioned above, capacity on a freeway weaving segment is a function of numerous factors. Among these factors, a weaving segment features the four types of traffic movements categorized by different O-D, including freeway-to-freeway, freeway-to-ramp, ramp-to-freeway, and ramp-to-ramp. In these four movements, weaving maneuvers contribute to the capacity difference between basic freeway capacity and weaving capacity (as shown in FIGURE 5.1). Basic freeway capacity means the capacity under normal driving behaviors with no weaving maneuvers. In other words, the weaving ratio is zero, which achieves the highest capacity, the basic freeway capacity. Once the weaving ratio is greater than zero, the capacity reduces to the "weaving capacity". The basic freeway capacity is the normal capacity of the equivalent freeway segment as defined in Lertworawanich and Elefteriadou [70, 75]. The difference between basic freeway capacity and weaving capacity is brought by weaving maneuvers (i.e. lane changing behaviors). In short, lane changing behaviors by weaving vehicles influence capacity.

Previous studies indicated that the highest concentration of flow and rate of lane changing occur in a "critical region". Within the critical region, a function of vehicle flows and lane changing rates can be defined as the weaving capacity [96]. Based on this definition, this study applies a four-step procedure to estimate weaving capacity (see FIGURE 5.2). First, basic geometry and traffic information is needed to determine configuration characteristics of a segment. With these configuration characteristics, the maximum length of a weaving segment ($L_{\max}$) is computed referring to HCM 2010. As defined in HCM 2010, volume ratio (VR) is the ratio of weaving flow rate over total flow rate at a weaving segment, and N_{WL} is the number of lanes from which a weaving maneuver may be made with one or no lane changes. Then, only the segment whose length (L_s) is less than $L_{\max}$ is regarded as a weaving segment. Second, the region with the highest concentration of lane changes is selected as a critical region within the weaving segment. Meanwhile, the traffic data requires further reduction to determine the weaving and non-weaving flow rate. Next, for each lane that is involved in the weaving maneuvers, its critical density is applied in the MH model. The results obtained from the MH model are the maximum lane changes that weaving vehicles can actually make. With all the information in hand, the capacity estimation problem is established as a linear optimization problem by applying the aforementioned definition of capacity, while weaving capacity is solved with several constraints for traffic movements.

5.2.2 Capacity Estimation Model

Weaving is the crossing of two or more traffic streams traveling in the same general direction. FIGURE 5.3 presents two configurations of weaving segments, along with the symbols used to describe traffic streams. To apply the proposed model, the studied freeway corridor is divided into several segments (i =1, 2,..., M). As defined in HCM 2010, one-sided and two-sided weaving segments differ in number of mandatory lane changes required to complete the weaving maneuvers.

In this research, the capacity of ramp weaves is assumed to be the summation of the traffic flows for the four movements over number of lanes. Thus, the weaving capacity can be mathematically expressed as Equation (5.1). In addition, several constraints (Equation (5.2)-(5.4)) are also employed. Equation (5.2) and Equation (5.4) are to limit the flow of traffic movements from exceeding the equivalent basic freeway and ramp capacity. The constraints for weaving flows ($\max\left(q_{RR}\right)$, or $\max\left(q_{FR}\right)$ and $\max\left(q_{RF}\right)$) are capacity for weaving movements, which are computed based on the MH model.

Previous research revealed that weaving capacity is highly dependent on the proportion of weaving flow [70, 74, 96-98]. Weaving flows from each origin must keep their ratios in demand. Thus W_1 and W_2 in Equation (5.3) are defined. Having formulated all the constraints, the capacity at a weaving segment can be easily estimated by using a linear optimization technique.

$$c_W = \max\left(q_{FF} + q_{FR} + q_{RF} + q_{RR}\right) / N_{F,i} \tag{5.1}$$

$$\begin{aligned}
q_{FF} + q_{FR} + q_{RF} + q_{RR} &\le c_{BF} \times N_{F,i} \\
q_{FF} + q_{RF} &\le c_{BF} \times N_{F,i+1} \\
q_{FR} + q_{RR} &\le c_{BR} \times N_{OFR,i} \\
q_{FF} + q_{FR} &\le c_{BF} \times N_{F,\mathrm{i}-1} \\
q_{RF} + q_{RR} &\le c_{BR} \times N_{ONR,\mathrm{i}}
\end{aligned} \tag{5.2}$$

$$\begin{aligned}
\frac{q_{FF}}{q_{FF} + q_{FR}} &= W_1 = \frac{D_{FF}}{D_{FF} + D_{FR}} \\
\frac{q_{RR}}{q_{RF} + q_{RR}} &= W_2 = \frac{D_{RR}}{D_{RF} + D_{RR}}
\end{aligned} \tag{5.3}$$

$$
\begin{aligned}
&0 \le q_{FF} \le c_{BF} \times N_{F,i} \\
&0 \le q_{FR} \le \min\left(c_{BF}, c_{BR}\right) \times N_{OFR,\mathrm{i}} \\
&0 \le q_{RF} \le \min\left(c_{BF}, c_{BR}\right) \times N_{ONR,\mathrm{i}} \\
&0 \le q_{RR} \le \max\left(q_{RR}\right) \quad \text{(two-sided)} \\
&or \\
&0 \le q_{FF} \le c_{BF} \times N_{F,i} \\
&0 \le q_{FR} \le \max\left(q_{FR}\right) \\
&0 \le q_{RF} \le \max\left(q_{RF}\right) \\
&0 \le q_{RR} \le c_{BR} \times \min\left(N_{ONR,i}, N_{OFR,i}\right) \quad \text{(one-sided)}
\end{aligned} \tag{5.4}
$$

where, c_{BF} is the basic freeway capacity; c_{BR} is the basic ramp capacity; N_F is the number of lanes on freeway; N_{ONR} is the number of lanes on on-ramps; and N_{OFR} is the number of lanes on off-ramps.

5.2.3 Multilane Hybrid Model

Modeling the whole process of lane changing requires compatibility to deal with random human maneuvers. Throughout the literature, lane changing models have three components: 1) lane changing inducement mechanism; 2) generation of a spatial-temporal inserting point; and 3) the behaviors following lane changing.

The inducement mechanism falls into two categories: mandatory and discretionary [99]. This study assumes that lane changes in weaving segments are mandatory. In other words, lane changes are required before or at diverging segments, otherwise a vehicle needs to decelerate or stop for an acceptable lane changing gap. Moreover, similar to methods in [76, 100], a new term was introduced in the lane changing model, τ_{LC}, which is the actual time for a vehicle to change its lane. The net lane changing rate from lane l to lane l'

at time step i is computed as Equations (5.5)-(5.6), which were evaluated in previous studies [76, 77].

$$\Phi\left(\rho_l^{x,i}, \rho_{l'}^{x,i}\right) = \min\left\{1, \frac{\mu\left(\rho_{l'}^{x,i}\right)}{\lambda\left(\rho_{l'}^{x,i}\right)}\right\} \frac{\pi\left(\rho_l^{x,i}, \rho_{l'}^{x,i}\right)\lambda\left(\rho_l^{x,i}\right)W_l}{v_{f,l}} \tag{5.5}$$

where, $\rho_l^{x,i}$ and $\rho_{l'}^{x,i}$ are density on lane l and lane l' respectively; λ is the demand (sending) function: $\lambda\left(\rho_{l'}^{x,i}\right) = \min\left\{v_{f,l'}\rho_{l'}^{x,i}, c_{l'}^{i}\right\}$; μ is the supply (receiving) function: $\mu\left(\rho_{l'}^{x,i}\right) = \min\left\{\left(\rho_{Jam,l'} - \rho_{l'}^{x,i}\right)\omega_{l'}, c_{l'}^{i}\right\}$; W is the ratio of weaving vehicles, which can be expressed by W_1 and W_2 in terms of segment configuration; and π is a fraction of decision-makers per unit time wishing to change from l to l'. Lane changes for weaving maneuvers are assumed to be mandatory; thus, Equation (5.6) is applied,

$$\pi\left(\rho_l^{x,i}, \rho_{l'}^{x,i}\right) = \frac{1}{\tau_{ll',LC}} \tag{5.6}$$

When this model is implemented, a critical region where most weaving vehicles make lane changes is selected as the lane changing generation point. The required inputs for modeling mandatory lane changing is the lane-specific traffic state data for each lane changing generation point, i.e. $\rho_l^{x,i}$ and $\rho_{l'}^{x,i}$. The other parameters (free-flow speed v_f, capacity c, jam density ρ_{Jam}, and shockwave speed ω) are calibrated from the macroscopic fundamental diagrams.

5.3 Capacity Estimation Results

5.3.1 Study Site and Data Collection

To carry out and evaluate the proposed capacity estimation method, two weaving segments from WMD were studied (FIGURE 5.4). These two segments are classified as a two-sided and a one-sided weaving segment.

Site 1 is a two-sided weaving segment (FIGURE 5.4 (a)), where a right-hand on-ramp from 122 Street is followed by a left-hand off-ramp to Terwillegar Drive. With a high proportion of lane changing maneuvers between merging and diverging areas, a recurrent bottleneck is often triggered in this test segment. Based on the definitions in HCM 2010, the short length of the weaving segment (L_s) is 0.821 kilometer (km), which is less than the maximum length ($L_{MAX} = 1.782\ km$). Weaving vehicles must cross three lances. Only the ramp-to-ramp traffic is considered to be a weaving flow, while the through movement is not considered, as it does not need to change lanes and generally does not shift lane position in response to a desired exit leg. Site 2 is a one-sided weaving segment (FIGURE 5.4 (b)), originating at the on-ramp of 53 Avenue to the off-ramp of Fox Drive. On this weaving segment, short length ($L_s = 0.550\ km$) is less than $L_{MAX} = 1.445\ km$. As a result, ramp-to-freeway and freeway-to-ramp flows using Lane 1 and Lane 2 are considered weaving movements.

The field data used as inputs in this study was compiled from two separate sources: recorded videos for lane changing movements, mainline and ramp data, and VDS 1018 and VDS 1031 for 20 s traffic data. The upstream video cameras filmed traffic movements on the weaving segments. Both of the weaving segments were divided into three regions. All on-ramp vehicles merge in Region 1; thereafter, weaving vehicles start their weaving movements. Relevant lane changing movements were manually extracted and collected over 1 minute (min) intervals from traffic videos. Distributions of each traffic movement were also collected.

5.3.2 Field Data Analysis

- ***Lane Changing Distribution***

The number of lane changes in each region was collected from 04:00 PM to 06:00 PM on a typical weekday. In Site 1, Region 1 was indicated as the critical region in the weaving segment, as half of the lane changes occurred on it. Similarly, Region 1 on Site 2 was selected because it bore 63% of the lane changes. Same evidence was found in Cassidy et al. [96] and Kwon et al. [69] stating that the highest lane changing rates occur near the merge gore. Thus, in the following analysis, data in VDS 1018 and VDS 1031 was used.

- ***Lane-Specific Volume-Density Relationship***

Complete data sets from VDSs were available for the first half of 2013. To eliminate the impact of adverse weather conditions, only the data sets for May and June were selected (as those months typically bear mild weather conditions in Edmonton). FIGURE 5.5 exhibits the Volume-Density (V-D) plots from VDS 1018 and VDS 1031, which are located immediately downstream of the merging area.

In Site 1, Lane 1 and Lane 2 have similar capacity, but Lane 2 experiences a larger capacity drop during queue discharge periods. Meanwhile, Lane 2 and Lane 3 have similar V-D patterns, while Lane 2 has remarkably less than that of the leftmost lane. The large capacity drops on Lane 2 and Lane 3 are caused by queue formation. This phenomenon can be explained: weaving vehicles shift their lanes from Lane 1-2 and Lane 2-3 after entering the segment so that it easily forms a queue. Furthermore, the V-D plot shows the effect of the side friction: vehicles drive the most slowly on the rightmost lane but fastest on the leftmost lane. This observation is consistent with Kwon et al. [69]. Site 2 also experiences similar traffic patterns, yet the flow distinction among lanes is not as obvious as Site 1. Lane 1 bears the lowest flow rate and travel speed, meanwhile the capacity drops on the weaving lanes (Lane 2 and 3) are a bit more severe. Compared with Site 1, the flow rate on Site 2 is generally lower due to its geometric design. With a curve before the on-ramp of Fox Drive, vehicles usually drive a little slower but with larger spacing.

- ***Segment Capacity***

TABLE 5.1 summarizes traffic data from VDS 1018. The 20-s interval data of vehicle counts was aggregated into 5-min intervals. Then, the queue discharge condition was defined as the corresponding speed below 60 kilometer per hour (kph) for at least 15 min [70]. As presented in TABLE 5.1, this site is regularly an active bottleneck and there exists a capacity drop phenomenon. Variations of traffic demand and O-D result in different discharge flows. The capacity ranges from 1740 to 1850 vehicles per hour per lane (vphpl). However, discharge flow in the queue discharge period has a reduction variant from 5-20%. From this field data, capacity in this weaving segment is approximately 1850 vphpl and peak hours are from 04:00 PM to 06:00 PM.

- ***Model Results***

TABLE 5.2 (a) lists the model inputs, including flow rates, flow ratios, as well as basic capacity values. The value for τ_{LC} was set as the suggested value in [76], i.e. 3 s. The other parameters (v_f, ρ_{Jam} and ω) were calibrated from the macroscopic fundamental diagram for a separate lane .TABLE 5.2 (b) concludes the estimates from the methodology in HCM 2010 and the proposed method. In both configurations, the proposed method obtained similar results compared with HCM 2010. Also, the estimates from these two methods are consistent with field observations. The difference between field observation and estimation ranges from 30 vphpl to 40 vphpl, which is acceptable. The factors contributing the estimation errors are in two aspects. On one hand, the proposed methodology assumes that, on the weaving segment, no special driving maneuvers are conducted apart from the weaving maneuvers. In other words, non-weaving vehicles do not change lanes, accelerate, or decelerate, which is unrealistic in the real world. In real life, driving maneuvers are much more complicated than the assumption. On the other hand, geometric factors also contribute to the estimation errors. On Site 1, there is a curve downstream the weaving segment. Some of vehicles decelerate on the weaving segment, so too does upstream of

Site 2. As for Site 2, a left exit is 0.45 km downstream the weaving segment, which may attract more vehicles to change lanes. In short, the studied weaving segments are more complex than our assumption and simplification, so that errors exist in estimations by both the proposed method and HCM 2010. From these results, it can be concluded that the proposed method works well for capacity estimation and provides reasonable estimates.

- ***Sensitivity Analysis***

The weaving capacity may vary as the flow ratio of each stream changes; thus, a sensitivity analysis was conducted. With the proposed estimation model, flow ratio was individually varied across its entire range of plausible values (from 0 to 1) while all other parameters were held. The detailed results for the sensitivity analysis are exhibited in FIGURE 5.6.

FIGURE 5.6 illustrates the variation trend of weaving capacity for different flow ratios. For the two-sided weaving segment (as plotted in FIGURE 5.6 (a)), when ratio of through flow (W_1) is larger than 0.85, the weaving capacity stays at the basic capacity. However, once W_1 holds at a value less than 0.85, the weaving capacity decreases as the ratio of weaving flow (W_1) increases. This sensitivity indicates that an increase in weaving vehicles decreases weaving capacity, which was also found in [68, 74, 75]. Moreover, weaving capacity is rarely influenced by a small weaving flow; but, as weaving flow increases, the weaving capacity rapidly drops. The extremely low capacity, 500 vph, was caused by constraints of the basic ramp capacity, which rarely occurs in the real world.

Furthermore, similar trends were observed in the case of the one-sided weaving segment (FIGURE 5.6 (b)). Weaving capacity grows as the ratio of non-weaving flow increases (W_1). It is noted that these sensitivity results are from theoretical calculation. Capacity depends on number of lane changes, as well as the constraints of flow ratios. For this case, the range for W_1 is usually 0.6-1, while that for W_2 is below 0.4; this is why many capacity values in the calculation cannot happen in the real world. In addition, in this range, capacity increases as non-weaving flow (W_1) increases, but has little change as W_2 increases, because the capacity on the auxiliary lane is smaller than the mainline. If all the vehicles on the two weaving lanes are weaving vehicles, i.e. $W_1 = 0.66$ and $W_2 = 0$, the estimated capacity is 1080 vphpl. In this situation, the capacity for this four-lane segment equals the capacity for a three-lane basic freeway. For the other extreme situation, if there is no weaving on the segment, i.e. $W_1 = 1$ and $W_2 = 1$, the estimated capacity is 1400 vphpl. The weaving segment then equals to a four-lane basic freeway segment. These results are consistent with those from Lertworawanich and Elefteriadou [75].

5.3.3 Real-Time Maximum Discharge Flow Estimates

The proposed method was used to estimate the maximum discharge flow rate on Site 1. The real-time density was collected by loop detectors and used as a model input. The flow ratios (W_1 and W_2) were assumed fixed during the day.

When average traffic density was smaller than critical density, the maximum discharge flow was set to be the weaving capacity value; once the average density exceeded the critical density, the actual density was used as the model input and the maximum discharge flow was estimated. FIGURE 5.7 presents the flow measurement and estimated maximum discharge flow rate during the peak afternoon period (04:00 PM-06:00 PM) on May 21, 2013. From 04:00 PM, traffic demand increased, but did not reached capacity; thus, the maximum discharge flow remained at capacity. At 04:50 PM, when demand exceeded capacity, the weaving segment became congested and the maximum discharge flow decreased. It fluctuated until 06:00 PM, when traffic demand decreased and the traffic state returned to a free-flow condition. The real-time estimates of maximum discharge flow are slightly higher than the observed queue discharge flow. Therefore, the proposed method has the potential to be applied in traffic operation methods to better predict traffic dynamics.

5.4 Summary

This chapter proposed a capacity estimation approach that combined linear optimization with a lane changing model. This method was evaluated in two authentic weaving segments and found to be reasonably accurate.

There are four major findings of this research: 1) most lane changes happen near the merge gore, which can be considered the critical region, and the capacity there can represent the whole weaving segment; 2) the proposed approach provides similar results compared with HCM 2010 results and field observations; 3) when the weaving flow ratio is small, an increased number of weaving vehicles rarely changes weaving capacity, whereas, when weaving ratio is moderate or large, weaving behaviors notably decrease weaving capacity; and 4) the proposed approach can capture real-time maximum discharge flow, which is a main input for traffic operation strategies.

Based on the proposed weaving capacity estimation model, future work will make effort to implement the capacity estimation model in optimal traffic operation strategies. Furthermore, the estimation model can be applied to dynamic maximum discharge flow estimation. When a bottleneck is going to be or is already triggered in a weaving segment, it could help to find an optimal discharge flow rate from mainline and on-ramps. Then, by deploying a proper control rate, actual input flow rate in the weaving bottleneck can be adjusted. This can mitigate bottleneck severity. In the future, this research will be directed to develop dynamic traffic control strategies that can be implemented to relieve bottleneck severity. Driver maneuvers are complicated and also require more investigation.

TABLE 5.1. Field Observations, VDS 1018

Date	Max. 15 min		Max. Queue Discharge		Capacity Drop
	Capacity (vphpl)	Average Speed (kph)	Bottleneck Capacity (vphpl)	Average Speed (kph)	
06-May-2013	1793	60.95	1560	47.34	13.01%
13-May-2013	1740	69.43	1571	37.55	9.73%
21-May-2013	1837	67.95	1456	41.58	20.75%
23-May-2013	1840	64.87	1545	42.72	16.01%
29-May-2013	1665	57.14	1567	45.47	5.92%
04-Jun-2013	1849	63.37	1680	45.92	9.16%
06-Jun-2013	1789	72.01	1680	43.30	6.11%

TABLE 5.2. Capacity Estimation Results

(a) Model Inputs

	Observed Flow (vph)				Model Parameters			Basic Capacity (vphpl)	
	q_{FF}	q_{FR}	q_{RF}	q_{RR}	W_1	W_2	VR	c_{BF}	c_{BR}
Site 1	3006	1619	79	237	0.80	0.25	0.016	2100	1600
Site 2	4097	1593	441	9	0.72	0.02	0.3313	1400	1300

(b) Estimation Results

Capacity Estimates / Site	Field Observations		HCM 2010 Estimation (vphpl)	Proposed Method (vphpl)
	Max. 15 min (vphpl)	Max. Queue Discharge (vphpl)		
Site 1 21-May-2013	1837	1456	1857	1867
Site 2 16-May-2013	1299	1139	1285	1257

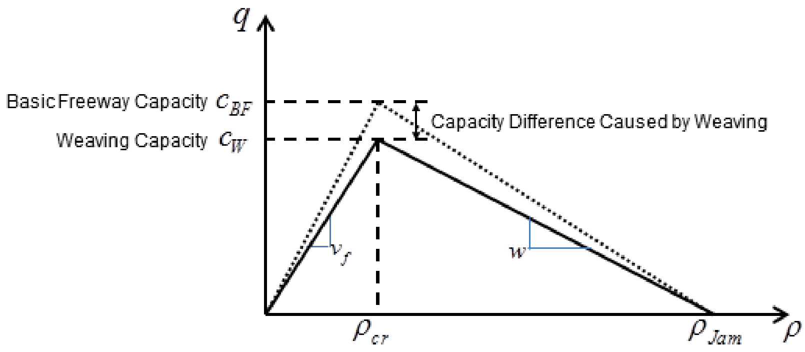

FIGURE 5.1. Triangular Fundamental Diagram.

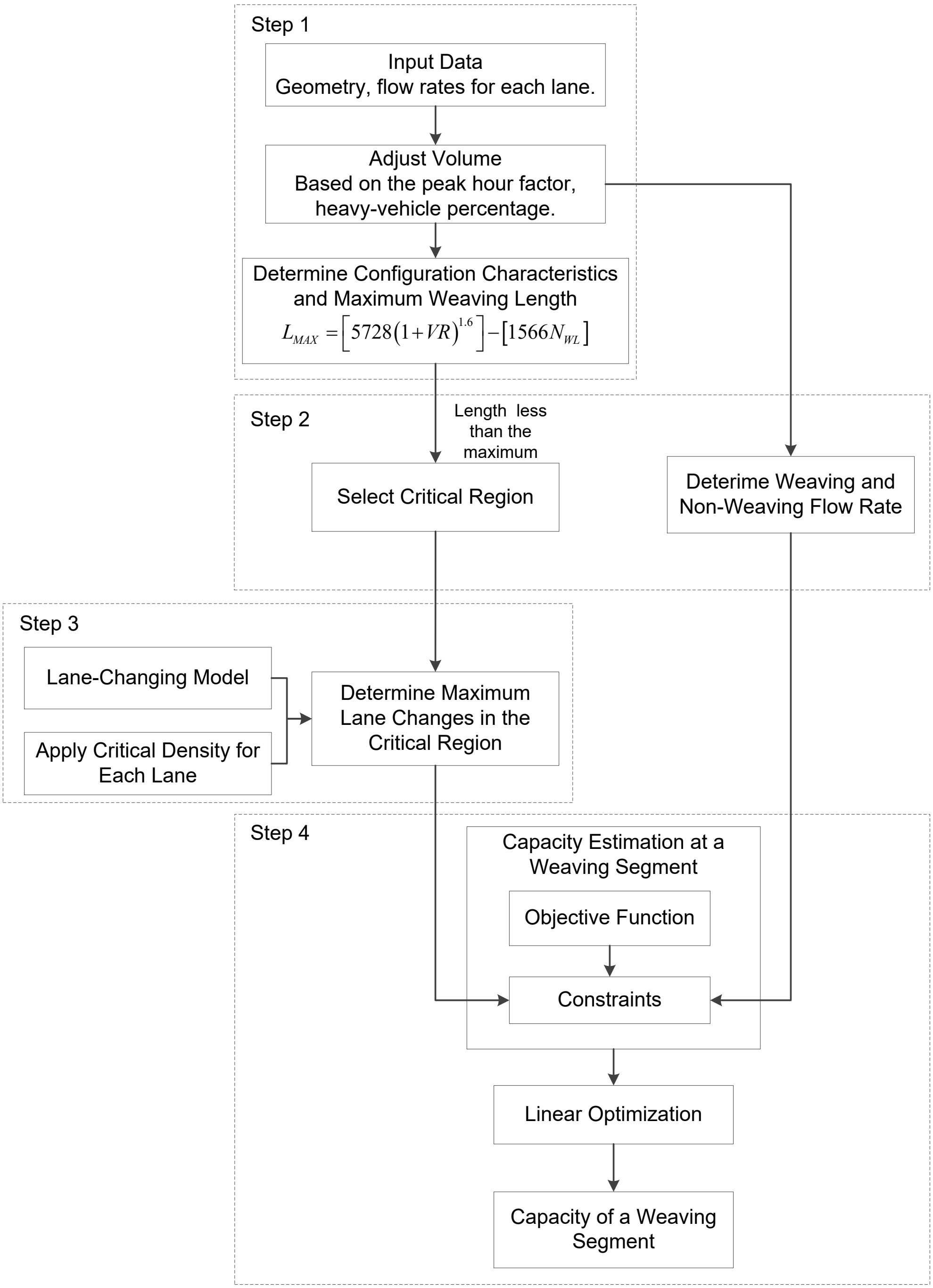

FIGURE 5.2. Methodology Flowchart.

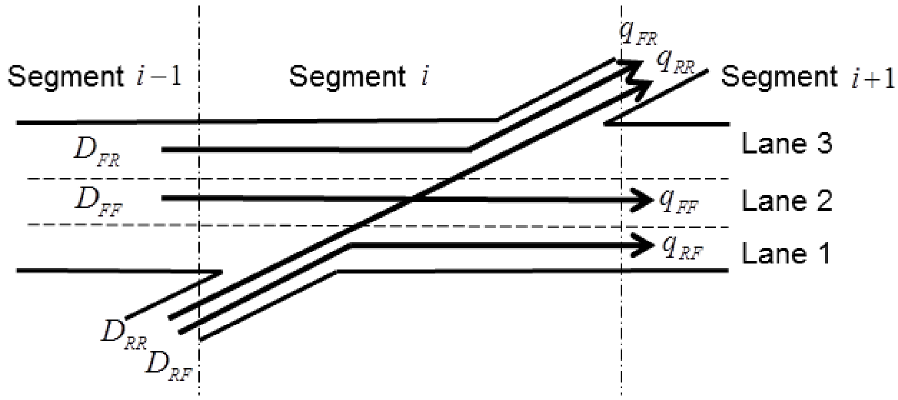

(a) Two-Sided Segment

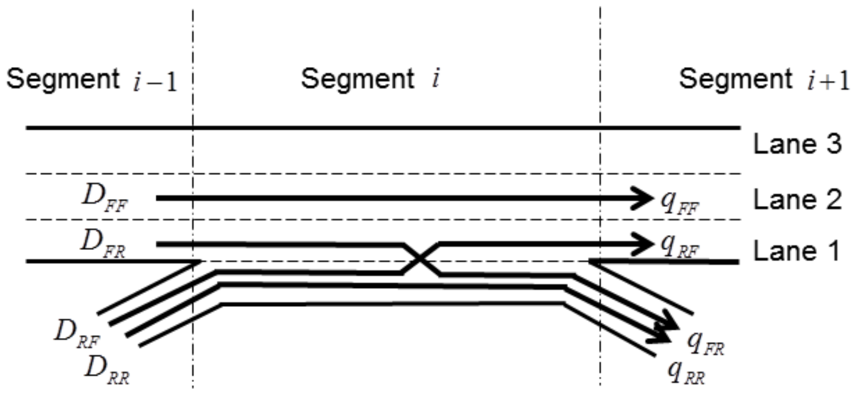

(b) One-Sided Segment

FIGURE 5.3. Sketches of Weaving Segments.

q_{FF} is the through traffic flow from freeway to freeway, at capacity;

q_{FR} is the traffic flow from freeway to off-ramp, at capacity;

q_{RF} is the traffic flow from the on-ramp to freeway, at capacity;

q_{RR} is the traffic flow from the on-ramp to off-ramp, at capacity;

D_{FF}, D_{FR}, D_{RF} and D_{RR} are the traffic demand for each traffic stream.

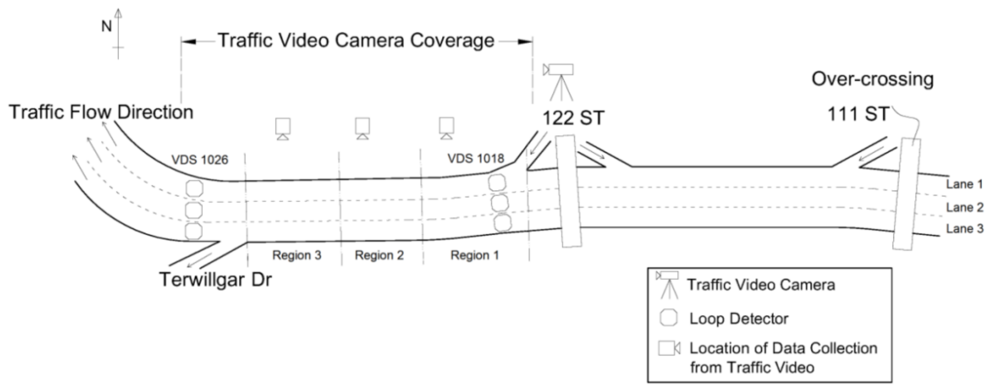

(a)

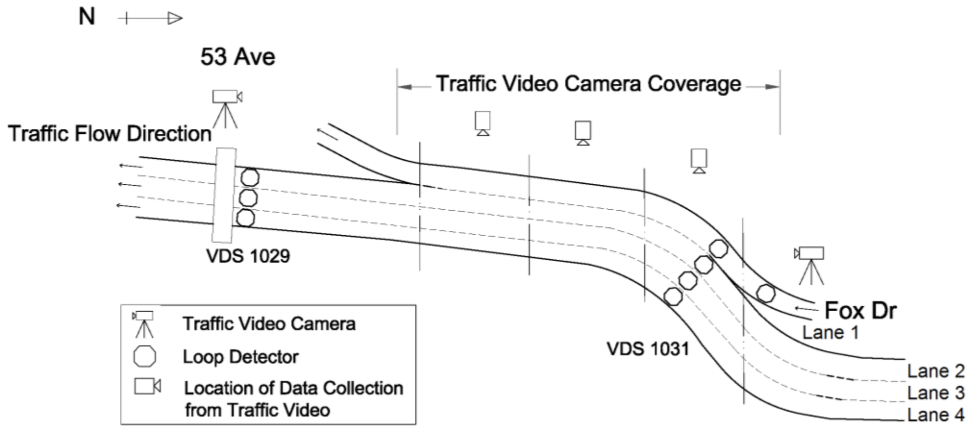

(b)

FIGURE 5.4. Study Site, Whitemud Drive, Edmonton, Alberta, Canada:

(a) Site 1, a Two-Sided Weaving Segment; (b) Site2, a One-Sided Weaving Segment.

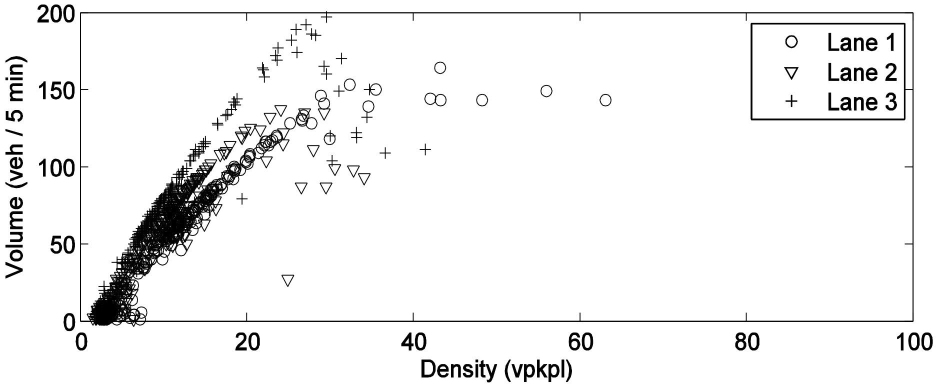

(a) VDS 1018, 21-May-2013

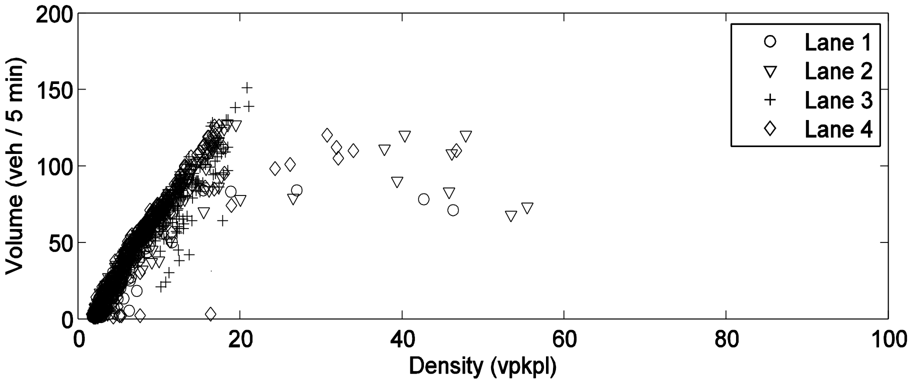

(b) VDS 1031, 16-May-2013

FIGURE 5.5. Volume-Density Plot at Weaving Segments.

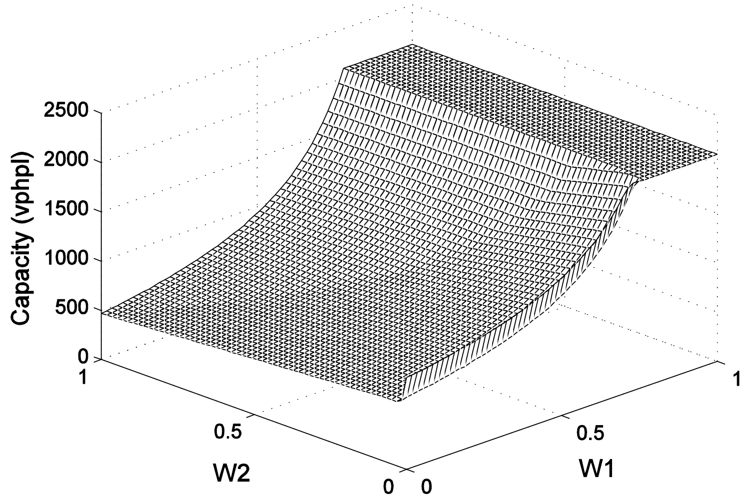

(a)

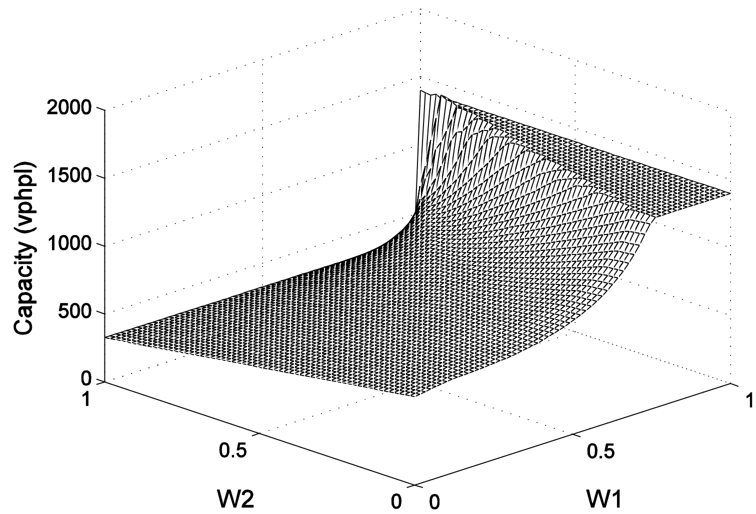

(b)

FIGURE 5.6. Capacity Estimates:

(a) the Two-Sided Weaving Segment (b) the One-Sided Weaving Segment.

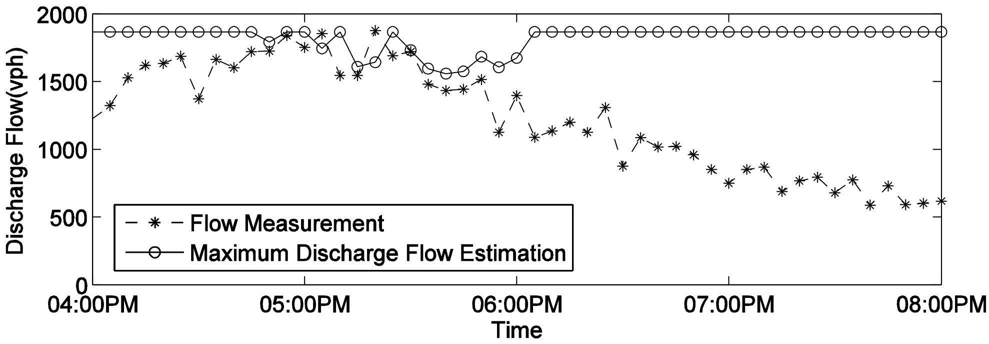

FIGURE 5.7. Maximum Discharge Flow Estimation, 21-May-2013

CHAPTER 6. MAINLINE AND RAMP FLOW INTERACTION UNDER PROACTIVE INTEGRATED FREEWAY CONTROL

6.1 Introduction

Active traffic and demand management (ATDM) methods, including ramp metering (RM), variable speed limits (VSL) and route guidance (RG), effectively and efficiently alleviate freeway congestion. Over the past decade, several ATDM methods that incorporate real-time data collection and facility coordination have been implemented in the field. So far, RM and VSL are the most commonly applied methods. RM is a ramp flow control that has no effect after vehicles enter the freeway mainline. The benefit of RM is subject to mainline and on-ramp demand levels. If on-ramps yield a low demand, there is little controllable traffic for RM, which may limit its performance. Conversely, if on-ramp demand is high, RM sometimes needs to be switched off in the case that the on-ramp queue spills back to surface streets. Thus, RM alone might be insufficient for freeway control in many cases. In contrast, VSL control is a mainline traffic flow control and a good supplement to RM, as the mainline carries more controllable traffic. Whereas, over-control of VSL may spread low speed to upstream traffic. Thus, much recent research has focused on integrated control of RM and VSL.

Depending on how the control strategy is designed, it can determine RM and VSL rates successively or simultaneously [67]. For example, Lu et al. determined VSL before RM [67]. In their method, VSL is determined first, based on the current traffic state. With the determined VSL, a first-order density dynamics is linearized and can be used to optimize RM rates. Likewise, Carlson et al. [101] integrated RM and VSL by considering RM first. The basic principle is that RM is applied for downstream congestion as long as the ramps are not full; otherwise, VSL is switched on.

Recently, many researchers have applied a tightly coupled second-order traffic dynamics to combine VSL and RM, and consider their optimal coordination and integration. The METANET model has been commonly applied. The original METANET model was extended to incorporate RM and VSL signals. The common objective function takes the total time spent (TTS) on both mainline and ramps, sometimes with a term that penalizes abrupt variations in RM and VSL signals. The differences among different studies are the applied control approach and optimization techniques. Hegyi et al. [6] fulfilled proactive integration using model predictive control (MPC). The nonlinear optimization problem was solved by a sequential quadratic programming (SQP) algorithm. Furthermore, one of their most recent studies [39] proposed a receding-horizon parameterized control approach based on MPC and state feedback control. A multi-start SQP algorithm was used to solve the optimal control variables. However, for real-life applications, computation time is the major concern. To this end, Ghods et al. [38] introduced a game theory to obtain optimal control inputs for the integration. The proposed optimization algorithm was verified in a macro-simulation, and its computation time was significantly reduced.

In previous research, although the performance of integrated control has been confirmed, some problems still exist. First, the aforementioned evaluation research applied the same macroscopic model in both traffic modeling and prediction. In other words, prediction in the proactive strategies was assumed to perfectly match future traffic measurements. This assumption is not achievable in real-world implementation. As a result of this infeasible assumption, real-life traffic disturbances and model errors are rarely considered, which may lead to overestimation of the control performance. Second, it is questionable whether integrated control always surpasses isolated control. Both RM and VSL have their own strengths and weaknesses, as explained before. Integration only takes advantage of both strategies and ideally avoids their disadvantages. However, the true effect of integrated or isolated control remains unknown in real-life applications. Lastly but most importantly, it is still unclear how RM and VSL cooperate and how their control rates change simultaneously. Mainline and ramp flows interact at weaving, merging or diverging segments. Traffic conditions on those segments are susceptible to recurrent congestion. Investigating the integration of RM and VSL can reveal the interaction between ramp flow and mainline flow. Little previous research has examined the integration results or explain how RM and VSL integrate, especially for the proactive algorithms that RM and VSL are determined simultaneously. Clarifying the relationships between RM and VSL and between mainline flow and ramp flow can help in integrated control algorithm design.

To bridge these research gaps, this study evaluates a proactive integrated control strategy. Traffic evolutions and driver responses are predicted by an extended METANET model and simulated within a micro-simulation environment, respectively. In this way, this study decouples traffic modeling and prediction. The evaluation varies mainline and ramp flow by changing mainline and ramp demand, and checks the integration performance by looking into the control variable profiles. The main objectives in this study are to: 1) identify the performance of integrated and isolated control in decoupled prediction and simulation environments, and explain potential control error sources; 2) evaluate the variations in control performance under different combinations of demand scenarios; and 3) investigate control variable profiles and explain the integration process and interaction between mainline and on-ramp flows.

The remainder of this study is organized into sections: Section 6.2 explains the ideas embedded in RM and VSL by the shockwave theory; Section 6.3 briefly introduces the integrated control method; and Section 6.4 is devoted to the investigation of integration performance.

6.2 RM and VSL Mechanism

FIGURE 6.1 graphs the effect of proactive RM and VSL on mitigating traffic congestion according to the shockwave theory. A weaving segment and a lane drop segment are used as examples. The time-space diagrams and fundamental diagrams exemplify the fundamental impact of proactive RM and VSL on traffic flow. In FIGURE 6.1 (a), due to high traffic demand (A) and limited bottleneck capacity between ramps (B), a small traffic jam propagates upstream (ω_{AB}) and is surrounded by free-flow traffic. The fundamental diagram shows the corresponding density and flow values for these states. The shockwave spreads upstream until demand is decreased (D). The proactive RM that resolves shockwaves works as shown in FIGURE 6.1 (b). A shockwave typically has low flow and low speed but high density. Once a shockwave (ω_{AB}) is predicted by traffic dynamics, RM is activated to decrease the bottleneck flow (A') to its capacity (C) by controlling on-ramp input flow. RM remains active until bottleneck flow (D) is lower than bottleneck capacity (C). Next, stopped vehicles are discharged into the mainline. In the whole process, RM improves mainline traffic speed and prevents the shockwave from propagating upstream.

Similar with RM, without VSL, it is assumed that during peak periods a shockwave is formed on a lane drop segment and propagates upstream (see FIGURE 6.1 (c)). When proactive VSLs are implemented (FIGURE 6.1 (d)), the traffic flow model forecasts the bottleneck activation (B) and shockwave propagation (ω_{AB}). When the shockwave is predicted, the upstream VSLs are activated. The two VSLs require drivers to decelerate and then accelerate according to the traffic direction. As seen in FIGURE 6.1 (d), the first VSL causes the traffic state in the speed-controlled area to change from state A to state B. State B has the same density but lower flow than state A, because the speed limits decrease while the density remains the same. Although the speed (v_B) propagating backwards is lower than the previous speed limit (v_A), it is still higher than the shockwave speed v_B in FIGURE 6.1 (c). The discharge flow at B is close to bottleneck capacity (D). Note that between the downstream bound of the VSL control area and upstream bound of the lane drop segment, there is an acceleration zone for vehicles accelerating and exiting the bottleneck. This is consistent with previous research [54]. Once the congestion is cleared (E), VSL control is deactivated. The boundary between state B and state E soon disappears and the traffic flow returns to normal.

6.3 Methodology

Mainline and ramp flows interact at freeway weaving, merging or diverging segments. Traffic conditions are sensitive when mainline and ramp demand levels are varied. RM and VSL work through limiting upstream mainline and ramp discharge flows from entering the downstream bottleneck. For different scenarios, the integrated control will generate different series of RM and VSL rates. The analysis attempts to demonstrate the cooperation between RM and VSL in control variable variation relationships.

6.3.1 *Control Strategy*

The applied integrated control of RM and VSL aims to achieve optimal network performance according to traffic states predicted in real time. Its MPC framework has a multi-module structure to collect field traffic data, predict traffic conditions, and optimize and apply control variables (see FIGURE 6.2).

A METANET-based dynamic traffic model, namely DynaTAM–RM&VSL (Dynamic Analysis Tool for Active Traffic and Demand Management–Ramp Metering and Variable Speed Limit), performs traffic state prediction and coordinates mainline and on-ramp flows. DynaTAM is an application-oriented software tool; its branches for RM and VSL were developed and presented by Wang et al. [90] and Hadiuzzaman et al. [10], respectively. DynaTAM–RM&VSL divides a freeway corridor into several segments (i =1, 2,..., N) of length L_i and lanes λ_i . For all segments, DynaTAM–RM&VSL predicts traffic density ρ in vehicles per kilometer per lane (veh/km/ln) and traffic speed v in kilometers per hour (km/h). The basic METANET model and the modifications have been introduced in previous research [10, 14, 90]. Note that DynaTAM–RM&VSL needs to be calibrated and validated before serving as a prediction model. The details of the prediction model and its calibration and validation are not repeated here. The sections below focus on the constraints and objective function in the optimization.

6.3.2 *Constraints*

Two inequality constraints are adopted for optimizing the RM rate r. First, Equation (6.1) makes an applicable flow rate lower than the difference between the mainline capacity $Q_{\max}$ and current flow rate q. Second, Equation (6.2) considers the limited storage space to avoid spillback from on-ramps to surface streets. To estimate an on-ramp queue length, this study uses a Kalman filter approach proposed by Vigos et al. [102].

$$q_{i-1}(k) + r_i(k) \le Q_{\max,i} \tag{6.1}$$

where, k is the time step index.

$$r_i(k) \ge r_{\min,i}(k) \text{ (when } w_{o,i}(k) > 95\% w_{cap}) \tag{6.2}$$

where, $r_{\min}$ is the minimum ramp metering rates in vehicles per hour (veh/h); w_o is the on-ramp queue length in vehicles (veh); w_{cap} is the on-ramp queue capacity in vehicles (veh).

The control strategy also constrains VSL rates for the VSL-controlled segments by two inequality constraints. First, Equation (6.3) restricts the optimal speed limit between the maximum and minimum values ($V_{\max}$ and $V_{\min}$). Second, Equation (6.4) limits the absolute speed change between two consecutive time steps within a maximum speed difference $V_{\max,\text{diff}}$ to maintain safe operation. This temporal constraint avoids abrupt speed limit change and ensures driver safety and comfort.

$$V_{\min} \le u_i(k) \le V_{\max} \tag{6.3}$$

$$\left|u_i(k+1) - u_i(k)\right| \le V_{\max,\text{diff}} \tag{6.4}$$

6.3.3 *Objective Function*

The objective function in the control framework is a weighted summation of the total travel time (TTT) on the mainline, the total waiting time (TWT) on ramps and the TTD on the mainline. As proved in much previous research [10, 67, 90, 103], minimizing TTT reduces mainline density and mitigates congestion; whereas, maximizing TTD accommodates more vehicles in the mainline. As RM and VSL may improve freeway mobility at the cost of preventing vehicles entering the traffic network, TTD is included in the objective function. Meanwhile, excessive ramp delay caused by ramp control may raise the public's doubts about efficiency. To alleviate extremely long delays, the waiting time of vehicles, which are forced to stop by ramp meters, should be weighted more than the absolute travel time [104]. In summary, the optimization problem is to find optimal control values to obtain the minimal value of the objective function J (Equations (6.5) and (6.6)) over a prediction horizon N_p . This optimization problem balances traffic mobility and infrastructure utility, as well as temporal equity of the mainline and on-ramp vehicles. The weighting factors (α_{TTT}, α_{TWT} and α_{TTD}) were selected in the simulation stage. To include time and distance indexes in one objective function, α_{TTT} and α_{TWT} should be related to speed. Typically, α_{TTD} is held at 1, and the values of α_{TTT} and α_{TWT} are tuned in the range of 20-100. In this study, the best network measures of effectiveness were achieved when α_{TTT} and α_{TWT} were 80 and 100.

$$J = \alpha_{TTT} TTT + \alpha_{TWT} TWT - \alpha_{TTD} TTD \tag{6.5}$$

$$
\begin{aligned}
TTT &= T\sum_{j=1}^{N_p-1}\sum_{i=1}^{N_m}\lambda_i L_i \rho_i\left(k+j\right) \\
TWT &= T\sum_{j=1}^{N_p-1}\sum_{i=1}^{N_m} w_{0,i}\left(k+j\right) \\
TTD &= T\sum_{j=1}^{N_p-1}\sum_{i=1}^{N_m}\lambda_i L_i \rho_i\left(k+j\right) v_i\left(k+j\right)
\end{aligned}
\tag{6.6}
$$

6.4 Simulation Test and Evaluation Results

6.4.1 Study Site

A westbound section (between 122 Street and 159 Street) of an urban freeway corridor, called Whitemud Drive (WMD), in Edmonton, Canada, was chosen (as shown in FIGURE 6.3). The posted speed limit is 80 km/h. As observed from historical data, two recurrent bottlenecks are often activated along this urban freeway. One is a two-sided weaving segment from the on-ramp of 122 Street to the off-ramp of Terwillegar Drive. The other one originates at the sharp curve before 149 Street, where the deceleration of vehicles causes a backward shockwave. However, in coordinated control, further upstream RM and/or VSL control restricts flow and affects downstream bottleneck traffic. To eliminate the effect from upstream control, this analysis starts with integrated local control at the first bottleneck. Weaving segments bear frequent weaving maneuvers, which are representative of the interaction between mainline and ramp flow. Thus, the performance of Segments 1 to 4 (the weaving segment and its adjacent 3 segments) was demonstrated.

The City of Edmonton has installed vehicle detection stations (VDSs) and traffic video cameras along this corridor. The VDSs collect 20-second intervals of volume, speed and occupancy data, and send this data to the city's central computer system for archival. To replicate real-world traffic conditions, the prediction and micro-simulation models were calibrated and validated with field data.

6.4.2 Micro-Simulation Model Setup

For the implementation of the proactive strategy, an online optimization method was developed based on traffic measurements and prediction using VISSIM and Visual C++ (as shown in FIGURE 6.4). To change the RM and VSL rates assigned to the freeway segments during the simulation, the VISSIM component object model (COM) application programming interface (API) is used. Moreover, the Visual C++ program is used to load the traffic network through the VISSIM API, and to start the simulation process.

For RM implementation, a signal control strategy, namely "single-lane one car per green", was applied in the signal state generator. It allows one vehicle to enter the freeway during each signal cycle with a minimum duration of 4.5 seconds (s) [105]. An uncontrolled single-lane on-ramp is capable of a throughput of 1800 veh/h. The minimum admissible ramp flow is typically 200-400 veh/h [106]. With this in mind, in the simulation, the cycle length was set from 5 s to 10 s at one-second (1-s) intervals. Each signal cycle consisted of 1-s green, 1-s yellow and remaining red signal indications. Once a ramp meter was required to shut off, its signal indication was set to green (cycle length is 0 s). It is important to note that the signal cycle length was converted from on-ramp flow obtained by solving the optimization problem.

In Canada, the implemented speed limits on freeways are multiples of 10 km/h. Thus, VSL signs update in increments or decrements of a value that is a multiple of 10 km/h. Hence, $V_{\max,\text{diff}}$ is 10 km/h. Furthermore, the upper and lower bounds of the posted speed limit are $V_{\max}$ =80 km/h and $V_{\min}$ =20 km/h. The VSL sign locations along the studied corridor are shown in FIGURE 6.3. VSL-1 was located far upstream of the bottlenecks and it urged drivers to decelerate. VSL-2 provided higher speed limits ahead of the bottleneck for drivers to accelerate and pass through the bottleneck as quickly as possible. In this study, VSL-2 was given a fixed value of 80 km/h. Thus, VSL-2 was not considered in the optimization problem.

The sequence of ramp and mainline inputs that minimizes the performance criterion over a given future prediction horizon (N_p =5 minutes (min)) can be determined. The control horizon (N_c) is 1 min. In this study, a 5-min prediction horizon was equivalent to a 15-step prediction, as length of each prediction time step (T) is 20 s. At each control horizon, these meter and speed limit rates are generated using a C++ program based on a decision tree-based solver.

6.4.3 Simulation Results

Integrated and coordinated control supports the maximum utilization of traffic infrastructure for the whole network rather than just an individual segment. The control performance at all four segments was considered in the analysis. The simulation tests replicated traffic conditions during PM peak hours (4:30PM-6:30PM) after a 5-min warm-up period (4:25PM-4:30PM). The warm-up period allowed vehicles to spread everywhere in the network. Then the result analysis removed the warm-up period. The peak hours contained low-demand and high-demand periods. Low demand was input into the network from 4:30PM to 4:40PM and from 6:00PM to 6:30PM, and high demand was loaded for the time period in between. The demand level in the high-demand period varied for the mainline and on-ramp. Moreover, as explained before, traffic conditions at weaving segments are sensitive to weaving maneuvers. Weaving maneuvers increase as weaving flow grows. The growth of congestion is much faster than the increase of weaving flow. This study selected mainline demand ranging from 3600 veh/h to 4000 veh/h and on-ramp demand from 800 veh/h to 1000 veh/h. Traffic congestion is sensitive to even a 100 veh/h increase in either mainline or on-ramp demand.

Possible sources of suboptimal or even adverse control performance are explained before presenting the results:

a) VSL limits flow by lowering the upstream speed limit. Assuming all drivers comply with VSL, the upstream of the bottleneck experiences lower speed, even though it may be free flow in the no-control case. In this way, VSL may actively spread a relatively low speed upstream. Although mobility at bottlenecks is improved by VSL, the decreased mobility at upstream segments may lower the overall performance;

b) RM limits flow by stopping on-ramp vehicles at entrances to the freeway mainline. Stopped vehicles at on-ramps may cause excessive waiting time. Thus, RM improves mainline mobility, but meanwhile results in delay to ramp vehicles;

c) Proactive integration considers a tradeoff among network-wide mainline travel time, ramp waiting time and network flow. However, the tradeoff may not be achieved in real-world applications due to the following: 1) The selection of control variables is limited to several discrete values for the convenience of signal setting. The assumption of discrete signals loses some control performance; 2) Occasional mistakes from the queue estimation model may generate incorrect RM control signals; 3) Traffic dynamics cannot promise to perfectly match real traffic evolutions even though they have been calibrated and validated; 4) Several constraints are applied to the optimization for safety concerns. For example, as the speed limit becomes lower and lower, it cannot recover to the normal value quickly once congestion is about to be alleviated; 5) Proactive control optimizes the traffic performance over a short term, but the resulting traffic condition may not be optimal over the whole peak period.

In summary, either isolated or integrated control can theoretically mitigate congestion. In real implementation, the aforementioned factors keep control performance from reaching its optimum level. With this in mind, the following analysis examines control performance under different scenarios of traffic demand.

TABLE 6.1 lists the control performance results from the simulation tests. Each case was run 10 times with random seed numbers in the micro-simulation, and the performances have been averaged. Overall, in the no-control cases, TTT and TTD increased as the ramp and mainline demand grew. In other words, congestion became more severe as the demand increased and the network carried more vehicles. When control strategies were applied, the performance generally improved by a distinct difference. After comparing TTS (TTS=TTT+TWT) among control scenarios in each demand combination, the control performance was assessed, as shown by cell shading in TABLE 6.1. The darker the shading is, the better the performance. We can observe that the integrated control performed best among all control options when both mainline and on-ramp demand were relatively high (the bottom right side). Otherwise, isolated control may be a better option. In conclusion, integrated control is not always better than isolated control. On one hand, VSL is enough for low on-ramp demand (see the rows when on-ramp demand is 800 veh/h). At this time, integration with RM adds excessive ramp waiting time (TWT) and thus loses some performance in TTS. RM performs better if on-ramp demand grows (see the column when mainline demand is 3600 veh/h). Similarly, integration with VSL increases mainline travel time (TTT). On the other hand, if we look at the bottom right of TABLE 6.1, integration of RM and VSL acts as a combination of isolated RM and VSL. The TTT and TWT values under integration are between those under isolated RM and VSL, which provides evidence for the balancing effect of integration on the mainline travel time and ramp waiting time.

An interesting phenomenon can be observed from TABLE 6.1: VSL or RM sometimes leads the traffic condition to become even worse (on-ramp demand is 900 veh/h and mainline demand is 3800-4000 veh/h). The reasons why traffic control may obtain unsatisfactory effects, no matter whether it is isolated or integrated, were explained qualitatively before. The following analysis will look at a set of simulation results from a typical scenario (mainline demand is 3900 veh/h and on-ramp demand is 900 veh/h), quantitatively investigate the causes and detail how integrated control coordinates RM and VSL.

FIGURE 6.5 shows the control performance under different control strategies. In particular, FIGURE 6.5 (a) profiles speed to show traffic evolutions. It is obvious that without any control, congestion originates from Segment 3 and propagates to the farthest upstream segment. The low speed on the farthest upstream segment prevents vehicles from entering the traffic network. It can be shown from TABLE 6.1 that the TTD even decreased from

17529.43 veh*km to 17390.54 veh*km when the mainline demand increased from 3800 veh/h to 3900 veh/h.

When VSL was applied to Segment 2, the backward shockwave caused by VSL propagated upstream. The low average speed on Segment 1 blocked the freeway mainline entrance. Even though some improvement was achieved on downstream segments, the overall TTT grew (no-control: 325.28 veh*h, VSL: 333.8 veh*h) and TTD remained the same (no-control: 17390.54 veh*km, VSL: 17394.44 veh*km). FIGURE 6.5 (b) profiles the control variable variations. Isolated VSL control generated very low speed limits during peak hours. The unsatisfactory performance of VSL was due to the formed mainline queue. Other than the general error sources explained before, two other factors were attributable to the unsatisfactory performance. Firstly, as neither estimation nor a constraint for mainline queue length was built into the control algorithm, the mainline queue was not predictable. If the bottleneck kept getting worse, the algorithm continued suggesting lower speed limits for the upstream VSL-controlled segment. Once low speed limits were achieved, the algorithm could not recover speed limits immediately as a result of the safety constraint (Equation (6.4)). Secondly, the traffic dynamics took flow measurements on Segment 1 as the demand for downstream traffic prediction. No measurement or prediction of speed and density was taken for Segment 1. The algorithm mistakenly assumed that the low flow from Segment 1 was due to low mainline demand rather than congestion. Therefore, VSL led to a negative improvement.

It is crucial to ensure the farthest upstream segment does not encounter congestion before and after deploying the proactive control algorithm. The high TTT and low TTD profiles of VSL in FIGURE 6.5 (c) can also come to this conclusion.

The control performance of isolated RM on Segment 3 was better than that of isolated VSL. The TTT was reduced by 6.2% (no-control: 325.28 veh*h, RM: 305.04 veh*h). An apparent correlation between RM cycle length and speed profiles was that the longer a cycle length was, the higher the mainline speed was. RM with a longer cycle length discharged less ramp flow so that it prevented mainline traffic becoming worse. However, the control horizon lasted for one minute, suggesting that a long RM cycle length may form a long ramp queue and spillback to the surface street. Hence, most RM cycle lengths were less than 7 s long. The resulting ramp queue can be calculated from the TWT profile, as shown in FIGURE 6.5 (c). The maximum TWT of isolated RM happened at around 5:00PM, reaching 0.334 veh*h. The stopped vehicle number equaled to 20 veh (0.334 veh*h multiplied by 1 min). Assuming vehicle length and spacing equaled to 10 meters per vehicle (m/veh), the queue length was 200 m (20 veh multiplied by 10 m/veh). This queue length almost exceeded the ramp length of 250 m. Thus, in the next time step, the RM cycle length decreased so that TWT dropped. In conclusion, RM control impacts the network performance little when on-ramp demand is high, due to the limited on-ramp storage length.

In contrast, integrated control maximizes the utility of both control strategies. Combining VSL on Segment 2 with RM on Segment 3, traffic congestion was notably alleviated (see FIGURE 6.5 (a)). The bottleneck speed was remarkably higher and the duration of a low speed upstream was much shorter than in other scenarios. The integrated control obtained a 13.3% reduction in TTT (no-control: 325.28 veh*h, RM&VSL: 281.78 veh*h). In addition, the alleviation of speed drops on the farthest upstream segment attracted more vehicles to enter the network. The TTD increased from 17390.54 veh*km to 17838.77 veh*km. TWT under integrated control was 1 veh*h more than that in no-control scenario, but it was still 1 veh*h less than that in RM scenario. From the control signals in FIGURE 6.5 (b), RM reacted earlier than VSL at the onset of congestion. In the case of an excessive queue, VSL then took over. The average speed limits were higher than those determined by isolated VSL. Thus, the mainline queue was shorter. In the middle of the congested period, VSL itself could not control the congestion as the mainline queue length increased. At this time, RM helped in restricting ramp flow, resulting in a TWT increase. The speed at the bottleneck and the farthest upstream segment grew. Then RM stopped working until the demand was reduced. Traffic congestion recovered but there were still occasional traffic instabilities. It is important to note that the number of stopped vehicles were different between high- and low-demand periods even though RM cycle lengths were the same. That is why, although the RM cycle lengths were high, RM did not lead to an extremely long ramp waiting time during low-demand periods.

RM and VSL are basically flow control measures. To illustrate their effectiveness in flow control, FIGURE 6.5 (d) presents the flow profiles under integrated control. The upstream mainline (Segment 2) and on-ramp discharge flow was adjusted by VSL and RM, respectively. Then the mainline and on-ramp flows interacted at the weaving segment (Segment 3) and became the bottleneck flow. During the high-demand period, bottleneck flow slightly fluctuated around 4800 veh/h. VSL and RM worked together to maintain this stable bottleneck flow. Most of the time, the upstream mainline and on-ramp discharge flow were negatively correlated. Put simply, on-ramp flow reduced when the mainline flow increased, and vice versa. By this means, VSL and RM cooperated through limiting mainline and on-ramp input flows, and sustained a stable traffic condition.

FIGURE 6.5 (c) confirms that the proactive integrated control is superior to isolated control under high mainline and ramp demand. Integrated control shortens mainline travel time by mitigating the mainline queue, and meanwhile controls the on-ramp waiting time by balancing mainline and ramp travel time. This is done by proactive integration. The integration synthetically considers all possible control scenarios, takes advantage of both control strategies, and coordinates RM and VSL rates. The effect of the prediction is reflected in how RM and VSL react before the onset of congestion. Other than control signal profiles, the effect of the prediction is more obvious in speed profiles on Segment 2 (FIGURE 6.5 (a)) and TWT profiles on Segment 3 (FIGURE 6.5 (c)). The prediction module forecasts traffic evolutions and proposes control countermeasures. By responding to the predicted traffic condition, it is promising that bottleneck congestion can be prevented if demand is light. In the presented case, the demand was so high that the bottleneck congestion could not be prevented but could still be greatly alleviated. In addition, proactive integration is not always better than isolated control due to some potential errors in real implementation. RM improves freeway mobility, but only for short congestion scenarios with relatively high ramp demand. As the mainline carries more controllable flow, VSL outperforms RM when mainline demand is high. However, if the demand is extremely high at both the mainline and on-ramps, isolated control cannot operate optimally. In this case, the integration of RM and VSL maximizes their benefits and infrastructure utility.

6.5 Summary

Recurrent bottlenecks often limit discharge flow and lower freeway mobility. This study emphasized the applicability and effectiveness of a proactive integrated RM and VSL approach. It adopted a METANET-based traffic flow model within an MPC framework. By implementing this proactive control approach in a micro-simulation model, there were three major findings:

1) Proactive RM and VSL, no matter whether they are isolated or integrated, generally improve freeway mobility. After decoupling prediction and simulation models, the unsatisfactory performance originates from the built-in prediction model and control algorithm. The control benefits of integrated control can achieve improvements of up to 13.65% in TTS and 3.41% in TTD, varying with different combinations of mainline and on-ramp demand.

2) Considering the same demand scenario, the control performance among strategies differs. The light congestion that is caused by on-ramp flow can be alleviated by RM. When mainline demand becomes higher, VSL can control mainline flow and achieve more control benefits. However, isolated control fails to achieve the best control performance once mainline and ramp demand are both high. The integration of RM and VSL maximizes their own benefits.

3) For integrated control, RM reacts before VSL. When the demand keeps increasing, VSL takes over the control. During the most congested period, RM and VSL work simultaneously. After, RM is deactivated in the case of a long ramp queue. At the end of congestion, RM is activated occasionally to deal with remaining traffic disturbances.

This analysis could guide strategy selection during the ATDM planning stage. Prior to implementation, the causes of recurrent congestion must be carefully analyzed. Flow and corridor origin-destination surveys are recommended. Geometric and traffic situations vary among cases, so it is impossible to provide a quantitative guideline for strategy selection. However, the results from this study can still help. RM is beneficial for alleviating short-period congestion during peak hours without disturbing mainline traffic. Appropriate metering rates can improve freeway mobility and balance temporal equality between mainline and ramp vehicles. VSL functions under a higher demand, taking the risk of spreading congestion upstream. The performance of integrated RM and VSL exceeds isolated strategies for more severe congestion.

TABLE 6.1. Control Performance under Different Traffic Demand

On-ramp Demand (veh/h)		Mainline Demand (veh/h)	3600	3700	3800	3900	4000
800	No Control	TTT	237.99	247.89	285.21	311.85	326.68
		TWT	2.04	2.10	2.15	2.10	2.09
		TTD	16405.57	17010.34	17121.66	17312.67	17726.24
	VSL	TTT	219.65	234.65	241.61	252.12	323.70
		TWT	2.04	2.09	2.09	2.09	2.20
		TTD	16405.05	17009.07	17294.86	17676.83	17835.85
	RM	TTT	218.42	233.58	271.22	304.78	308.44
		TWT	5.18	3.61	3.27	4.68	4.61
		TTD	16405.08	17010.11	17294.92	17219.50	17765.35
	RM&VSL	TTT	221.74	235.22	257.90	280.76	301.50
		TWT	3.67	3.59	3.31	3.24	3.17
		TTD	16405.05	17009.88	17295.41	17640.25	17699.56
900	No Control	TTT	262.53	268.17	273.38	325.28	329.59
		TWT	2.59	2.54	2.39	2.64	2.52
		TTD	16853.21	17168.73	17529.43	17390.54	17542.15
	VSL	TTT	257.19	234.95	280.08	333.8	329.12
		TWT	2.54	2.56	2.34	2.57	2.56
		TTD	16861.96	17166.91	17528.25	17394.44	17635.70
	RM	TTT	223.94	253.81	269.94	305.04	329.00
		TWT	5.48	5.28	4.04	4.83	7.72
		TTD	16846.23	17157.93	17530.20	17539.99	17389.18
	RM&VSL	TTT	227.55	252.03	262.67	281.78	322.71
		TWT	4.88	3.57	3.47	3.67	6.03
		TTD	16840.04	17167.42	17454.28	17838.77	17679.23
1000	No Control	TTT	276.42	328.95	338.51	334.81	355.85
		TWT	2.39	2.82	2.79	2.39	3.44
		TTD	17040.57	16774.49	17243.51	17548.01	17236.82
	VSL	TTT	251.00	315.12	335.23	328.88	347.76
		TWT	2.3881	2.39	2.61	2.34	2.74
		TTD	17037.81	17057.53	17348.43	17602.64	16882.69
	RM	TTT	223.64	294.72	294.16	324.89	332.83
		TWT	12.29	7.45	6.58	8.93	7.87
		TTD	16863.70	17290.00	17330.01	17161.77	17521.57
	RM&VSL	TTT	228.50	285.97	295.29	321.44	322.57
		TWT	12.26	3.82	5.08	5.43	7.36
		TTD	16842.89	17347.12	17355.20	17568.99	17036.60

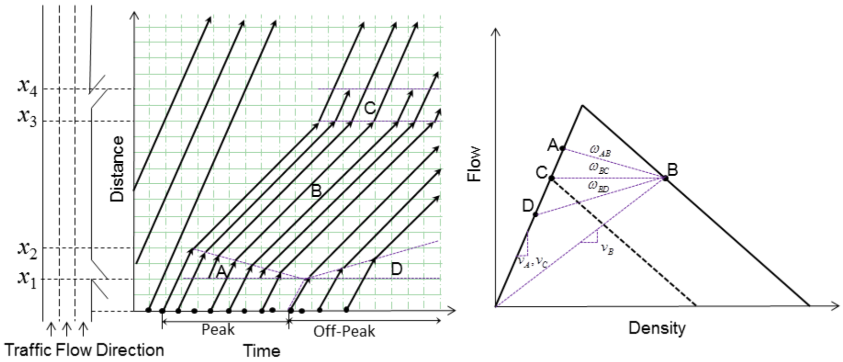

(a) before RM control

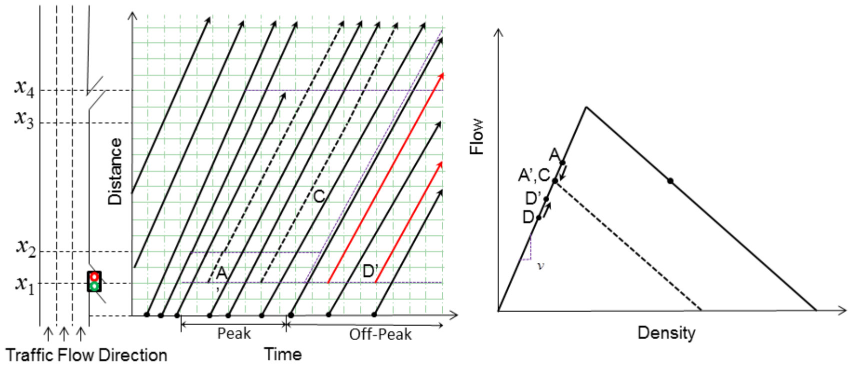

(b) after RM control

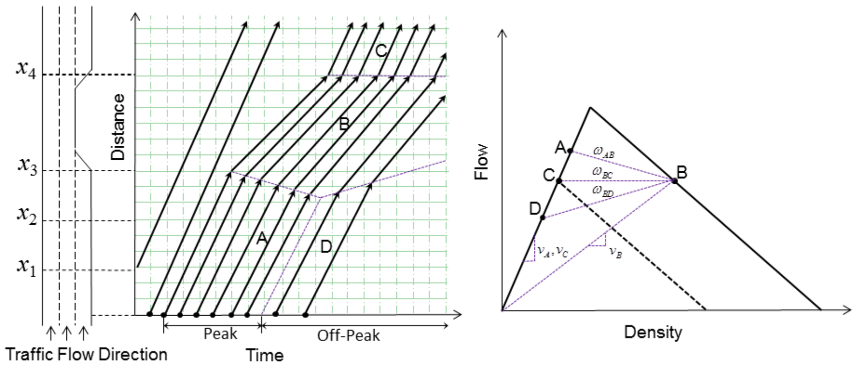

(c) before VSL control

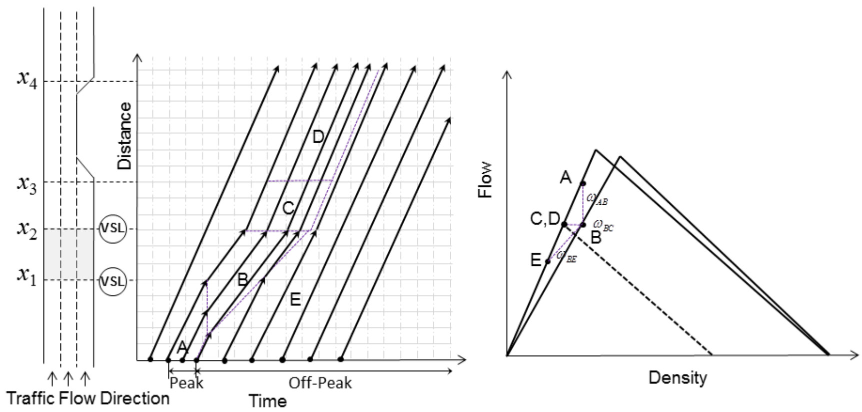

(d) after VSL control

FIGURE 6.1. Time-Space Diagram and Fundamental Diagram.

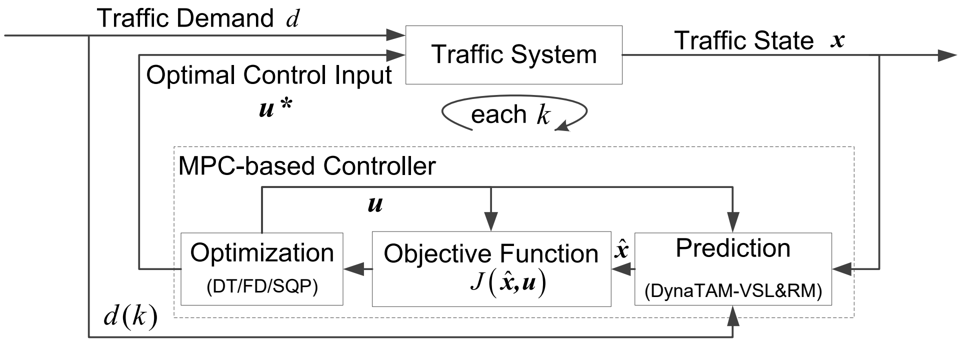

FIGURE 6.2. Proposed Framework of RM and VSL Integrated Control.

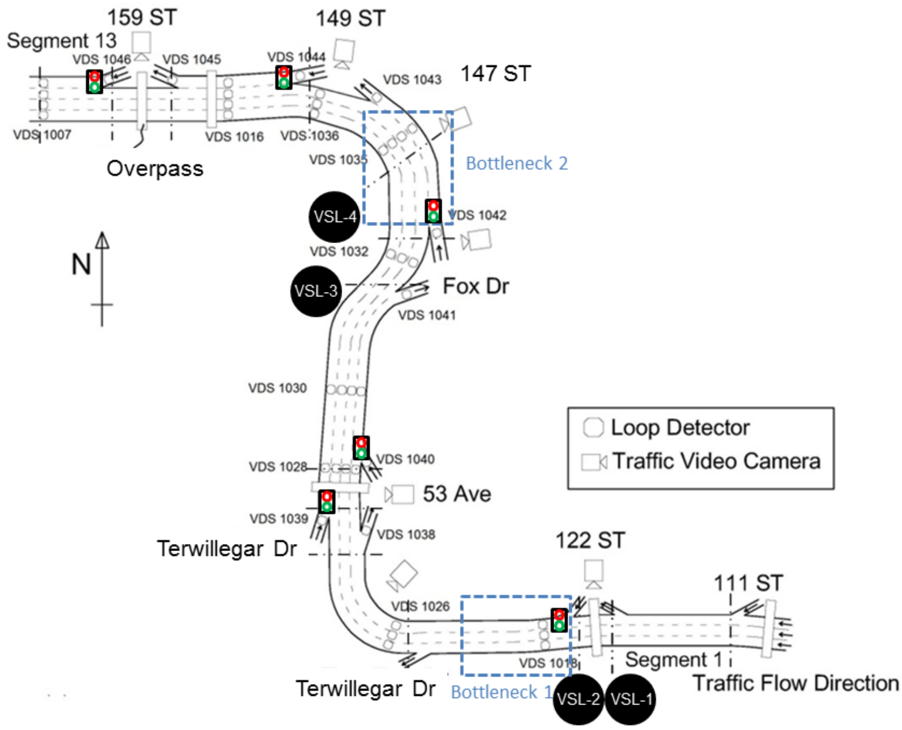

FIGURE 6.3. Study Corridor, WMD, Edmonton, Canada.

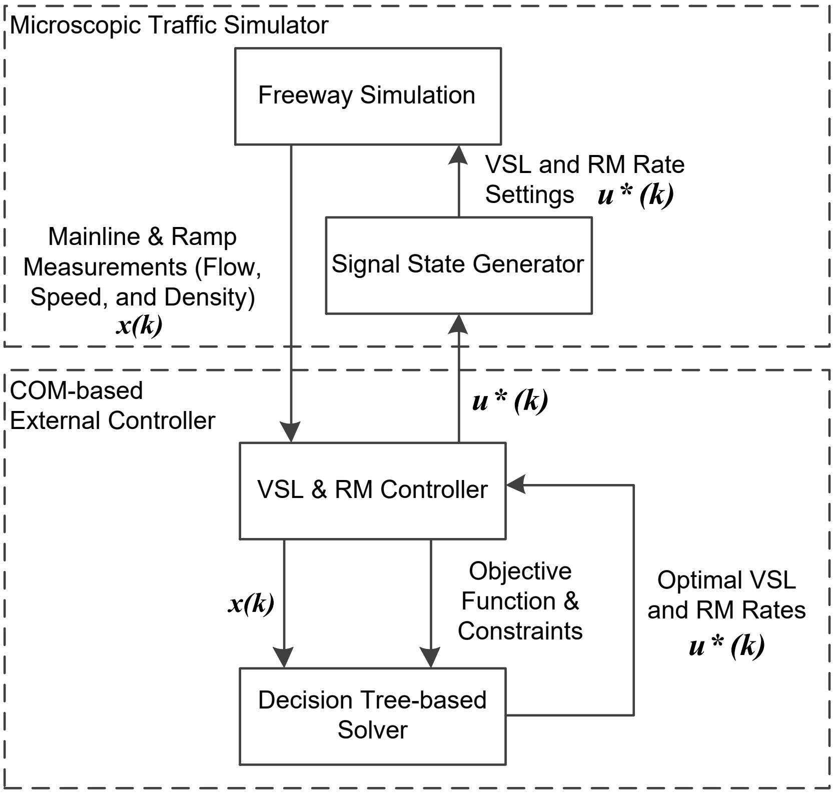

FIGURE 6.4. Simulation System Architecture of RM Controller.

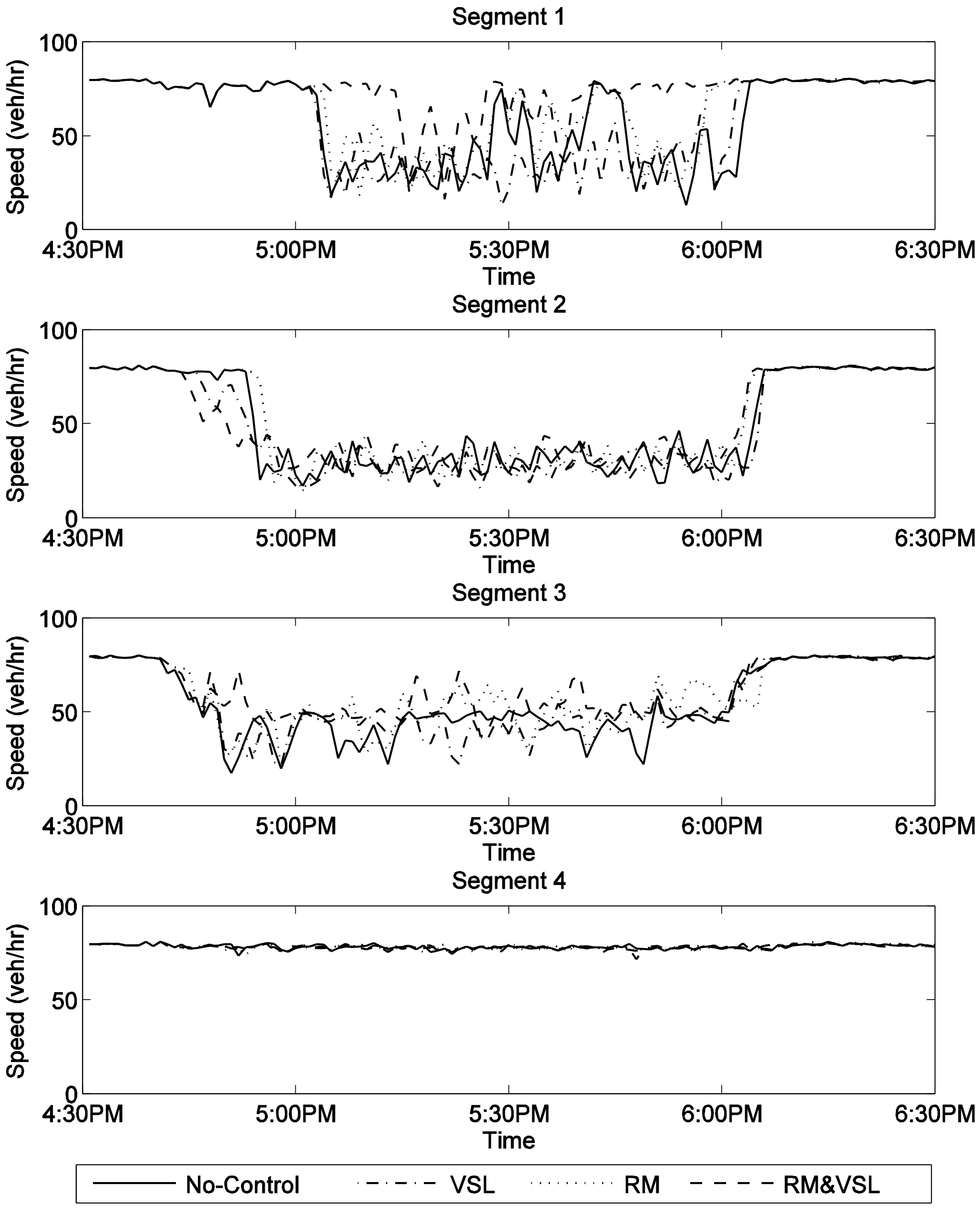

(a) Speed Profiles

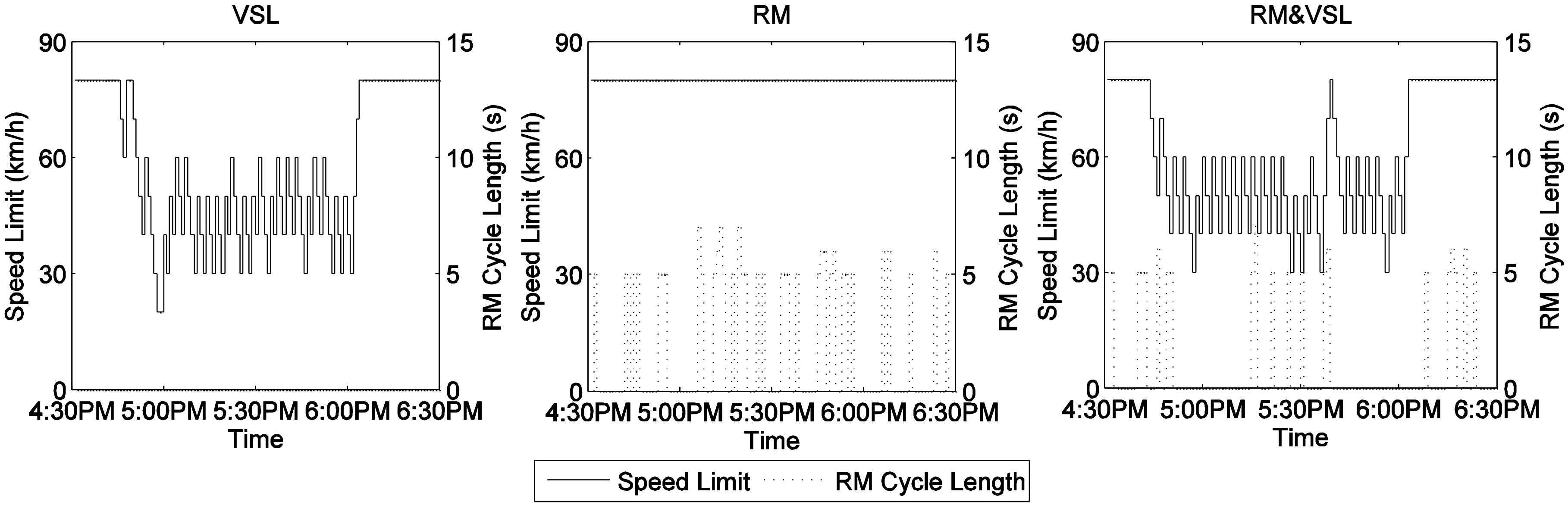

(b) RM and VSL Rates

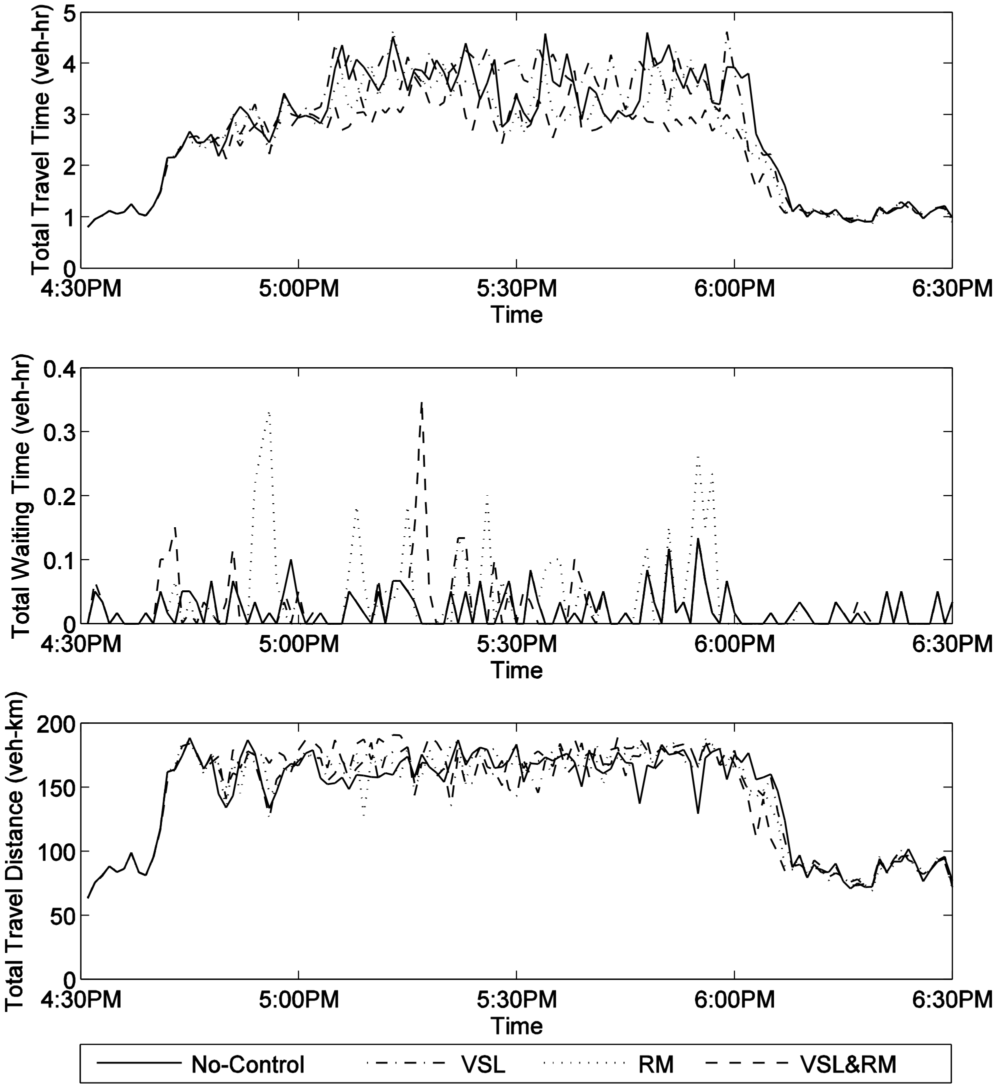

(c) MOEs

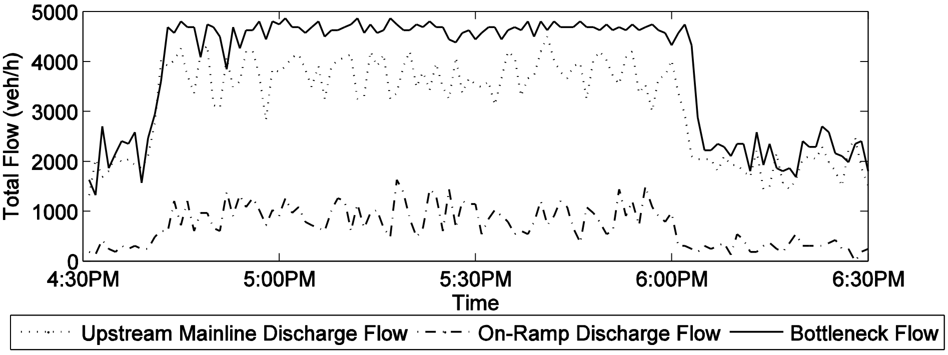

(d) Flow Profiles under Integrated Control

FIGURE 6.5. Network Performance.

CHAPTER 7. EFFECT OF SPEED LIMITS AT SPEED TRANSITION ZONES

7.1 Introduction

Speed limits provide the legal maximum or minimum speeds on roadways. Appropriate speed limits serve as a tradeoff for mobility and safety concerns. In turn, roadway mobility and safety performance depends on driver compliance with speed limits. In the past few decades, variable speed limits (VSLs) have been introduced to roadways. VSLs are an intelligent transportation system (ITS) measure that seeks to relieve congestion by limiting upstream flow, and meanwhile to improve traffic safety by homogenizing vehicular speed. Different from static speed limits, VSLs operate in either mandatory or advisory ways. Mandatory VSLs are legally equivalent to static speed limits, and may even be enforced to increase driver compliance. In contrast, advisory VSLs recommend driving speed limits but they are not enforced. Obviously, VSLs under different traffic environment bring distinct level of driver compliance. Similar with static speed limits, the safety and operational performance of VSLs is correlated with the level of driver compliance. Hence, VSL algorithms should consider driver compliance. In current practice, speed limit enforcement and education are common actions that attempt to improve driver compliance. More importantly, VSLs dynamically create and shift speed transition zones, where driver behavioral feedback are complicated. Then questions arise simultaneously:

How do drivers react to speed limits in speed transition zones? Which factors affect driver compliance? How to represent driver compliance under different combinations of conditions in VSL algorithms? Unfortunately, existing studies fail to answer these questions. An important point to note is that, providing greater insight into the effect of speed limits at speed transition zones is promising to enhance roadway design and operation. Consequently, this research aims to bridge these research gaps.

The existence of VSLs forms and moves speed transition zones dynamically. At speed transition zones, driver compliance varies caused by various factors, such as traffic flow characteristics, environmental, spatial and temporal conditions. Driver compliance reflects the driver feedback to VSLs. The resulted driver compliance influences VSL control performance. In this way, driver compliance correlates with VSLs. Therefore, understanding effect of speed limits at speed transition zones is a key issue in VSL design and implementation. Whereas, existing studies are unable to propose a convincing solution to deal with this issue. To this end, this research focuses on driver behaviors at speed transition zones and quantifies the impact factors of driver compliance. There are five objectives of this research: 1) test the spatial and temporal variations of driver behaviors at speed transition zones; 2) evaluate the temporal and spatial effect of speed limit signs and education tools; 3) investigate into various factors that may affect driver compliance and rank their contributions; 4) analyze the correlation between various factors and driver compliance, and propose a potential driver compliance estimation method; 5) based on driver behaviors at speed transition zones, provide suggestions and guidelines for VSL algorithm design and implementation.

With these objectives in mind, this study gathered field data from two consecutive speed transition zones on 97th Street, Edmonton, Canada. The analysis is expected to guide future VSL design and implementation. The reminder of this research is organized into sections: Section 7.2 details study site selection, data collection, experimental design and analysis methods; and Section 7.3 is devoted to exploring the temporal and spatial effect of speed limits, identifying critical impact factors on driver compliance, and discussing VSL design and implementation practice.

7.2 Study Methodology

7.2.1 Selection of Study Site

This study selected two sections from the southbound of 97th Street between 176th Avenue and 137th Avenue in Edmonton, Canada. The corridor is a major arterial that connects highways and enters the city from north along the centerline. The studied section yields speed transitions and experiences frequent collisions. Two speed transition zones were designed to allow drivers reduce speed from 80 kilometers per hour (km/h) to 60 km/h in two steps. Conventional signs post reduced speed limits, accompanied by advance warning signs (R2-1 and W3-5 types of signs according to Manual on Uniform Traffic Control

Devices [107]). These two sites were selected for this study because conventional static speed limits and mandatory VSLs are legally equivalent. The driver feedback to conventional static speed limit should be the same as that to VSLs, but its characteristics are much easier to be captured. For safety concern, City of Edmonton installed dynamic speed display signs (DSDSs) from June to August 2010, expecting to improve driver compliance with speed limits. DSDSs, as one kind of speed education device, reminded drivers to adjust speed by real-time measuring and displaying oncoming vehicular speed, but no enforcement was applied. FIGURE 7.1 exhibits the layout of the study site schematically, including sign placement and data collection. The total length of the study site is 4.3 kilometers (km) and drivers would not expect speed transitions at its beginning. Along the study site, the corridor is straight with a clear view that ensures the sign information is delivered. Traffic signals operate in the middle and the end of the study site, where speed limit signs are installed approximately 200-300 meters (m) upstream. The distance between signs and signals are long enough for vehicle speed not being affected by signals in off-peak time. Advance warning signs are placed 150 m upstream of the speed limit signs. Initially, static signs indicating speed limits of 70 km/h and 60 km/h were in operation, and during part of the test DSDSs were set aside by the static speed limit signs.

7.2.2 Data Collection

City of Edmonton installed data collection devices at four locations: two at the upstream of the speed transition zones and two at the speed limit sign locations. As presented in FIGURE 7.1, Site 1 is at the entry of the first study section where drivers are supposed to travel at their initial speed of 80 km/h. Passing Site 1, drivers notice the warning sign for speed limit reduction and enter the first speed transition zone. When drivers are approaching the speed limit sign at Site 2, they are supposed to adjust their speed and complete deceleration ahead of Site 2. Similarly, Site 3 and Site 4 are outside and in the end of the second speed transition zone, respectively. During the test, once DSDSs were set aside by the speed limit signs, they displayed drivers' arriving speed and reminded them to adjust their speed.

Data collection devices detected and recorded traffic data continuously from May to September of 2010. Data set of volume, speed and density along with other related parameters were available for the test period. Meanwhile, volume data were automatically aggregated into a 15-minute interval and meanwhile categorized into bins respect to speed and vehicle length. Speed bins were divided as follows: 0-50 km/h, 51-55 km/h, 56-60 km/h, 61-65 km/h, 66-70 km/h, 71-75 km/h, 76-80 km/h, 81-85 km/h, and 86-100 km/h. In terms of vehicle length, vehicles with a length less than 8.4 m were classified as light vehicles while others were classified as heavy vehicles. Additionally, to account for impact of adverse weather (e.g. rainfall, hail), weather data from

Environment Canada were linked with traffic data. In this way, traffic data were categorized into favorable and adverse weather. In the end, sunset and sunrise information from National Research Council of Canada were fused with traffic data to obtain temporal impact from time of day. To sum up, a total 14 weeks of fused data was archived to investigate driver behaviors at speed transition zones.

7.2.3 Experimental Design

This experiment aimed to evaluate the effect of speed limits at speed transition zones. The comparative test was conducted in three phases: 1) drivers were informed speed limit reductions by static speed limit signs; 2) speed limit education devices were in place aside of static speed limit signs; 3) speed limit education devices were removed. The detailed test schedule is listed in TABLE 7.1. Note that, during Phase 2, the devices were turned on and off alternately to clarify the influence of activated speed education. The result analysis primarily focuses on temporal and spatial variations of driver behaviors under static speed limit signs or education devices. It analyzes main contributing factors affecting driver behaviors at speed transition zones. Secondly, comparisons between Phase 1 and Phase 2 can reveal the impact of speed education on speed reduction. Meanwhile, comparisons between Phase 1 and Phase 3 can show whether effectiveness of speed education last after devices were removed. Alternations of device conditions in Phase 2 can show the impact of activated or inactivated education device on driver behaviors. A total of 13382, 52365 and 14212 data points were collected in Phase 1, 2 and 3, respectively. Data from June 29th to 30th, July 1st to 3rd and August 19th to 22nd were lost due to device failure.

Congestions also influence vehicular speed. To erase the impact of congestion on speed, this study divided traffic conditions into free flow and congestion by comparing headway values to be higher or lower than 2 seconds (s). The 2-s headway is recommended by Government of Alberta to drivers. Thus, this analysis began with removing the data points with average density higher than $\rho^{v}_{threshold}$, which was converted from 2-s headway based on Equation (7.1).

$$\rho^{v}_{threshold} = \frac{1}{L + v \times h_{threshold}} \tag{7.1}$$

where, $\rho^{v}_{threshold}$ (in vehicles per kilometer per lane, veh/km/ln) is the threshold of density at vehicular speed v (in km/h); L is vehicle length in km; and $h_{threshold}$ is the threshold of headway in hours. From the data set, average vehicle length L is 0.006 km and speed v takes 80 km/h, 70 km/h and 60 km/h for each location. Then, $\rho^{80}_{threshold}$, $\rho^{70}_{threshold}$ and $\rho^{60}_{threshold}$ equal to 20, 22.3 and 25 veh/km/ln, respectively.

This study evaluates the effect of speed limits by following indicators: average speed, standard deviation of speed, and driver compliance. Among these indicators, the analysis concentrates on driver compliance. The reasons why average speed rather than the 85th percentile operating speed is selected as an indicator can be explained in two aspects. Average speed is a common variable in traffic flow prediction models. Analysis results for average speed are easy to be incorporated into traffic flow models. Additionally, during our data analysis, average speed was positively correlated with 85th percentile speed. Hence, average speed was chosen.

This study investigates the temporal and spatial variations of driver behaviors, and tests the possible contributing factors, i.e. vehicle type, time of day, weather condition, speed limit value, existence of activated enforcement or education devices, and surrounding traffic speed. At last, the analysis ranks the contributions of the factors.

7.2.4 Analysis Method

- ***Statistical Tests***

A two-sample t test with pooled variance for average speed and driver compliance were conducted to assess the statistical significance of driver behavior difference between various scenarios. Average speed and driver compliance were calculated for each scenario. Each test compared the mean values of driver behaviors between two scenarios, which suggested that the two-sample t-test with pooled variance was appropriate for this analysis. The null and alternative hypotheses were no difference ($H_o : \mu_1 = \mu_2$) and reduction ($H_a : \mu_1 > \mu_2$) in driver behaviors. For example, in the temporal analysis, Phase 1 is considered as a baseline. T values between every two scenarios were calculated to test the statistical significance at a 0.001 level. The hypotheses tests are summarized in TABLE 7.2.

- ***Linear Regression***

To quantify the contribution of each variable to driver compliance, a linear regression model was established after the correlations between variables and driver compliance were identified. The linear regression model covers traffic flow parameters as well as vehicular, environmental and temporal factors. Linear regression is one of the most straightforward methods which can quantify the impact of various variables on driver compliance. Linear regression is an appropriate option for the data set in this study because the dependent variable y is continuous and independent variables x may include binary and continuous variables. Furthermore, due to the continuous attribute of y, the commonly used method, binary logistic model, cannot be applied in this data set. Let y denote the driver compliance with the speed limit in a certain time interval (15 minutes in this case). If $y = 0$, it means zero compliance; however, if $y = 1$, it means full compliance.

$$y = b_0 + b_1 x_1 + b_2 x_2 + ... + b_n x_n \tag{7.2}$$

where $b_0, b_1, ..., b_n$ are coefficients for independent variables $x_1, x_2, ..., x_n$. The dependent variable y and independent variables x should be quantitative. It is important to note that categorical variables need to be recoded to binary (dummy) variables before being applied in linear regression. Least squares method is used to obtain coefficient values for best predict of the dependent variable. All statistical analysis was conducted in IBM SPSS Statistics version 20.

7.3 Data Analysis and Results

7.3.1 Temporal and Spatial Variations of Driver Behaviors

Temporal variation analysis focused on the variations of speed-related parameters from Phase 1 to Phase 3, while spatial variation analysis investigated the variations of speed-related parameters from Site 1 to Site 4 in each phase. TABLE 7.3 (a) summarizes results of average speed and driver compliance from the three-phase experiments. Their variations were in different extent across sites. Generally, for the sites where education devices were placed (Site 2 and Site 4), average speed was reduced when education devices were in force. For example, average speed at Site 2 was 74.41 km/h in Phase 1, and it was remarkably reduced to 71.90 km/h in existence of the activated education device. However, average speed rose again once education devices were turned off or even removed. Driver compliance grew with the usage of education devices, but dropped again when devices were not in force. This phenomenon can also be observed in FIGURE 7.2 (a). The results from statistical tests were listed in TABLE 7.3 (a). These results suggested that speed limit education takes only temporary rather than everlasting effect. When speed education devices are inactivated or removed, drivers performs as no education used to show up. These results were consistent with a previous study [84]. Thus, in following analysis, Phase 1, Phase 2 (off) and Phase 3 were combined into one category, during which drivers reduced speed in response to static speed limit signs. In contrast, drivers decelerated reacting to speed education devices during Phase 2 (on). Another point noticed from FIGURE 7.2 (a) is that positive impact of speed education decreases after some time when it keeps being activated for a long time. The experiment tried 2-day, 7-day and 14-day durations. The optimum effect achieved in the 7-day duration case. In the 2-day and 7-day cases, driver compliance increased day by day continuously; but in the 14-day case, driver compliance increased in the first 7 days and dropped in succession after then.

Subsequently, we looked into spatial variations of driver behavior (as presented in TABLE 7.3 (b) and FIGURE 7.2 (b) and (c)). Drivers approached Site 1 at their original speeds. When they noticed the speed limit warning sign or speed education device, they decelerated and met the speed limit until they reached the speed limit signs at Site 2. Then, they continued to speed down from Site 2 to Site 3. Arriving Site 4, they tried to achieve the posted speed limit. All phases experienced the same spatial variation of average speed (shown in FIGURE 7.2 (b) and (c)). However, an interesting phenomenon was noticed in FIGURE 7.2 (c) that standard deviation of speed increased from Site 2 to Site 3. Similar changes happened for driver compliance. Speed limit on Site 2 and Site 3 are both 70 km/h but driver compliance on Site 3 is apparently higher than that on Site 2. Therefore we infer that some incompliant vehicles might continue to decelerate after Site 2 due to surrounding traffic speed and enlarged the standard deviation. Surrounding traffic includes leading vehicles and vehicles on neighbor lanes. Speed trends found above confirmed the effectiveness of speed limit signs on reducing speed. Also, activated speed education enhances their effectiveness. The shift in percentile speed profile (see FIGURE 7.3) also validates these conclusions.

Throughout the hypothesis results in TABLE 7.3 (b), only Site 2 yielded statistically significant reduction in average speed. Meanwhile, Site 2 and Site 4 bore significant improvement in driver compliance. Speed limit education decreased average speed by 2.5 km/h and increased driver compliance by 8% at maximum. These results all proved the observation above: speed education increases driver compliance indeed, but only in a limited space in close proximity; speed education have no effect on upstream traffic (350 m upstream in our case). The latter conclusion is opposite to an existing study [81]. Hence, it can be inferred that effectiveness of speed limit signs or education devices is site-specific. In addition, the major concern to post lower speed limit in the study site is to adapt drivers to speed limits in urban arterial as well as to ensure traffic safety. Existing studies indicated speed variance to be a major contributing factor in collisions. The reduction in standard deviation of speed in Site 2 observed from FIGURE 7.3 examined the safety effectiveness of speed education.

Last but not the least, driver compliance in Site 2 was always higher than that in Site 4 during any phase. Site 2 and Site 4 are both the end of speed transition zones which require speed decrements of 10 km/h. The distinction in compliance revealed driver compliance is also affected by speed limit values. The lower the speed limit value is, the lower driver compliance it

In sum, various factors contribute to driver compliance: existence of activated speed education devices, speed limit values and surrounding traffic speed. In the following analysis, we included vehicular, environmental and temporal factors involved in existing studies: vehicle type, weather condition, and time of day.

7.3.2 Linear Regression

Last subsection verified the tight associations between several variables and driver compliance. Their associations showed linear relationships. To evaluate the level of association between each impacting variable and driver compliance, below applies linear regression as a quantitative analysis. Although the calibrated linear regression model can dynamically estimate driver compliance, regression parameters are site-specific and need to be calibrated before certain applications. As a result, regression here is only to rank the variable contributions to driver compliance. Variable descriptions and statistics are listed in TABLE 7.4. Among the variables, speed limit value was categorical originally, but it has been recoded to binary variables before being applied in linear regression. Surrounding traffic speed was calculated as the mean value of average speed on the current lane in the last data collection interval and average speed on the neighbor lane(s) in the current data collection interval. For an individual vehicle, its speed partly depends on speeds of its surrounding vehicles, such as leading vehicles and vehicles on neighbor lane(s). Likewise, its speed affects it following and adjacent vehicles. Thus, when speeds are averaged over a short time interval, they should keep their correlations. Surrounding traffic speed was processed from speed measurements before being input into linear regression. Linear regression results are presented in TABLE 7.5.

The adjusted R square of 0.826 in TABLE 7.5, as a measure of goodness-of-fit, indicates the established linear relationship fits the data set. The significance value of 0.000 show the significant linear relationships between y and x. For the resulted regression coefficients, the unstandardized coefficients b for binary variables (x_2 to x_6) reveal the amount of change in y when a binary variable changes from 0 to 1 and other variables remain. For example, if speed limit varies from 80 km/h to 70 km/h (x_4=1), driver compliance will decrease by 26.9%. Thus, among the binary variables, speed limit value (x_4 and x_5) are the most critical variables to driver compliance, amounting to -26.9% and -55.9%, respectively. However, unstandardized coefficients between binary and continuous variables are not comparable. Hence, this study determined the importance of each independent variable x to the dependent variable y by comparing the absolute values of standardized coefficients beta. The impact of variables on driver compliance from high to low is as follows: speed limit of 60 km/h, surrounding traffic speed, speed limit of 70 km/h, weather condition, time of day, activated speed education device, and vehicle type. As desired, higher proportion of heavy vehicles, nighttime and adverse weather result in driver compliance increase.

In addition, spearman correlations explain the full impact of each variable and their correlation with dependent variable. Spearman correlation may range from 0 to 1, indicating the lowest to highest linear correlation. The resulted correlations demonstrated the high linear correlation between driver compliance and speed limit, activated education device and surrounding traffic speed.

7.3.3 Discussion

The statistical tests examined the significant influence of several selected factors on compliance. The linear regression quantified the extent of effect on driver compliance. The regression performance revealed the potential of linear regression in estimating or predicting driver compliance. Overall, speed limit value is the most critical factor. In speed transition zones, the lower a speed limit is, the fewer drivers comply with the speed limit. Also, vehicles tend to follow the speeds of their leading and adjacent vehicles so that surrounding traffic speed also notably affects compliance. For a certain speed limit value, to temporally improve the level of driver compliance, the only way is to implement speed limit education devices. Other commonly used factors in previous driver compliance research, including vehicular, environmental and temporal factors, also have relatively slight impact on driver compliance.

The existence of VSLs dynamically creates speed transition zones. The observations and results should be considered in VSL algorithm design and implementation, especially for model-based proactive algorithms. First of all, in real world, the operational speeds cannot achieve expected VSLs in most of the time. For mobility purpose, VSLs are often placed at the upstream of bottlenecks to limit the discharge flow to the bottlenecks. Without VSLs, the upstream may not encounter congestion during peak hour. However, sometimes VSL even provides speed limit as low as 30 km/h. Driver compliance will be very low in this situation. Equally important, different VSL values cause different driver compliance. Whereas, existing proactive algorithms consider either full compliance or static driver compliance during prediction. Due to this limitation, real-world traffic cannot reach the predicted conditions. Then the prediction-based VSL algorithms may suggest an unreasonable or unachievable speed limit in next time step. Thus, proactive VSLs should dynamically estimate driver compliance and include it in traffic dynamics. Especially for relatively low speed limit, compliance should be cautiously considered. As an illustration, speed dynamics in METANET model should be modified. The free-flow condition of its built-in fundamental diagram needs to include the driver compliance variable. Driver compliance varies according to the changes in the aforementioned factors. If the compliance with one speed limit is low, the predicted traffic speed can hardly reach the optimum. In this situation, the control algorithm will try a lower speed limit to achieve the optimal future traffic speed. Similarly, if the compliance with one speed limit is high enough to the optimal future traffic speed, a higher speed limit will be tried in case of excessive traffic disturbances. Based on dynamic estimation of driver compliance, the predicted speed can better reflect future speed transition.

Secondly, VSLs should reduce step by step in consecutive segments to achieve low speed limits. Sudden decrease of speed limits also result in insufficient driver compliance. In the control algorithm, temporal and spatial constraints for VSL values are required. Thirdly, speed limit education or enforcement devices can increase driver compliance, but the temporal and spatial effect is very limited. Similar with VSL signs, education devices should be installed at locations where drivers are exactly expected to change their speed. Next, this analysis assessed driver compliance with two regulatory (mandatory) speed limits. The generated driver compliance was unsatisfactorily low, not to mention the scenarios under advisory driving speed. Possible low driver compliance should be considered at VSL planning stage. If allowed, regulatory VSLs are preferable. Last but not the least, extensive public education is important. Driver response to speed limit is directly influenced by those from leading vehicles and adjacent vehicles. Public education is the best way to improve overall compliance.

7.4 Summary

VSLs are a promising countermeasure to resolve traffic mobility and safety problem. It aims to adjust upstream discharge flow or smooth bottleneck speed transitions. Driver compliance is a critical factor for control performance. Because of the major role of driver compliance in real-life implementation, this research presented an analysis of the complex driver speed behaviors at speed transition zones. The analysis was conducted by statistical tests and linear regression. The observations and results can guide future VSL algorithm design and implementation.

There are four major findings of this research: 1) Driver compliance varies mainly due to speed limit value, surrounding traffic speed and existence of activated speed education. All the key factors are controllable in filed by strategy design, public education and speed limit education or enforcement tools. Other vehicular, environmental and temporal factors are also significant but their importance is relatively low. 2) All contributing factors exhibit close correlation with driver compliance. Linear regression can reflect most of its features so that it is promising for real-time compliance estimation and prediction. The dynamic driver compliance model is potential to be embedded in the traffic flow prediction model to better prediction traffic evolutions in VSL control. 3) Distinct speed limit yields different level of driver compliance. VSL algorithm design should involve driver compliance estimation or prediction. 4)

Speed education is an effective tool for short-term compliance improvement. Its temporal and spatial impact is limited.

TABLE 7.1. Experiment Plan

Phases	Phase 1: Static Speed Limit Signs	Phase 2: DSDSs set aside static signs							Phase 3: After removal of DSDSs
		On	Off	On	Off	On	Off	On	
Duration (Days)	11	2	12	2	5	7	7	14	14
Date	Jun 10-20, 2010	June 21, 2010 – August 08, 2010							Aug 09-22, 2010

TABLE 7.2. Hypotheses Tests

	Parameters	Hypotheses Test	Hypothesis of Interest (H_a)
Temporal Variations	Average Speed	$H^T{}_0: S_{phase\ 1} = S_{phase\ i}$ $H^T{}_a: S_{phase\ 1} > S_{phase\ i}$	Average speed in Phase i (i =2, 3) is less than that in Phase 1.
	Driver Compliance	$H^T{}_0: CR_{phase\ i} = CR_{phase\ 1}$ $H^T{}_a: S_{phase\ i} > S_{phase\ 1}$	Compliance in Phase i (i =2, 3) is larger than that in Phase 1.
Spatial Variations	Average Speed	$H^S{}_0: S^{sign}_{site\ i} = S^{enforcement}_{site\ i}$ $H^S{}_a: S^{sign}_{site\ i} > S^{enforcement}_{site\ i}$	Average speed is reduced under speed enforcement compared with under static speed limit sign for each site location.
	Driver Compliance	$H^S{}_0: CR^{enforcement}_{site\ i} = CR^{sign}_{site\ i}$ $H^S{}_a: CR^{enforcement}_{site\ i} > CR^{sign}_{site\ i}$	Compliance is increased under speed enforcement compared with under static speed limit sign for each site location.

TABLE 7.3. Speed Parameter Variations

(a) Temporal Variations

Average Parameter Values among samples		Speed Transition Zone 1		Speed Transition Zone 2		Hypothesis on $H^{T}{}_{0}$		
		Site 1	Site 2	Site 3	Site 4	t value	t critical value	Decisions*
Average Speed (km/h)	Phase1	77.61	74.41	67.70	67.15	/	/	/
	Phase 2 (on)	76.06	71.90	67.38	66.34	-5.42	3.62	R
	Phase 2 (off)	76.11	72.48	67.64	65.86	-4.17	4.48	F
	Phase 3	75.91	74.14	67.89	66.29	-3.77	5.04	F
Driver Compliance	Phase1	55.56%	40.37%	58.35%	28.12%	/	/	/
	Phase 2 (on)	57.41%	48.36%	56.40%	30.87%	4.40	3.62	R
	Phase 2 (off)	57.82%	45.94%	55.46%	32.87%	1.09	4.48	F
	Phase 3	57.55%	42.77%	56.48%	31.50%	4.03	5.04	F

*R means reject and F means fail to reject.

(b) Spatial Variations

Parameters for Statistical Tests among Samples		Hypothesis on H^{S}_{0} t value[a]	Decisions[b]
Average Speed (km/h)	Site 1	-2.56	F
	Site 2	-5.89	R
	Site 3	-1.47	F
	Site 4	-3.05	F
Driver Compliance	Site 1	1.35	F
	Site 2	5.05	R
	Site 3	-0.46	F
	Site 4	4.05	R

[a] t critical value =3.62

[b] R means reject and F means fail to reject.

TABLE 7.4. Description of Independent Variables

Independent Variable		Attribute	Value	Mean	SD[a]
Vehicle Type	x_1	Continuous	Percentage of light vehicles	0.95	0.08
Time of Day	x_2	Binary	1 – daytime; 0 – nighttime	0.66	0.47
Weather Condition	x_3	Binary	1 – adverse weather; 0 –favorable weather	0.10	0.30
Speed Limit Value[b]	x_4	Binary	1 – speed limit of 70 km/h; 0 –other speed limit	0.40	0.49
	x_5	Binary	1 – speed limit of 60 km/h; 0 –other speed limit	0.46	0.50
Active Enforcement	x_6	Binary	1 – with active enforcement; 0 – no enforcement	0.63	0.48
Surrounding Traffic Speed	x_7	Continuous	Average speed	69.01	7.51

[a]SD: Standard Deviation

[b]When x_4 and x_5 are both zero, it indicates that the speed limit is 80 km/h

TABLE 7.5. Linear Regression Model Summary

Model Summary								
R^2=0.826			Adjusted R^2=0.826			SE[a] =0.09619		
Variable	Unstandardized Coefficients		Standardized Coefficients	Sig.[b]	95.0% C.I[c] for B		Spearman Correlations
	b	S.E. [a]	beta		Lower	Upper	
Constant	2.555	0.009	/	0.000	2.538	2.571	/
x_1	-0.043	0.007	-0.014	0.000	-0.056	-0.030	-0.095
x_2	-0.008	0.001	-0.016	0.000	-0.010	-0.006	0.081
x_3	0.015	0.002	0.019	0.000	0.011	0.018	0.067
x_4	-0.269	0.002	-0.572	0.000	-0.272	-0.265	0.303
x_5	-0.559	0.002	-1.209	0.000	-0.563	-0.554	-0.530
x_6	-0.008	0.002	-0.017	0.000	-0.011	-0.005	-0.545
x_7	-0.025	0.000	-0.815	0.000	-0.025	-0.025	-0.411

a SE: Standard Error

b Sig.: Significance

c C.I.: Confidence Interval

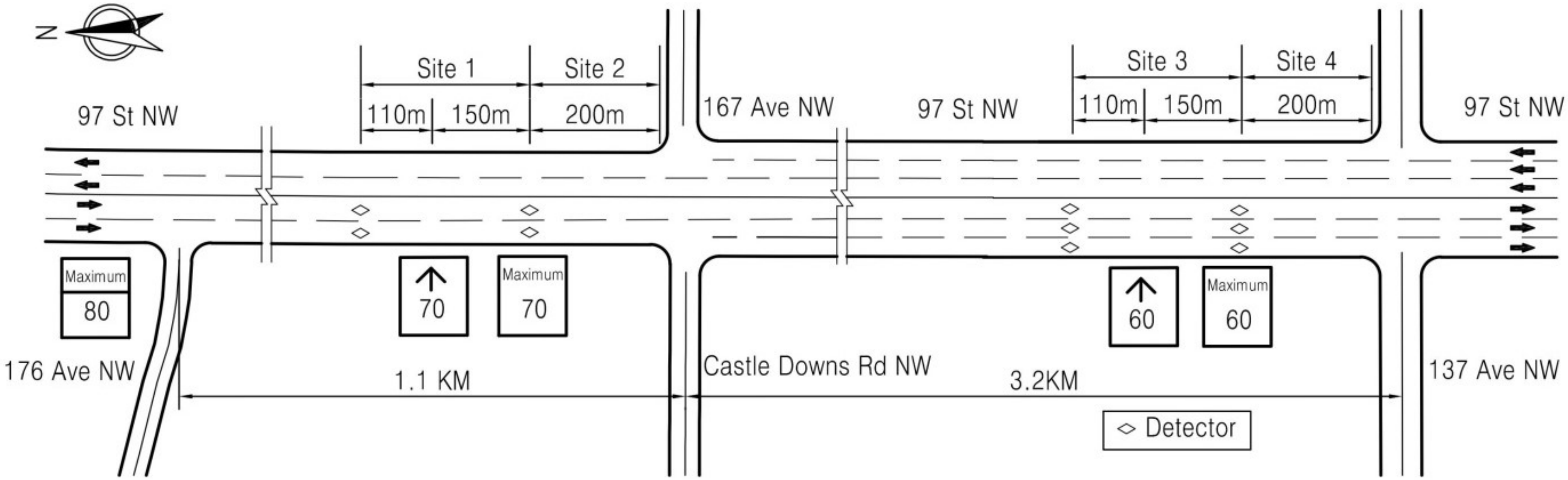

FIGURE 7.1. Layout of the Study Site.

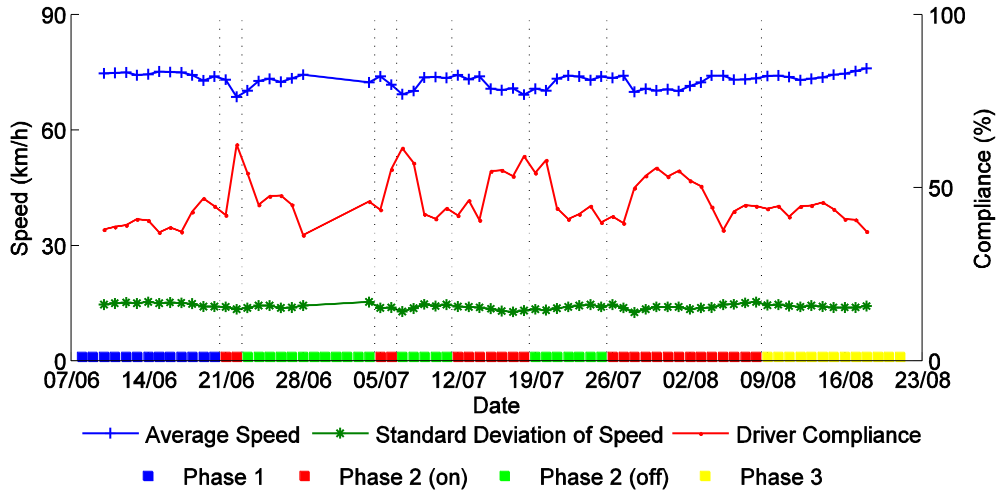

(a) Temporal Variation on Site 2

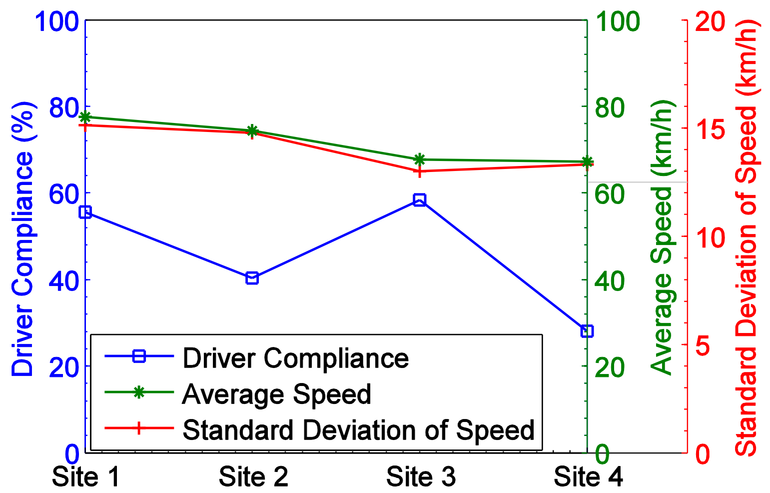

(b) Spatial Variation under Speed Limit Signs

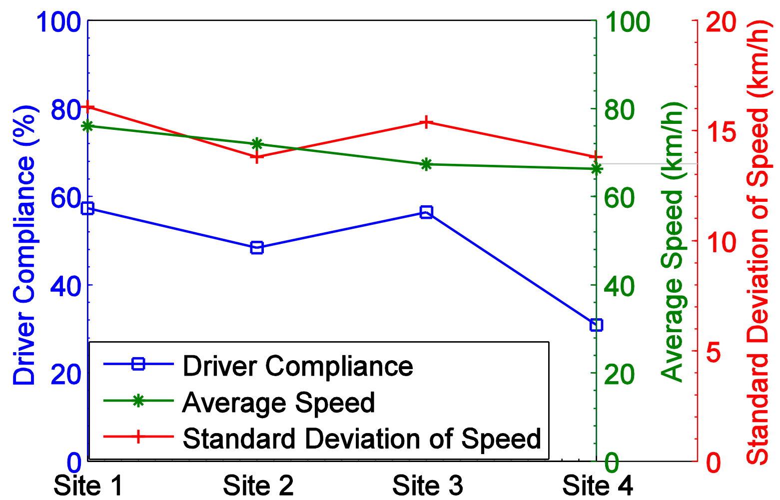

(c) Spatial Variation under Speed Enforcement

FIGURE 7.2. Variations of Speed Parameters.

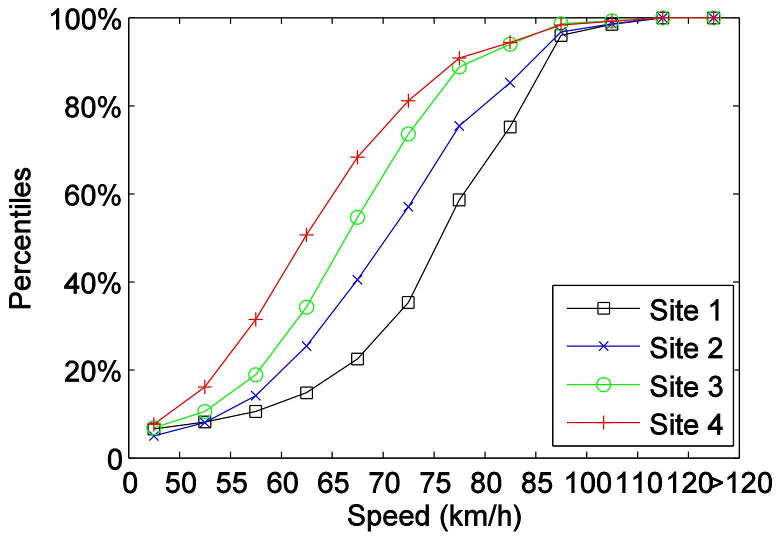

(a) Speed Limit Sign

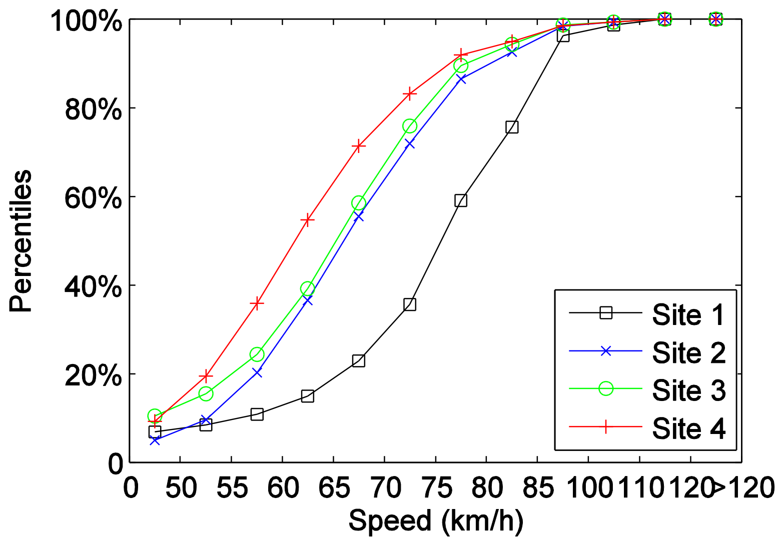

(b) Speed Enforcement

FIGURE 7.3. Percentile Speed Profile.

CHAPTER 8. IMPLEMENTATION OF VARIABLE SPEED LIMITS: PRELIMINARY TEST ON WHITEMUD DRIVE, EDMONTON, CANADA

8.1 Background

Variable speed limits (VSLs) are an intelligent transportation system (ITS) measure that seeks to relieve roadway congestion by limiting flow, and improve safety by homogenizing vehicle speeds. In practice, VSLs have been implemented in the U.S. [108-111] and Europe [112]. VSLs can serve as either mandatory or advisory speed limits; in other words, VSLs can post speed limits that drivers must obey, or act as recommended driving speeds that are not legally enforced. These two categories may generate different levels of driver compliance. In addition, in terms of control algorithms, VSLs can be categorized broadly into rule-based and model-based control. Rule-based VSLs preselect thresholds (e.g. traffic flow, occupancy or mean speed) and make real-time decisions, while model-based VSLs obtain optimal control variables through the optimization of a pre-established model with traffic measurements. So far, most field implementations have used rule-based algorithms.

Rule-based VSL strategies have been widely deployed. For example, the Washington State Department of Transportation (DOT) [108-110] and Florida DOT [111] established an essential principle of VSL strategies: an upstream variable message sign (VMS) displays a reduced speed limit once congestion happens downstream; then, the VMS shows a normal speed limit when the downstream segment recovers from congestion. Updated speed limits and their temporal and spatial variance are constrained by certain safety considerations. Field evaluations have reported that drivers followed VSLs, resulting in reduced stop-and-go frequency and improved traffic safety. However, VSLs in Florida [111] resulted in even more congested traffic situations during rush hours, which was caused by detector failure. It follows then that the control algorithm is critical and the key to VSL reliability. To improve VSL reliability, Minnesota DOT [113] implemented VSLs that required operators to oversee and verify the calculated VSL suggestions. VSLs reduced collisions by 30% and increased capacity by 22%. Furthermore, Chang et al. [114] integrated VSLs with travel time information and conducted a field test to alleviate recurrent bottlenecks. VSLs achieved a higher throughput and smoother speed transitions. The lessons learned from the above field tests can be summarized as follows: 1) a lack of VSL standards and public education may cause driver confusion and even lower driver compliance; 2) VSL control algorithms must reliably generate reasonable rates; otherwise, VSL leads to low driver compliance or worse traffic conditions. Most rule-based strategies apply predefined trigger conditions to adjust VSLs, but they are not designed to adapt to future temporal and spatial variations of congestion. Thus, recent research focuses on model-based VSL strategies.

Model-based VSL strategies are designed as either responsive or proactive. Various studies [6, 10, 53] have evaluated them using simulation tools. Whereas, to the author's knowledge, the only model-based VSL applied in real-world tests is named the SPEed Controlling ALgorithm using Shockwave Theory (SPECIALIST) [65]. It translates the shockwave theory into a practically applicable algorithm. The main steps of SPECIALIST are shockwave detection, solvability assessment, control scheme generation and control scheme application [66]. Even though model-based VSLs have proved to be effective in simulations, especially proactive ones [6, 10], their real-life benefits are still unapparent. The following factors may be attributable:

1) Absence of reliable field application software for proactive VSLs: Most existing software tools are suitable for offline evaluation, but few of them have adopted proactive strategies for online and real-time implementation.

2) Accuracy of prediction models: Proactive VSL features a prediction module. Accurate prediction represents traffic evolutions of free flow, congestion and especially the transitions between them; otherwise, the controller may generate false speed suggestions.

3) High computation time for proactive control: Proactive control, such as model predictive control (MPC), is usually challenged for its excessive computation time during optimization.

To fill in the research gap and overcome the problems mentioned above, this study presents the preliminary test for a VSL strategy implemented on

Whitemud Drive, Edmonton, Canada. The whole proactive VSL strategy is composed of traffic sensors, VMSs, a proactive control software tool, real-time database, and communication component among modules. Among these components, this paper emphasizes its control software tool. The developed software tool, named Dynamic Network Analysis Tool for Active Traffic and Demand Management-Variable Speed Limit (DynaTAM-VSL), realizes proactive VSL based on MPC and is suitable for field applications. FIGURE 8.1 explains the DynaTAM-VSL mechanism. VMSs display the VSL calculated based on predicted downstream traffic conditions. VSL-1 and VSL-2 generally provide lower speed limits than VSL-3. Ideally, all arriving vehicles slow down to the VSL-1 and VSL-2 values, then accelerate to the VSL-3 value so that they can travel quickly and smoothly through the bottleneck segment.

This study reports the preliminary test of the proactive VSL implementation. The preliminary test concentrates on evaluating VSL control performance and reliability. During the field test, five VSLs were deployed along the test bed. The results from this field test serve as a reference for future implementation and move VSL forward to the next phase of permanent applications. The remainder of this study is organized into sections: Section 8.2 describes the VSL field test plan and some field observations of the study site; Section 8.3 briefly introduces the control algorithm; Section 8.4 details the DynaTAM-VSL software structure; and then, Section 8.5 analyzes the performance and reliability of DynaTAM-VSL.

8.2 Proactive Variable Speed Limit Field Test Plan

8.2.1 Variable Speed Limit Implementation Procedure

The deployment of an ITS strategy includes hardware implementation, software design and realization, communication setup and database design and management. Real-time or historical traffic data, video records, incident and weather data are fused and transmitted to the database and software by a certain communication technique. The traffic control countermeasures are then transmitted back to the traffic facilities, e.g. signs and signals. However, to generate reasonable control countermeasures (VSLs in this case), the following steps are required.

- ***Step 1: Process traffic data***

On one hand, traffic data from the sensors need to be checked for consistency and be imputed if necessary. On the other hand, traffic data are collected at a certain interval, which may not match the required time interval in the application. Thus, data smoothing and aggregation must be conducted before being inputted to the control algorithm.

- ***Step 2: Identify possible bottleneck location(s)***

Bottlenecks limit the traffic flow on roadways. VSLs are designed to avoid or postpone the activation of bottlenecks. Bottleneck activation can be identified by occupancy-to-flow ratio [115], occupancy thresholds [116], or speed drop [75, 117, 118]. Once the bottleneck location is identified, the cause of the bottleneck needs to be determined. The common cause is driver behavior changes in response to different geometric features, e.g. curve, weaving or lane drop. Ultimately, all this information supports the placement of VMSs. The basic considerations for determining the location of VMSs are the following: 1) the relative distance between a VMS and a bottleneck; 2) normal vehicular deceleration and acceleration rates; and 3) the visibility of VMSs. Placing a VMS upstream of a bottleneck is recommended. With VMS location information in hand, the design of the control algorithm is explained in Step 3.

- ***Step 3: Design the variable speed limit control algorithm***

The proactive VSLs aim to provide drivers with speed suggestions that are reasonable, reliable and beneficial for traffic mobility and safety. An accurate traffic prediction model should be able to predict future traffic states based on measurements. Equally important, the prediction model should be embedded in a predictive control framework. In this study, a modified METANET model was applied as the traffic prediction model, and embedded in the MPC framework as described in previous research [10].

- ***Step 4: Calibrate and validate prediction model parameters***

The control algorithm always contains some unknown parameters or thresholds. Therefore, these parameters or thresholds need to be calibrated and validated by comparing real and predicted traffic states. This step confirms that the control algorithm represents real traffic evolutions and takes effective control measures.

- ***Step 5: Realize expected functions in DynaTAM-VSL software***

The DynaTAM-VSL software should fulfill all necessary functionalities, including representing detailed network information, managing traffic data, simulating traffic scenarios, measuring performance and optimizing control strategies.

- ***Step 6: Implement and evaluate control performance***

The VSL control is planned to be implemented and evaluated in two stages. The first stage is to perform an offline test without sending VSL results to the traffic network. This stage fixes possible bugs, and makes necessary modifications and adjustments for the software. Essentially, this phase resembles a field scenario with 0% driver compliance. Afterward, the second stage implements VSLs at the study site, and drivers are shown recommended driving speed. This stage focuses on further analysis of the control performance with respect to traffic mobility. During the second stage, the following issues need to be checked: detector data availability and accuracy, database connection, VSL suggestion reasonability and VSL control performance. This study concentrates on the second stage.

8.2.2 Study Site

The westbound direction of an urban freeway corridor, called Whitemud Drive, in Edmonton, Canada, was selected as the test bed for this study. The westbound section from 111 Street to 170 Street has six on-ramps and six off-ramps. Whitemud Drive is a three-lane freeway with a posted speed limit of 80 kilometers per hour (km/h). Serving as a part of Edmonton's inner ring road, the annual average daily traffic (AADT) of its westbound section alone was greater than 90,000 vehicles in 2014 [119]. Also, it experienced a total of 277 accidents in 2012. Due to high peak-hour demand and notable variations in geometric features (i.e. sharp curve, weaving or lane drop), this freeway corridor often suffers from recurrent congestion.

The City of Edmonton has installed vehicle detection stations (VDSs) and traffic video cameras along this corridor. The VDSs are placed on the roadway mainline, on-ramps and off-ramps. They collect traffic data, such as volume, speed and occupancy every 20 seconds (s), and send the data to the City's central computer system for archival. Complete historical data from VDSs are available from 2011 to 2015. FIGURE 8.2 schematically shows VDS and camera locations.

8.2.3 Bottleneck Identification

The scope of this study is limited to relieving recurrent bottlenecks. As Edmonton often experiences adverse weather conditions in winter, the weather records for bottleneck identification were checked to ensure there was enough visibility for driving. Also, the traffic incident records of this corridor were checked to eliminate the impact of incidents. From the daily measurements, on an average weekday, the AM and PM peaks start at 7AM and 4PM respectively. After the onset of the congestion, the speed drops fast, from 80 km/h to as low as 20 km/h. FIGURE 8.3 shows the speed contour maps for westbound sections, plotted from loop detector data on May 14th, 2015. As observed, two recurrent bottlenecks are often activated. One is a two-sided weaving segment from the on-ramp of 122 Street to the off-ramp of Terwillegar Drive. The other one originates near Fox Drive. Its upstream segment carries high traffic demand but little traffic exits using the Fox Drive off-ramp. At the same time, the number of lanes drops from four to three. In this sense, this segment can be defined as a virtual lane drop segment.

In summary, based on field observations and bottleneck information, the weaving segment after 122 Street on-ramp and the segment around Fox Drive were selected as critical segments for VSL control implementation. Five sets of portable VMSs were placed. Their locations are presented in FIGURE 8.2. The VSLs in this study function as advisory driving speeds. Driving speeds during peak periods are recommended to drivers but not enforced.

8.3 Variable Speed Limit Control Algorithm

For the purpose of implementation, DynaTAM-VSL applies the control algorithm developed by Hadiuzzaman et al. [10], which was proved to be effective in simulation [10, 90, 120]. It is designed to mitigate congestion during peak hours, and its main objectives are to reduce vehicle travel time as well as to accommodate more vehicles in the traffic network. Within an MPC-based control framework (as manifested in FIGURE 8.4), the control algorithm collects traffic flow data, predicts future traffic states, and optimizes and applies control variables. Referring to the modules shown in FIGURE 8.4, the data collection module performs traffic data extraction, imputation, smooth processing and aggregation; the traffic state prediction module applies a METANET-based traffic flow model to predict traffic evolutions in the near future; and the optimization module calculates the optimal control set according to a specific objective function.

Traffic measurements $\boldsymbol{x}=\left[\rho_i(k), v_i(k)\right]$ (ρ is traffic density and v is traffic speed) are collected at each time step k. At each time step of prediction horizon N_p, the prediction module takes current measurements $\boldsymbol{x}$ and predicts traffic state $\boldsymbol{x}$ based on the density and speed dynamics, which were modified by Hadiuzzman et al. [10] from the original METANET model [14]. In order to replicate the control consequence under VSLs, the prediction module includes the vector of VSL values $\boldsymbol{u}$. On the other hand, at each control time index k_c, the control algorithm optimizes the vector of VSL values u^*. The selected objective function J is expected to achieve optimal traffic states by finding the future trend of VSL values. The optimization problem considers temporal, spatial and discrete constraints.

In this study, the control horizon N_c is one minute and the prediction horizon N_p is five minutes. Every minute, optimal control inputs are generated by prediction and optimization for the next five minutes. The rolling horizon scheme in MPC assumes that only control inputs for the first minute are actually applied in the traffic network. The control inputs calculated for next four minutes are not actually implemented but only work as initial guesses for the next cycle. Detailed introductions to the prediction model, control algorithm and solution technique have been presented by Hadiuzzman et al. [10] and are not repeated here. During the field test, for the operator's convenience, the updated VSL values stayed for 5 minutes and then another cycle started.

8.4 DynaTAM-VSL Software Implementation

DynaTAM-VSL software can analyze, simulate and optimize traffic networks in offline or online mode. It was coded with C++ based on an object-oriented design, and achieved several functionalities. FIGURE 8.5 demonstrates the integration of DynaTAM-VSL with all components. Details of the integration are described below.

8.4.1 Real-time Data Collection and Storage

The traffic data collection devices take measurements from the traffic network and send them to the City of Edmonton’s database. DynaTAM-VSL retrieves necessary data from the database and organizes and stores them. It utilizes Standard Template Library (STL) to organize the data structure so that the fewer pointers and structured text files are needed. In case of occasional sensor failures or data transmission problems, DynaTAM-VSL performs a data consistency check and imputation prior to its use in the control algorithm. Lastly, DynaTAM-VSL stores the data in the Structured Query Language (SQL) server as “Whitemud Traffic Database” using Microsoft Access. In addition, the database applies “hash_map” to improve the efficiency of data searches and path storage.

8.4.2 Optimization of Control Algorithm

DynaTAM-VSL extracts real-time and historical traffic data to estimate current traffic states. With the information in hand, the current traffic state is illustrated in the user interface. The color of each link indicates the severity of traffic congestion. Subsequently, future traffic states are calculated by the prediction model. The proactive control performs using the rolling horizon concept of MPC, as explained in the last section.

8.4.3 Variable Speed Limit Implementation

When obtaining the optimal values for VSL control variables, DynaTAM-VSL stores the optimal speed limit values and their control performance measurements in its database. At the same time, it sends a message containing the suggested speed limits to an operator in the Transportation Management Center (TMC) of the City of Edmonton. To ensure a reasonable speed limit suggestion, this operator is in charge of confirming and posting suggested speed limits. The operator can decide whether to accept the proposed speed limits by observing the real-time traffic via traffic video cameras. If the operator accepts the request, the VSLs are displayed on the VMSs using wireless communication, under the National Transportation Communications for Intelligent Transportation System Protocol (NTCIP). Any action by the operator is recorded in the database.

8.5 Analysis of Online Test Results

8.5.1 Flow Pattern

As traffic flow fluctuates from day to day, this analysis selected weekdays in the year of 2015 with similar traffic flow patterns to evaluate VSL control performance. For the no-control case, no VMS was placed on the roadside. In the VSL-control case, VMSs were placed and activated during peak hours. The preliminary VSL tests were conducted from August 11th to September 4th, 2015. The VSL control was operated during AM and PM peaks (6:30 AM-8:30 AM and 4:30 PM- 6:30 PM). Recurrent congestion happened at Bottleneck 1 during PM peaks. Hence, the time period from 4:30 PM to 6:30 PM was selected for the analysis below. FIGURE 8.6 (a) and FIGURE 8.7 (a) plot five-minute aggregated volume variations from VDS 1018 over time. These figures present the no-control (May 14th and May 20th) and VSL-control (August 12th and August 26th) cases, respectively. Both days experienced recurrent congestion at Bottleneck 1. The plots indicate that traffic patterns were stable regardless of the VSL deployment. As a result, they are comparable in the before-and-after VSL evaluation.

In addition, a statistical significance t-test was applied to identify whether the flow patterns from the VSL-control and no-control cases are significantly different. A confidence interval of 95% was chosen. Its corresponding t-critical value for the two-tailed test was 1.98. TABLE 8.1 summarizes the statistical test results for two days with similar flow patterns.

Since all t-statistics values are lower than the t-critical value, it verifies that there was no vital difference between the flow profiles of each of the two days compared.

TABLE 8.1 also lists the results for VSL performance evaluation, including average speed, total travel time (TTT, in vehicle hours, veh*h) and total travel distance (TTD, in vehicle kilometers, veh*km). The detailed analysis is presented below.

8.5.2 Speed Comparison

Theoretically, the deceleration and acceleration when vehicles pass a congested bottleneck cause a drop in capacity. VSLs reduce upstream discharge flow by lowering the speed limits, and subsequently increase speed limits after vehicles pass downstream bottlenecks. VSLs reduce vehicle travel time and avoid or relieve the occurrence of congestion and capacity drop. In this way, VSLs smooth speed transitions and reduce stop-and-go conditions. FIGURE 8.6 (b) and FIGURE 8.7 (b) present the speed profiles at Bottleneck 1, as well as the VSL rates. As desired, on the whole, the speeds on bottleneck segments under VSL control were higher than those under the no-control scenario. The bottleneck speeds were increased by VSL control and the drastic speed drop was prevented. Quantitatively, VSLs increased the average speed from 59.87 km/h to 73.06 km/h at Bottleneck 1 on August 12th. Likewise, the average bottleneck speed was increased from 65.27 km/h to 74.04 km/h on August 26th. VSL control smoothed the speed transitions between free flow and congestion, and ensured a stable traffic flow and safe driving environment. In addition, the variation trend of VSL rates was close to that of bottleneck speeds. This indicates that the traffic prediction model built in the control can predict traffic changes, particularly for speed drops. During the test, VSL-1 and VSL-2 were given the same VSL rates. For VSL-1, the segment speed in historical peak-hour data was generally free flowing. The suggested speed was lower than its peak-hour speed. It proves the suggested speed limits are reasonable and achievable. Reasonable and achievable speed suggestions encourage drivers to cooperate in improving traffic mobility, rather than confuse them and result in worse conditions.

Standard deviation of speed (SDS) was revealed to be the highest statistically significant variable that impacts traffic collisions. In this case, SDS was calculated every five minutes. Accordingly, FIGURE 8.6 (c) and FIGURE 8.7 (c) compare time-varying SDS at Bottleneck 1 under no-control and VSL-control cases. Take FIGURE 8.6 (c) as an example. SDS in the no-control scenario varied from 4.5 km/h to 17.7 km/h. Particularly at the beginning of the PM peak, the SDS started to rise to as much as 14 km/h. This suggests a high probability of collisions and congestion occurring. After VSL deployment, SDSs fluctuated from 3.3 km/h to 15.1 km/h during the PM peak. VSLs reduced SDS impressively overall and improved traffic safety.

8.5.3 Comparison of Travel Time and Throughput

Shorter travel time is the main direct benefit for drivers, and more discharged traffic is a major concern for traffic agencies. Hence, the objectives in the VSL optimization problem are to minimize TTT and, meanwhile, maximize TTD. Equations (8.1) and (8.2) calculate TTT and TTD. TTT is related to traffic density. Thus, during one control horizon, minimizing TTT reduces mainline density and mitigates congestion, but may prevent vehicles from entering the traffic network. Whereas, TTD is related to traffic flow. Maximizing the TTD at the same time can improve traffic throughput and accommodate more vehicles in the mainline. Although no-control and VSL-control cases may result in similar TTD across the whole time period, their TTDs for each step of the control horizon may be distinguished.

$$TTT = T\sum_{j=1}^{N_p-1}\sum_{i=1}^{N_m}\lambda_i L_i \rho_i\left(k+j\right) \tag{8.1}$$

$$TTD = T\sum_{j=1}^{N_p-1}\sum_{i=1}^{N_m}\lambda_i L_i \rho_i\left(k+j\right)v_i\left(k+j\right) \tag{8.2}$$

where, T is the length of a discrete time step (20 s in this study); L and λ are segment length and number of lanes.

On August 12th, when only Bottleneck 1 was considered, TTT was reduced from 221.07 veh*h to 169.75 veh*h in the control case for the whole PM peak. Meanwhile, TTD was similar in both cases as their traffic demand were similar. These results suggest that the VSL control improves traffic mobility. Also, at the corridor level, TTT achieved 1,134.7 vehicle hours (veh*h) in the no-control case and 1,104.9 veh*h in the VSL-control case in total. The implemented VSL decreased TTT by 2.6%. Similarly, TTD reached 77,482.7 vehicle kilometers (veh*km) in the no-control case and 87,928.8 veh*km in the VSL-control case. Similar observations can be found for August 26th. Thus, upstream flow control can benefit downstream traffic flow.

FIGURE 8.6 (d) and (e) exhibit the evolutions of TTT and TTD at the bottleneck. When FIGURE 8.6 (d) and (e) are analyzed combined with FIGURE 8.6 (b), the performance of VSL can be demonstrated. After 4:30 PM, when the traffic demand gradually increased, DynaTAM-VSL worked by applying VSL values from high to low. Due to its prediction module, DynaTAM-VSL is capable of predicting traffic states in the near future and applying corresponding control variables. That is why the VSL decreased before a speed drop could occur at the bottleneck. The speed control in advance can reduce traffic flow and prevent speed drop at the bottleneck. This effect is obvious between 4:30 PM to 5:10 PM in FIGURE 8.6 (b). During this period, the driver compliance was high, and the TTT in the VSL-control case was less than that in the no-control case. However, as the demand increased after 5:10 PM, the bottleneck speed suddenly dropped from 80 km/h to 40 km/h, approximately. The VSL value decreased simultaneously. Restricted by the VSL maximum variance (10km/h) and VSL rate duration (5 minutes) in the algorithm, VSL changes could not keep up with the speed drops. When the VSL reached 40 km/h, the traffic flow was limited to a low level so that speed at the bottleneck started to increase. The time when the bottleneck speed returned to free-flow speed speed in the VSL-control case was 15 minutes earlier than in the no-control case. VSL control shortened the congestion duration and saved drivers' travel time.

At the beginning of the field test, for operators' convenience, the updated VSL values were implemented for five minutes and then another cycle started. After a problem with the VSL rate duration was found, the duration was reduced to one minute from August 17th onward. Thus, FIGURE 8.7 (b) shows a more reasonable profile of speed suggestions but more frequent speed variations. The frequent speed variation may risk traffic safety. TTT on the bottleneck was decreased from 198.13 veh*h to 167.87 veh*h on August 26th. FIGURE 8.7 (d) and (e) show the benefits from VSL control in detail. In addition to the two comparisons above, the performance evaluation results are given in TABLE 8.1.

In summary, this proactive control approach can predict bottleneck states and forecast whether a bottleneck will be triggered. When an active bottleneck is signaled, the VSL rates are lowered to prevent upstream flow from reaching bottleneck capacity. When the bottleneck activation signal is lifted, the control reverts to higher VSL rates and discharges more vehicles from the mainline. The measures of effectiveness under proactive control, including average speed, SDS, TTT and TTD, outperformed those under no control.

8.6 Summary

Excessive peak-hour demand triggers recurrent bottlenecks and constrains discharge flow on freeways. Simulation tests have exhibited the benefit of proactive freeway control algorithms for relieving recurrent bottlenecks. Compared with reactive freeway control algorithms, proactive algorithms take advantage of their prediction module. Unfortunately, real-life performance of proactive control is still unapparent, so this paper presents a field evaluation of proactive VSL control realized by DynaTAM-VSL. The preliminary test was completed on a freeway corridor and indicated that proactive VSL control is reasonably effective.

There are four major findings of this research: (1) in the preliminary test, DynaTAM-VSL suggested reasonable and reliable speed limits and favorable driver compliance; (2) DynaTAM-VSL achieved improved average speed at the bottleneck and reduced TTT over the corridor; (3) well-established proactive control strategies are efficient and applicable in real-time field implementation; and (4) proactive control benefits from its prediction module, which considers future traffic evolutions in advance.

TABLE 8.1. VSL Performance during the Test

Comparisons		Demand Pattern	Average Speed at Bottleneck 1 (km/h)		TTT at Bottleneck 1 (veh*h)		TTD at Bottleneck 1 (veh*km)	
VSL Control	No Control	T-stat Value	VSL Control	No Control	VSL Control	No Control	VSL Control	No Control
Aug. 12	May 14	0.82	73.06	59.87	169.75	221.07	10957	10986
Aug. 17	May 25	0.12	72.66	69.12	169.62	183.39	11181	11083
Aug. 18	May 05	0.34	76.73	64.44	160.23	205.18	11616	11131
Aug. 20	May 14	0.47	79.40	59.87	144.31	221.07	10860	10986
Aug. 25	May 05	0.19	74.67	64.44	170.03	205.18	11475	11131
Aug. 26	May 20	0.86	74.04	65.27	167.87	198.13	11472	11289
Aug. 27	May 14	0.55	73.96	59.87	169.28	221.07	11537	10986

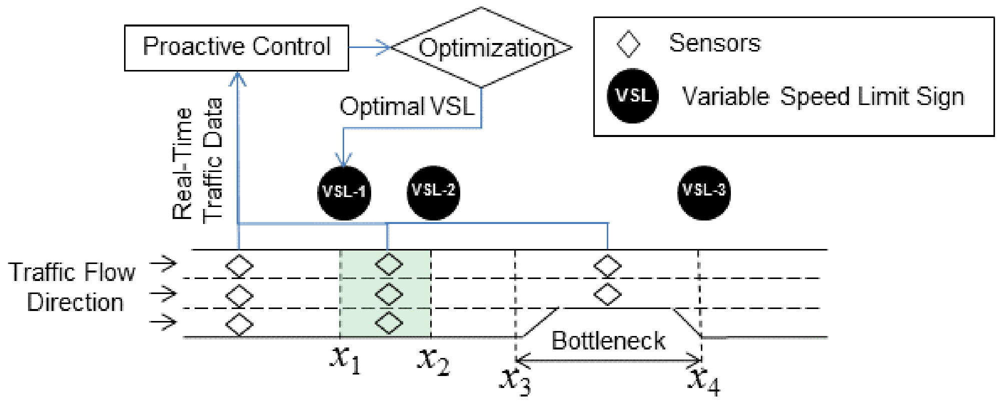

FIGURE 8.1 DynaTAM-VSL Mechanism.

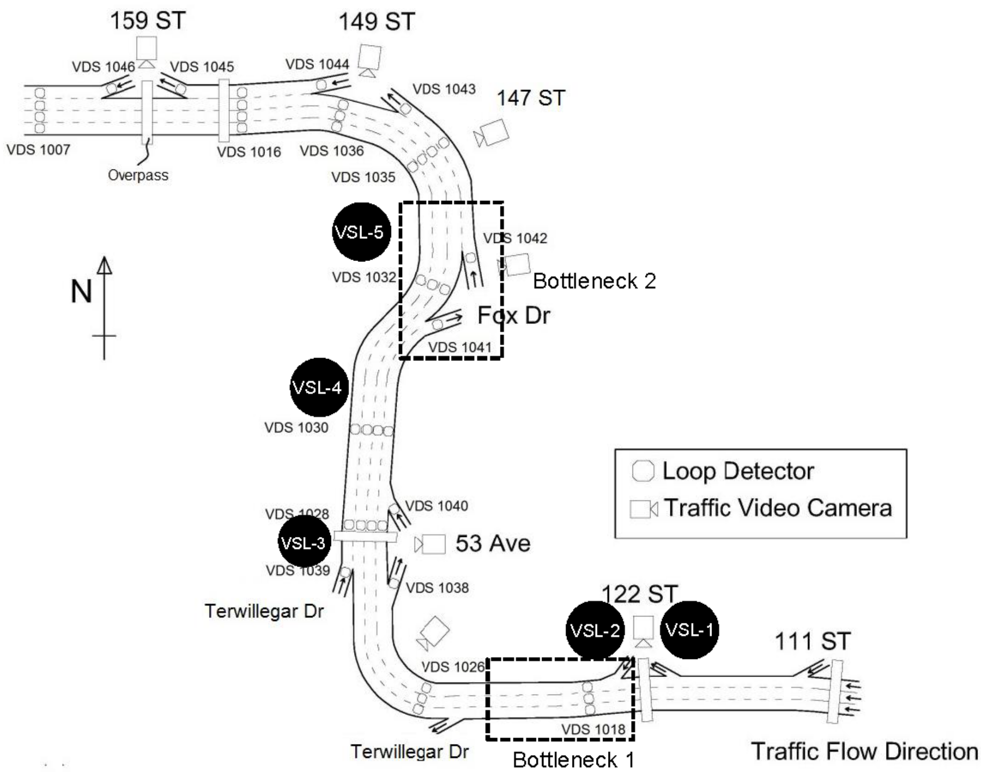

FIGURE 8.2 Study Site.

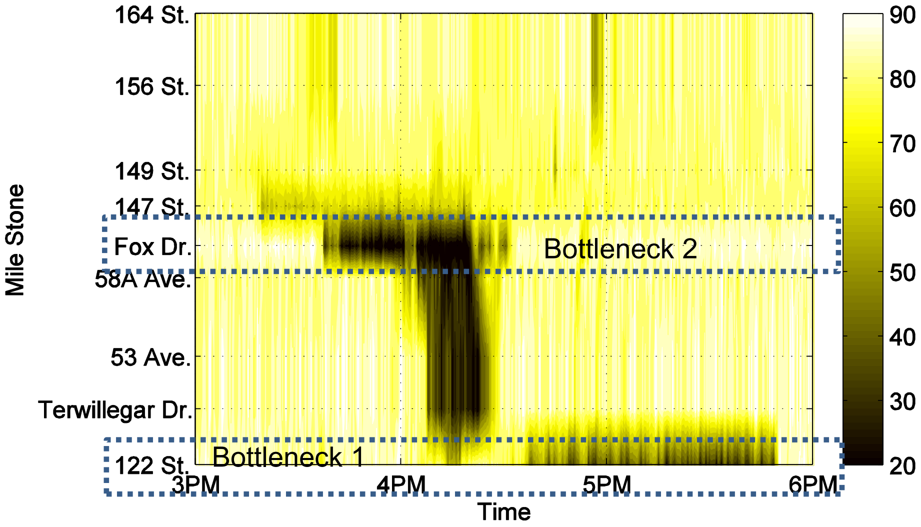

FIGURE 8.3 Speed Contour Maps, May 14, 2015.

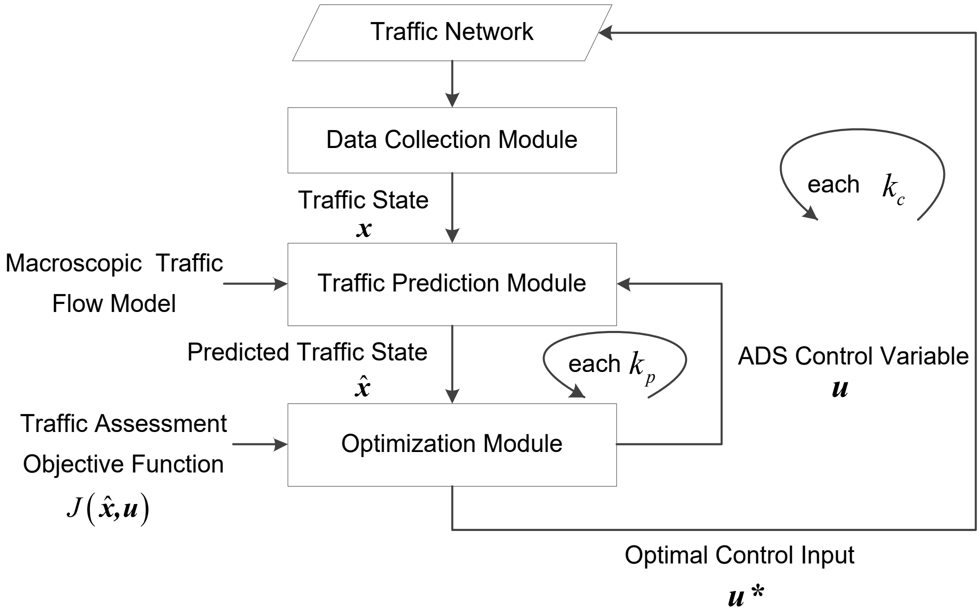

FIGURE 8.4 MPC-based Control Framework.

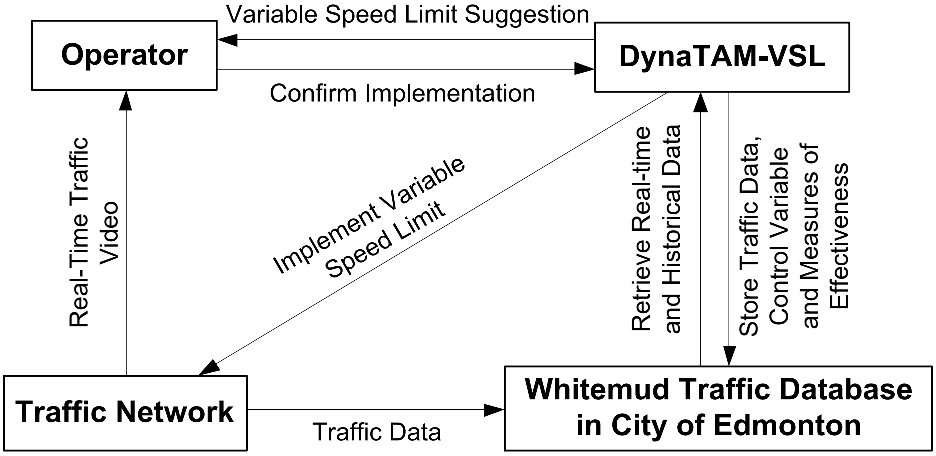

FIGURE 8.5 Integration of DynaTAM-VSL.

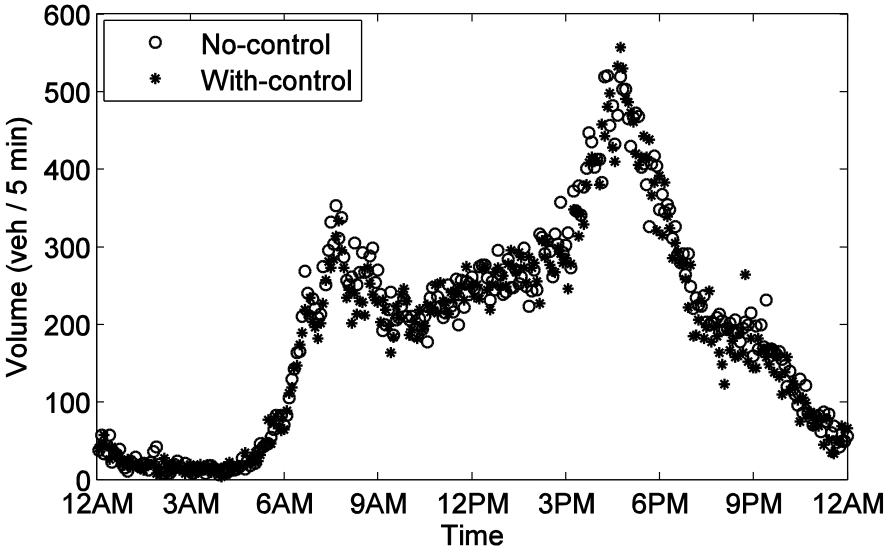

(a) Distributions of Traffic Volume

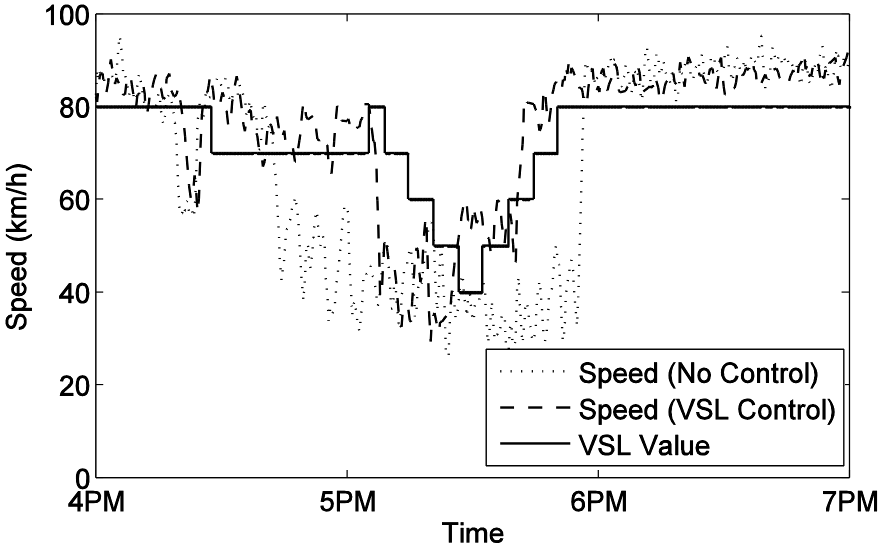

(b) Speed Profiles and VSL Signal for VSL-2

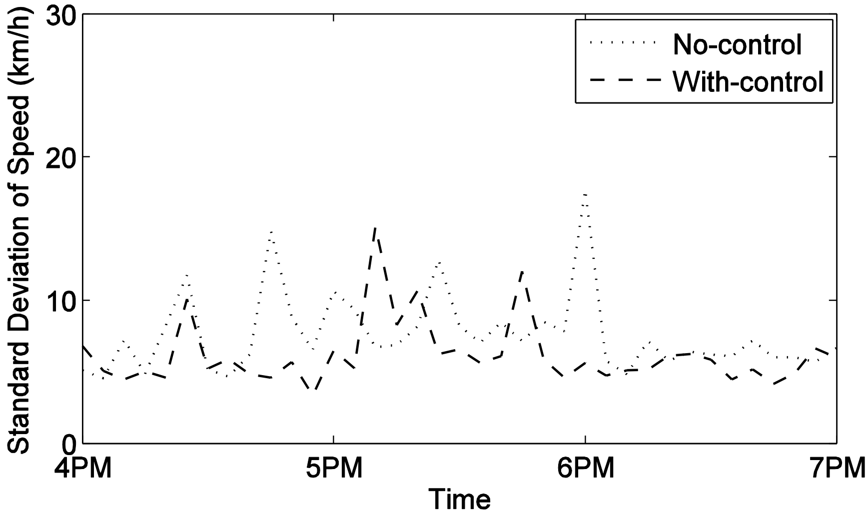

(c) Time-Varying Standard Deviation of Speed

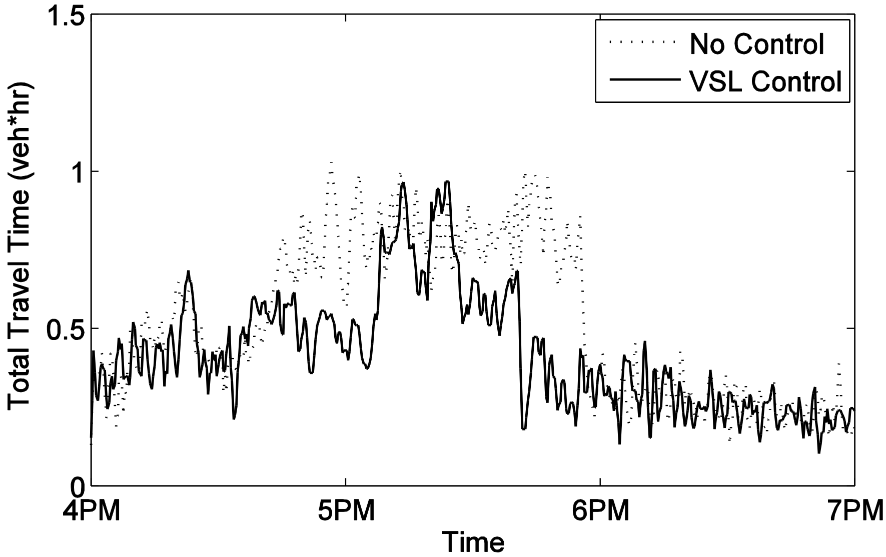

(d) Evolution of TTT during the PM Peak

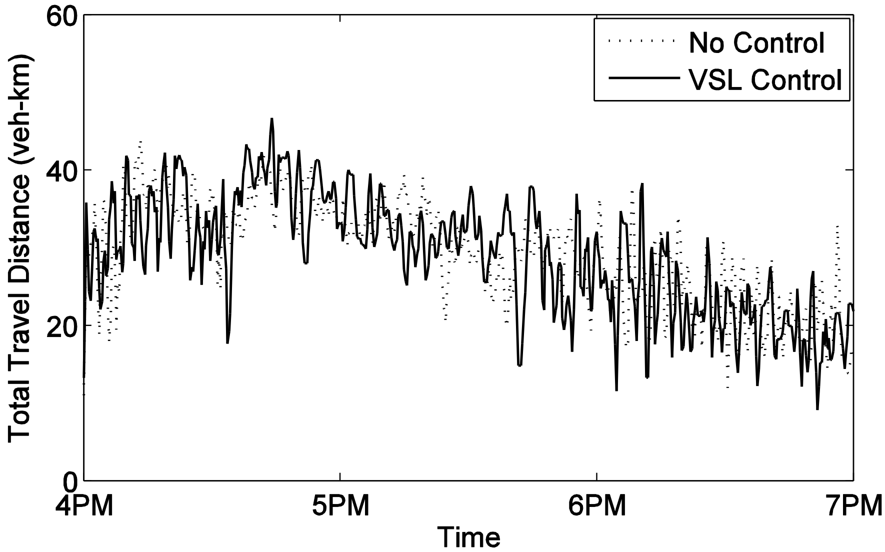

(e) Evolution of TTD during the PM Peak

FIGURE 8.6 Comparisons between No-Control (May 14th) and VSL-Control (Aug 12th) Scenarios at Bottleneck 1.

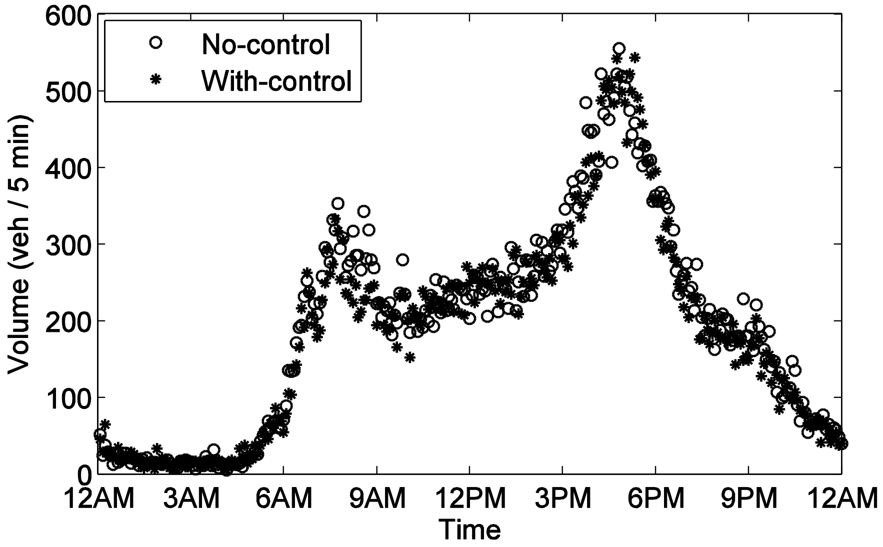

(a) Distributions of Traffic Volume

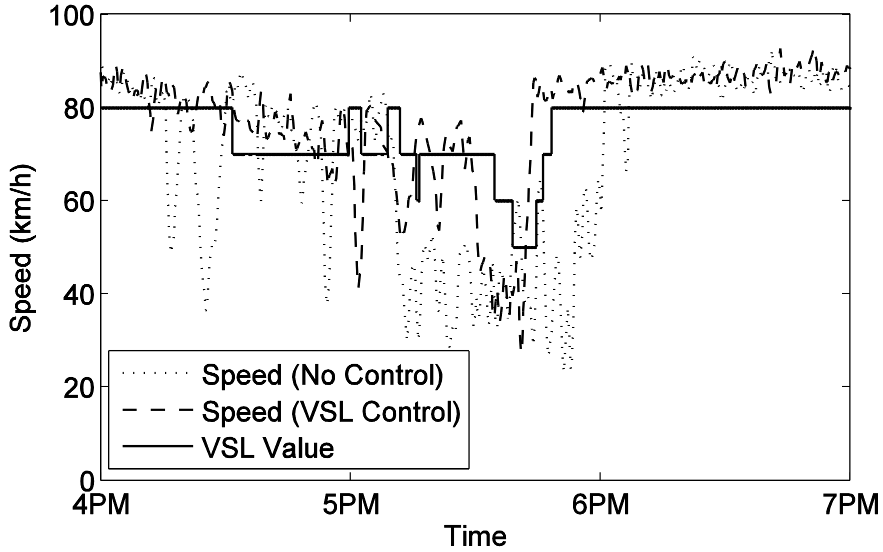

(b) Speed Profiles and VSL Signal for VSL-2

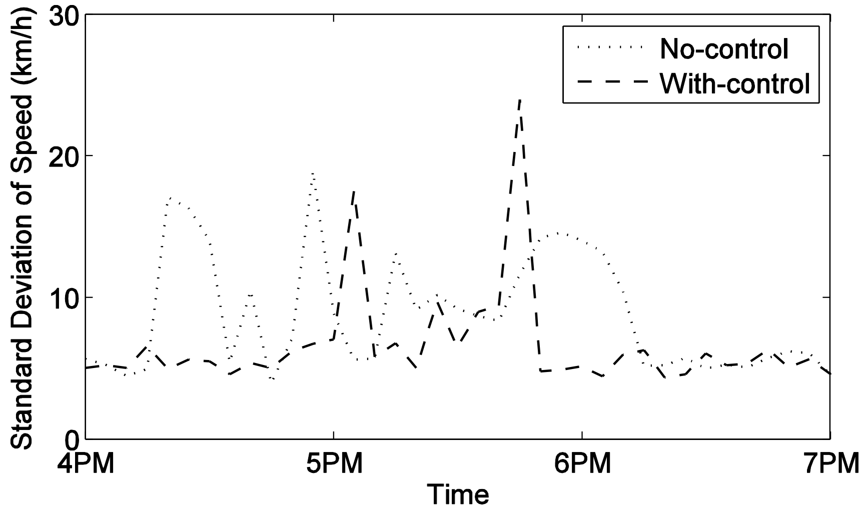

(c) Time-Varying Standard Deviation of Speed

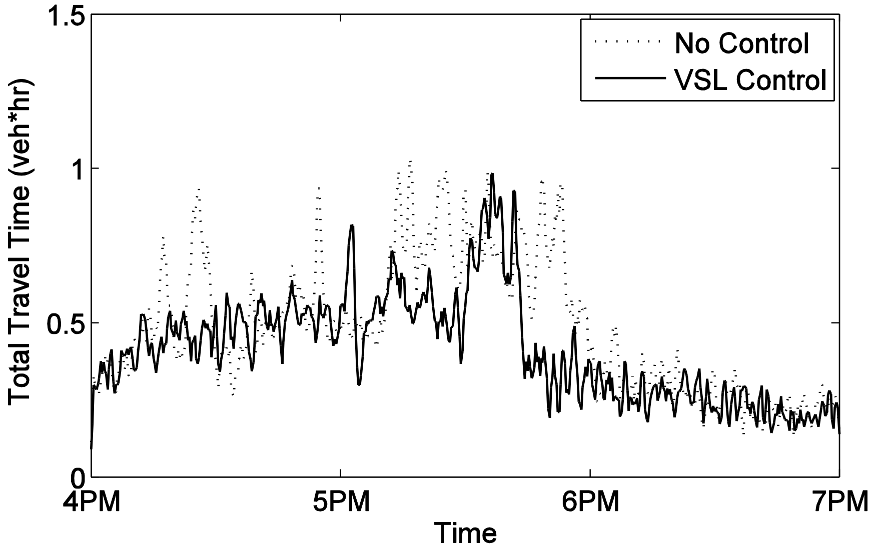

(d) Evolution of TTT during the PM Peak

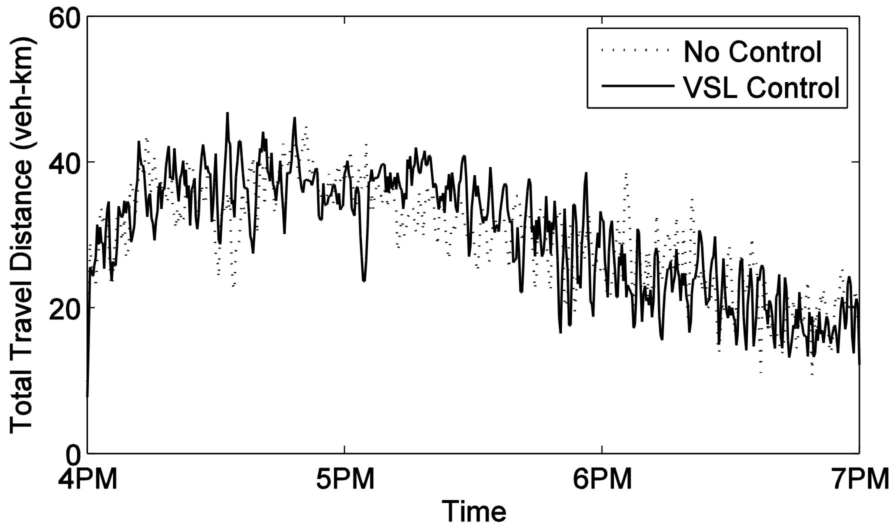

(e) Evolution of TTD during the PM Peak

FIGURE 8.7 Comparisons between No-Control (May 20th) and VSL-Control (Aug 26th) Scenarios at Bottleneck 1

CHAPTER 9. CONCLUSIONS AND FUTURE RESEARCH

9.1 Conclusions

This research studies several important issues in freeway proactive integrated control. They include prediction model calibration and validation, RM control considering dynamic weaving capacity estimation, theoretical model development for weaving capacity estimation, mainline and ramp flow interaction under integrated control, effect of speed limits at speed transition zones and preliminary VSL field test. Main findings of this research are concluded as follows.

CHAPTER 3 calibrated and validated a modified METANET model for a complicated corridor, where multiple bottlenecks exist. According to the calibration and validation results, the following main conclusions were obtained:

(1) The METANET model with modifications can generally reflect and predict real traffic states under complex traffic conditions with multiple bottleneck locations. The modification of METANET accommodates the unpredictability of bottleneck activation. METANET is applicable as a prediction module in proactive traffic control implementation, such as the VSL or RM field test on the study site.

(2) The speed dynamics in METANET is a weighted summation of traffic state change inducements: speed at the last time step acts as a baseline

for prediction; the relaxation term makes the predicted speed follow the fundamental speed-density relationship; and the convection term and anticipation term consider the impact of upstream speed and downstream density respectively. All terms collaborate and contribute to model prediction accuracy, but they may cause prediction errors as well.

(3) The obtained values for parameters τ, η, and κ from calibration give the feedback for the model prediction performance. The values of segment-specific parameters show the driver behavior characteristics.

(4) The prediction performance by segment-specific parameters surpasses that by global parameters, despite the potential problems produced by the segment-specific parameters.

After the prediction performance of METANET model was verified, CHAPTER 4 proposed a METANET-based traffic flow model, DynaTAM-RM, which was considerate of dynamic weaving impacts. DynaTAM-RM was used within an MPC framework. DynaTAM-RM, providing real-time estimated weaving capacity, was evaluated and analyzed on the WMD test bed. There are four major findings of this study.

(1) Weaving segment capacity drop was observed at bottleneck activation, which reveals the necessity of considering weaving capacity.

(2) According to the weaving capacity estimation model and its sensitivity analysis, the proposed RM control is a promising congestion mitigation method.

(3) The RM control variables were optimized in MPC by DynaTAM-RM considering dynamic weaving capacity.

(4) DynaTAM-RM with dynamic weaving capacity was simulated, evaluated and shown to be effective: the model provided a 9.71% decrease in TTT, a 3.32% increase in TTD and an 8.40% increase in TF, all of which were better improvements than those made with a static weaving capacity.

Weaving capacity estimation model can enhance freeway operation strategies. CHAPTER 5 proposed a capacity estimation approach that combined linear optimization with a lane changing model. This method was evaluated in two authentic weaving segments and found to be reasonably accurate. There are four major findings of this research.

(1) Most lane changes happen near the merge gore, which can be considered the critical region, and the capacity there can represent the whole weaving segment.

(2) The proposed approach provides similar results compared with HCM 2010 results and field observations.

(3) When the weaving flow ratio is small, an increased number of weaving vehicles rarely changes weaving capacity, whereas, when weaving ratio is moderate or large, weaving behaviors notably decrease weaving capacity.

(4) The proposed approach can capture real-time maximum discharge flow, which is a main input for traffic operation strategies.

CHAPTER 6 emphasized the applicability and effectiveness of a proactive integrated approach of RM and VSL. It adopted a METANET-based traffic flow model, DynaTAM-RM&VSL, within an MPC framework. By implementing this proactive control approach in a micro-simulation model, there are three major findings.

(1) Proactive VSL and RM, no matter they are isolated or integrated, generally improves freeway mobility. After decoupling prediction and simulation models, the unsatisfactory performance originates from the built-in prediction model. Their benefits can achieve up to 20% in TTT and 3.4% in TTD, changing along with different combinations of mainline and on-ramp demand.

(2) Considering the same demand scenario, control performance among strategies differs. RM helps only for short congestion duration scenarios with relatively low mainline and ramp demand. As mainline carries more controllable flow, VSL outperforms RM when mainline and ramp demand is higher. However, if demand is extremely high, as most cases presented, isolated control cannot meet the operational requirements. Integration between RM and VSL maximizes their own benefits and infrastructure utility.

(3) In integrated control, RM reacts before VSL. When demand keeps increasing, VSL takes over the control until congestion continues to grow. During the most congested period, RM and VSL work simultaneously. After

then, RM is deactivated in case of long ramp queue. At the end of congestion, RM is activated occasionally to deal with remaining traffic disturbance.

CHAPTER 6 could guide strategy selection during ATDM planning stage. Prior to implementation, the causes of recurrent congestion are required to be carefully analyzed. RM strategies are good for relieving short period congestion in peak hours without disturbing mainline traffic. Appropriate metering rates can improve freeway mobility and balance temporal equality between mainline and ramp vehicles. VSL functions under a higher demand taking the risk of spreading congestion further upstream. The performance from integration of RM and VSL exceeds isolated strategies for much severer congestion. Proactive integrated control is potentially implementable in the field. If appropriately designed, the proposed integrated approach can lead to better network-wide mobility performance.

RM is a mandatory traffic control but driver response to VSL is complex. CHAPTER 7 presented an analysis of the complex driver behaviors at speed transition zones. The analysis was conducted by statistical tests and linear regression. The observations and results can guide future VSL algorithm design and implementation. There are four major findings.

(1) Driver compliance varies mainly due to speed limit value, surrounding traffic speed and existence of active speed enforcement. All the key factors are controllable in filed by strategy design, public education and

enforcement. Other factors are also significant but their importance is relatively low.

(2) All contributing factors exhibit close correlation with driver compliance. Linear regression can reflect most of its features so that it is promising for real-time compliance estimation and prediction.

(3) Distinct speed limit yields different level of driver compliance. VSL algorithm design should involve driver compliance estimation.

(4) Speed enforcement is an effective tool for short-term compliance improvement. Its temporal and spatial impacts are limited.

CHAPTER 8 presents a field evaluation of proactive VSL control realized by DynaTAM-VSL. The preliminary test was completed on a freeway corridor and indicated the proactive VSL control to be reasonably effective. There are four major findings of this research.

(1) In the preliminary test, DynaTAM-VSL suggested reasonable and reliable speed limits and favorable driver compliance.

(2) DynaTAM-VSL achieved a 12.4% improvement in average speed at the bottleneck and a 2.6% reduction in TTT over the corridor.

(3) Well-established proactive control strategies are efficient and applicable in real-time field implementation.

(4) Proactive control benefits from its prediction module, which considers future traffic evolutions in advance.

9.2 Recommendations for Future Research

Freeway control is a complicated research area, which involves various research aspects. From this research, several potential future research topics are identified. The recommendations for future research are list below.

(1) Macroscopic traffic flow model needs to be calibrated and validated in traffic control scenarios, other than in no-control scenarios. Traffic control strategies may change driver behaviors. Model parameters under traffic control have to be identified and compared those under no-control scenarios.

(2) The physical relationship between weaving capacity and its characteristics (e.g., gap acceptance behaviors at weaving segments) needs to be theoretically developed. Driver maneuvers at weaving segments are complicated as observed in this research. Microscopic driver behaviors at weaving segments require more investigation based on detailed vehicle trajectory data.

(3) The capacity estimation model needs to be implemented in integrated traffic operation strategies. Mainline and on-ramp flows at weaving segments are controlled by integrated control and also impact on weaving capacity. The proactive integrated control applies the theoretical weaving capacity estimation model can assess the model performance and the control improvement after considering weaving capacity estimation. Essentially, the estimation model can be applied to dynamic maximum discharge flow estimation. When a bottleneck is going to be or is already triggered in a weaving segment, it could help to find

an optimal discharge flow rate from mainline and on-ramps. Then, by deploying a proper control rate, actual input flow rate in the weaving bottleneck can be adjusted. This can mitigate bottleneck severity. In the future, this research will be directed to develop dynamic traffic control strategies that can be implemented to relieve bottleneck severity.

(4) RM is a mandatory measure while VSL can be mandatory or advisory. The driver compliance issue is the major concern for VSL implementation. In future research, it is necessary to consider driver compliance in the integrated control from VSL filed implementation. Also, future work needs to be devoted to improving driver compliance prediction performance and including compliance prediction in traffic dynamics.

(5) Driver compliance is a complicated maneuver. This study applied an empirical way to represent it. In the future, driver compliance can be investigated using theoretical models, such as car-following model. Besides, inclement weather challenges traffic operation during Edmonton's winter time. Compliance under inclement winter weather requires more insight.

(6) When congestion requires low discharge flow from upstream, VSL calculated without consideration of driver compliance may discharge higher flow and congestion still occurs. Based on dynamic driver compliance prediction, target speed will be adjusted by the speed limit value and its resulting driver compliance. Considering the adjusted target speed, the traffic prediction

can better reflect future traffic conditions. In this way, the target speed is achievable and reasonable.

(7) Based on DynaTAM-VSL and the results from the preliminary test, future work will make an effort to enhance the control algorithm so that it can be adopted for various scenarios. The VSL maximum variance constraint and duration of the control variable were observed to be important for VSL performance during the test. The selection of their values needs to balance their mobility and safety consequence. Traffic situations usually evolve very fast. Small VSL variance or long control duration prevent VSL control from providing reasonable rates. However, frequent VSL variations may lead to traffic safety problem. Thus, the constraints need more careful consideration. The test in the next phase will be devoted to field evaluation after some necessary adjustments. The time gap between the two phases will deal with strategy adjustments and deeper public education.

(8) Further research will be conducted involving incidents and inclement weather conditions in the VSL algorithm. Incidents or inclement weather conditions result in non-recurrent bottlenecks, which are also a major concern for freeway operation. In particular, Edmonton experiences adverse weather conditions in winter, with driving visibility seriously affected. Incorporating incident and weather factors in the control algorithm could help VSLs to suggest more feasible speed limits. Then, the VSL strategy can adjust the optimal

discharge flow, mitigate bottleneck severity and ensure traffic safety and mobility at the same time.

REFERENCES

[1] H. Shi and A. Ziliaskopoulos, "Traffic Flow Control using Variable Speed Limits," in *Traffic and Transportation Studies* ed, 2002, pp. 658-665.

[2] A. Hegyi, "Model predictive control for integrating traffic control measures," C815671 Dr., Technische Universiteit Delft (The Netherlands), Ann Arbor, 2004.

[3] Y. Wang, M. Papageorgiou, and A. Messmer, "Predictive Feedback Routing Control Strategy for Freeway Network Traffic," *Transportation Research Record: Journal of the Transportation Research Board,* vol. 1856, pp. 62-73, 01/01/ 2003.

[4] Y. Wang, M. Papageorgiou, G. Sarros, and W. Knibbe, "Feedback Route Guidance Applied to a Large-Scale Express Ring Road," *Transportation Research Record: Journal of the Transportation Research Board,* vol. 1965, pp. 79-88, 01/01/ 2006.

[5] T. Bellemans, B. De Schutter, and B. De Moor, "Anticipative model predictive control for ramp metering in freeway networks," in *American Control Conference*, 2003, pp. 4077-4082.

[6] A. Hegyi, B. De Schutter, and H. Hellendoorn, "Model predictive control for optimal coordination of ramp metering and variable speed limits," *Transportation Research Part C: Emerging Technologies,* vol. 13, pp. 185-209, 2005.

[7] T. Bellemans, B. D. Schutter, and B. D. Moor, "Model predictive control for ramp metering of motorway traffic: A case study," *Control Engineering Practice,* vol. 14, pp. 406-411, 2006.

[8] X.-Y. Lu, T. Z. Qiu, P. Varaiya, R. Horowitz, and S. E. Shladover, "Combining Variable Speed Limits with Ramp Metering for freeway traffic control," presented at the American Control Conference (ACC), 2010, 2010.

[9] S. K. Zegeye, B. D. Schutter, J. Hellendoorn, E. A. Breunesse, and H. Andreas, "A Predictive Traffic Controller for Sustainable Mobility Using Parameterized Control Policies," *IEEE Transactions on Intelligent Transportation Systems,* vol. 13, pp. 1420-1429, 2012.

[10] M. Hadiuzzaman, T. Qiu, and X. Lu, "Variable Speed Limit Control Design for Relieving Congestion Caused by Active Bottlenecks," *Journal of Transportation Engineering,* vol. 139, pp. 358-370, 2013.

[11] A. Spiliopoulou, M. Kontorinaki, M. Papageorgiou, and P. Kopelias, "Macroscopic traffic flow model validation at congested freeway off-ramp areas," *Transportation Research Part C: Emerging Technologies,* vol. 41, pp. 18-29, 4// 2014.

[12] M. S. Grewal and H. J. Payne, "Identification of Parameters in a Freeway Traffic Model," *Systems, Man and Cybernetics, IEEE Transactions on,*

vol. SMC-6, pp. 176-185, 1976.

[13] C. F. Daganzo, "The cell transmission model: A dynamic representation of highway traffic consistent with the hydrodynamic theory," *Transportation Research Part B: Methodological,* vol. 28, pp. 269-287, 1994.

[14] A. Messmer and M. Papageorgiou, "METANET: a macroscopic simulation program for motorway networks," *Traffic Engineering & Control,* vol. 31, pp. 466-470, 1990.

[15] M. Cremer and M. Papageorgiou, "Parameter identification for a traffic flow model," *Automatica,* vol. 17, pp. 837-843, 11// 1981.

[16] M. Papageorgiou, J.-M. Blosseville, and H. Hadj-Salem, "Macroscopic modelling of traffic flow on the Boulevard Périphérique in Paris," *Transportation Research Part B: Methodological,* vol. 23, pp. 29-47, 2// 1989.

[17] M. Papageorgiou, J.-M. Blosseville, and H. Hadj-Salem, "Modelling and real-time control of traffic flow on the southern part of Boulevard Peripherique in Paris: Part I: Modelling," *Transportation Research Part A: General,* vol. 24, pp. 345-359, 1990.

[18] D. Yin and T. Z. Qiu, "Compatibility analysis of macroscopic and microscopic traffic simulation modeling," *Canadian Journal of Civil Engineering,* vol. 40, pp. 613-622, 2013/07/01 2013.

[19] X.-Y. V. Lu, Pravin P.; Horowitz, Roberto, "An Equivalent Second Order Model with Application to Traffic Control," presented at the 12th IFAC Symposium on Control in Transportation Systems, Crowne Plaza Hotel, United States of America, 2009.

[20] J. R. D. Frejo, A. Nunez, B. De Schutter, and E. F. Camacho, "Model predictive control for freeway traffic using discrete speed limit signals," presented at the Control Conference (ECC), 2013 European, 2013.

[21] L. G. Neudorff, J. E. Randall, R. Reiss, and R. Gordon, "Freeway Management and Operations Handbook," U.S. Department of Transportation2003.

[22] A. Wattleworth, "Peak Period Analysis and Control of a Freeway System," *Highway Research Record,* vol. 157, pp. 1-21, 1965.

[23] M. Papageorgiou and A. Kotsialos, "Freeway ramp metering: an overview," *IEEE Transactions on Intelligent Transportation Systems,* vol. 3, pp. 271-281, 2002.

[24] D. P. Masher, D. W. Ross, P. J. Wong, P. L. Tuan, H. M. Zeidler, and S. Peracek, "Guidelines for Design and Operating of Ramp Control Systems," Stanford Research Institute, Menid Park, CA1975.

[25] H. Hadj-Salem, J. M. Blosseville, and M. Papageorgiou, "ALINEA: a local feedback control law for on-ramp metering; a real-life study," in *Road Traffic Control, Third International Conference on*, 1990, pp. 194-198.

[26] M. Papageorgiou, H. Hadj-Salem, and F. Middelham, "ALINEA local

ramp metering: Summary of field results," *Transportation Research Record: Journal of the Transportation Research Board,* pp. 90-98, 1997.

[27] I. Papamichail, M. Papageorgiou, V. Vong, and J. Gaffney, "Heuristic Ramp-Metering Coordination Strategy Implemented at Monash Freeway, Australia," *Transportation Research Record: Journal of the Transportation Research Board,* vol. 2178, pp. 10-20, 2010.

[28] L. N. Jacobson, K. C. Henry, and O. Mehyar, "Real-Time Metering Algorithm for Centralized Control," *Transportation Research Record: Journal of the Transportation Research Board,* pp. 17-26, 1989.

[29] M. Papageorgiou, J.-M. Blosseville, and H. Haj-Salem, "Modelling and real-time control of traffic flow on the southern part of Boulevard Peripherique in Paris: Part II: Coordinated on-ramp metering," *Transportation Research Part A: General,* vol. 24, pp. 361-370, 9// 1990.

[30] R. Lau, "Ramp Metering by Zone - The Minnesota Algorithm," Minnesota Department of Transportation1997.

[31] C. D. o. Transportation, "Preliminary SWARM Study Report," California, U.S.2000.

[32] A. Kotsialos, M. Papageorgiou, M. Mangeas, and H. Haj-Salem, "Coordinated and integrated control of motorway networks via non-linear optimal control," *Transportation Research Part C: Emerging Technologies,* vol. 10, p. 65, 2002.

[33] I. Papamichail, K. Kampitaki, M. Papageorgiou, and A. Messmer, "Integrated Ramp Metering and Variable Speed Limit Control of Motorway Traffic Flow," in *Prepints (CD-ROM) of the 17th IFAC World Congress*, Korea, South, 2008.

[34] C. Taylor, D. Meldrum, and L. Jacobson, "Fuzzy ramp metering: Design overview and simulation results," *Transportation Research Record: Journal of the Transportation Research Board,* pp. 10-18, 1998.

[35] H. M. Zhang and S. G. Ritchie, "Freeway ramp metering using artificial neural networks," *Transportation Research Part C: Emerging Technologies,* vol. 5, pp. 273-286, 1997.

[36] Z. Hou, X. Xu, J. Yan, J. X. Xu, and G. Xiong, "A complementary modularized ramp metering approach based on iterative learning control and ALINEA," *IEEE Transactions on Intelligent Transportation Systems,* vol. 12, pp. 1305-1318, // 2011.

[37] I. Papamichail, A. Kotsialos, I. Margonis, and M. Papageorgiou, "Coordinated ramp metering for freeway networks - A model-predictive hierarchical control approach," *Transportation Research Part C: Emerging Technologies,* vol. 18, pp. 311-331, 2010.

[38] A. H. Ghods, L. Fu, and A. Rahimi-Kian, "An Efficient Optimization Approach to Real-Time Coordinated and Integrated Freeway Traffic Control," *IEEE Transactions on Intelligent Transportation Systems,* vol. 11, pp. 873-884, 2010.

[39] S. K. Zegeye, B. De Schutter, J. Hellendoorn, E. A. Breunesse, and A.

Hegyi, "A Predictive Traffic Controller for Sustainable Mobility Using Parameterized Control Policies," *Intelligent Transportation Systems, IEEE Transactions on,* vol. 13, pp. 1420-1429, 2012.
[40] H. Jack, R. Mohsen, and G. Nikolas, "Cooperative traffic control of a mixed network with two urban regions and a freeway," *Transportation Research Part B: Methodological,* vol. 54, pp. 17-36, 2013.
[41] J. M. Maciejowski, *Predictive Control with Constraints*: Prentice Hall, 2002.
[42] J. M. McDermott, S. J. Kolenko, and R. J. Wojcik, "Chicago Area Expressway Surveillance and Control," Illinois Department of Transportation, Oak Park1979.
[43] J. M. McDermott, "Freeway Surveilance and Control in Chicago Area," *Journal of Transportation Engineering,* vol. 106, pp. 333-348, 1980.
[44] I. Cambridge Systematics, "Twin Cities Ramp Meter Evaluation – Final Report," Cambridge Systematics, Inc., Oakland, California2001.
[45] I. Cambridge Systematics, "MnDOT Ramp Meter Evaluation: Phase II Evaluation Report," Oakland, California2002.
[46] A. Horowitz, J. Wu, and J. P. Duarte, "Evaluation of Ramp Meter Effectiveness for Wisconsin Freeways, A Milwaukee Case Study," Wisconsin Department of Transportation, Madison, WI2004.
[47] G. Xie, B. Hoeft, and G. Grayson, "Ramp Meters Evaluation: Using ITS Archived Data," *Journal of Transportation Engineering,* vol. 138, pp. 447-454, 2012.
[48] B. Park and S. S. Yadlapati, "Development and Testing of Variable Speed Limit Logics at Work Zones Using Simulation," presented at the Presented at 82nd Annual Meeting of the Transportation Research Board, Washington, D.C., 2003.
[49] K. Kyeong-Pyo and C. Gang-Len, "A robust model for optimal time-of-day speed control at highway work zones," *Intelligent Transportation Systems, IEEE Transactions on,* vol. 7, pp. 115-123, 2006.
[50] P. Allaby, B. Hellinga, and M. Bullock, "Variable Speed Limits: Safety and Operational Impacts of a Candidate Control Strategy for Freeway Applications," *Intelligent Transportation Systems, IEEE Transactions on,* vol. 8, pp. 671-680, 2007.
[51] P. W. Lin, K. P. Kang, and G. L. Chang, "Exploring the effectiveness of variable speed limit controls on highway work-zone operations," *Journal of Intelligent Transportation Systems: Technology, Planning, and Operations,* vol. 8, pp. 155-168, // 2004.
[52] A. Alessandri, A. Di Febbraro, A. Ferrara, and E. Punta, "Nonlinear optimization for freeway control using variable-speed signaling," *Vehicular Technology, IEEE Transactions on,* vol. 48, pp. 2042-2052, 1999.
[53] R. C. Carlson, I. Papamichail, and M. Papageorgiou, "Local Feedback-Based Mainstream Traffic Flow Control on Motorways Using Variable

Speed Limits," *Intelligent Transportation Systems, IEEE Transactions on,* vol. 12, pp. 1261-1276, 2011.
[54] R. C. Carlson, I. Papamichail, M. Papageorgiou, and A. Messmer, "Optimal mainstream traffic flow control of large-scale motorway networks," *Transportation Research Part C: Emerging Technologies,* vol. 18, pp. 193-212, 4// 2010.
[55] L. L. Chen, A. D. May, and D. M. Auslander, "Freeway ramp control using fuzzy set theory for inexact reasoning," *Transportation Research Part A: General,* vol. 24, pp. 15-25, 1// 1990.
[56] A. H. Ghods, A. Kian, and M. Tabibi, "Adaptive freeway ramp metering and variable speed limit control: a genetic-fuzzy approach," *Intelligent Transportation Systems Magazine, IEEE,* vol. 1, pp. 27-36, 2009.
[57] X.-Y. Lu, P. Varaiya, R. Horowitz, D. Su, and S. Shladover, "A new approach for combined freeway Variable Speed Limits and Coordinated Ramp Metering," presented at the Intelligent Transportation Systems (ITSC), 2010 13th International IEEE Conference on, 2010.
[58] Z. Jianlong, A. Boitor, and P. Ioannou, "Design and evaluation of a roadway controller for freeway traffic," presented at the Intelligent Transportation Systems, 2005. Proceedings. 2005 IEEE, 2005.
[59] D. Su, X.-Y. Lu, P. Varaiya, R. Horowitz, and S. E. Shladover, "Variable Speed Limit and Ramp Metering Design for Congestion Caused by Weaving," presented at the 90th TRB Annual Meeting, Washington, D.C., 2011.
[60] M. Hadiuzzaman and T. Z. Qiu, "Cell transmission model based variable speed limit control for freeways," *Canadian Journal of Civil Engineering,* vol. 40, pp. 46-56, 2013/01/01 2013.
[61] UK Highways Agency, "M25 Controlled Motorways: Summary Report," 2004.
[62] R. Bertini, S. Boice, and K. Bogenberger, "Dynamics of Variable Speed Limit System Surrounding Bottleneck on German Autobahn," *Transportation Research Record: Journal of the Transportation Research Board,* vol. 1978, pp. 149-159, 01/01/ 2006.
[63] E. van den Hoogen and S. Smulders, "Control by variable speed signs. Results of the Dutch experiment," presented at the 7th Int. Conference on Traffic Monitoring and Control, London, England, 1994.
[64] M. Papageorgiou, E. Kosmatopoulos, and I. Papamichail, "Effects of Variable Speed Limits on Motorway Traffic Flow," *Transportation Research Record: Journal of the Transportation Research Board,* vol. 2047, pp. 37-48, 12/01/ 2008.
[65] A. Hegyi and S. P. Hoogendoorn, "Dynamic speed limit control to resolve shock waves on freeways - Field test results of the SPECIALIST algorithm," presented at the Intelligent Transportation Systems (ITSC), 2010 13th International IEEE Conference on, 2010.
[66] A. Hegyi, S. P. Hoogendoorn, M. Schreuder, H. Stoelhorst, and F. Viti,

"SPECIALIST: A dynamic speed limit control algorithm based on shock wave theory," presented at the Intelligent Transportation Systems, 2008. ITSC 2008. 11th International IEEE Conference on, 2008.

[67] X.-Y. Lu, P. Varaiya, R. Horowitz, D. Su, and S. Shladover, "Novel Freeway Traffic Control with Variable Speed Limit and Coordinated Ramp Metering," *Transportation Research Record: Journal of the Transportation Research Board,* vol. 2229, pp. 55-65, 12/01/ 2011.

[68] Transportation Research Board, *Highway Capacity Manual*. Washington, D.C.: Transportation Research Board, 2010.

[69] E. Kwon, R. Lau, and J. Aswegan, "Maximum Possible Weaving Volume for Effective Operations of Ramp-Weave Areas: Online Estimation," *Transportation Research Record: Journal of the Transportation Research Board,* vol. 1727, pp. 132-141, 01/01/ 2000.

[70] P. Lertworawanich and L. Elefteriadou, "Capacity Estimations for Type B Weaving Areas Based on Gap Acceptance," *Transportation Research Record: Journal of the Transportation Research Board,* vol. 1776, pp. 24-34, 2001.

[71] Transportation Research Board, *Highway Capacity Manual*. Washington, D.C: Transportation Research Board, National Research Council, 2000.

[72] R. Roess and J. Ulerio, "Level of Service Analysis of Freeway Weaving Segments," *Transportation Research Record: Journal of the Transportation Research Board,* vol. 2130, pp. 25-33, 2009.

[73] H. Chen, H. Zhou, J. Zhao, and P. Hsu, "Safety performance evaluation of left-side off-ramps at freeway diverge areas," *Accident Analysis & Prevention,* vol. 43, pp. 605-612, 2011.

[74] R. Roess and J. Ulerio, "Capacity of Freeway Weaving Segments," *Transportation Research Record: Journal of the Transportation Research Board,* vol. 2130, pp. 34-41, 2009.

[75] P. Lertworawanich and L. Elefteriadou, "A methodology for estimating capacity at ramp weaves based on gap acceptance and linear optimization," *Transportation Research Part B: Methodological,* vol. 37, pp. 459-483, 2003.

[76] J. A. Laval and C. F. Daganzo, "Lane-changing in traffic streams," *Transportation Research Part B: Methodological,* vol. 40, pp. 251-264, 3// 2006.

[77] J. A. Laval and L. Leclercq, "Microscopic modeling of the relaxation phenomenon using a macroscopic lane-changing model," *Transportation Research Part B: Methodological,* vol. 42, pp. 511-522, 7// 2008.

[78] D. W. Soole, B. C. Watson, and J. J. Fleiter, "Effects of average speed enforcement on speed compliance and crashes: A review of the literature," *Accident Analysis & Prevention,* vol. 54, pp. 46-56, 5// 2013.

[79] C. Lee, S. Lee, B. Choi, and Y. Oh, "Effectiveness of Speed-Monitoring

Displays in Speed Reduction in School Zones," *Transportation Research Record: Journal of the Transportation Research Board,* vol. 1973, pp. 27-35, 2006/01/01 2006.

[80] T. Woo, S.-M. Ho, and H.-L. Chen, "Monitoring Displays Coupled with Speed Cameras: Effectiveness on Speed Reduction," *Transportation Research Record: Journal of the Transportation Research Board,* vol. 2009, pp. 30-36, 2007/01/01 2007.

[81] K. Santiago-Chaparro, M. Chitturi, A. Bill, and D. Noyce, "Spatial Effectiveness of Speed Feedback Signs," *Transportation Research Record: Journal of the Transportation Research Board,* vol. 2281, pp. 8-15, 2012/12/01 2012.

[82] J. Wasson, G. Boruff, A. Hainen, S. Remias, E. Hulme, G. Farnsworth*, et al.*, "Evaluation of Spatial and Temporal Speed Limit Compliance in Highway Work Zones," *Transportation Research Record: Journal of the Transportation Research Board,* vol. 2258, pp. 1-15, 2011/12/01 2011.

[83] F. Soriguera and M. Sala, "Freeway Lab: Testing Dynamic Speed Limits," *Procedia - Social and Behavioral Sciences,* vol. 160, pp. 35-44, 12/19/ 2014.

[84] A. Ardeshiri and M. Jeihani, "A speed limit compliance model for dynamic speed display sign," *Journal of Safety Research,* vol. 51, pp. 33-40, 12// 2014.

[85] J. Fang, Y. Luo, M. Hadiuzzaman, G. Liu, and T. Z. Qiu, "Safety Oriented Variable Speed Limit Control Method with Enhanced Driver Response Modeling," presented at the Transportation Research Board 94th Annual Meeting, Washington DC, 2015.

[86] B. Hellinga and M. Mandelzys, "Impact of Driver Compliance on the Safety and Operational Impacts of Freeway Variable Speed Limit Systems," *Journal of Transportation Engineering,* vol. 137, pp. 260-268, 2011/04/01 2011.

[87] F. Habtemichael and L. de Picado Santos, "Safety and Operational Benefits of Variable Speed Limits Under Different Traffic Conditions and Driver Compliance Levels," *Transportation Research Record: Journal of the Transportation Research Board,* vol. 2386, pp. 7-15, 2013/12/01 2013.

[88] L. Xiao-Yun, S. E. Shladover, I. Jawad, R. Jagannathan, and T. Phillips, "A Novel Speed-Measurement Based Variable Speed Limit/Advisory Algorithm for a Freeway Corridor with Multiple Bottlenecks," presented at the Transportation Research Board 94th Annual Meeting, Washington DC, 2015.

[89] H. Andreas, S. Bart De, and H. Hans, "Model predictive control for optimal coordination of ramp metering and variable speed limits," *Transportation Research Part C: Emerging Technologies,* vol. 13, pp. 185-209, 2005.

[90] X. Wang, M. Hadiuzzaman, J. Fang, T. Qiu, and X. Yan, "Optimal Ramp

Metering Control for Weaving Segments Considering Dynamic Weaving Capacity Estimation," *Journal of Transportation Engineering,* vol. 140, p. 04014057, 2014/11/01 2014.

[91] Y. Zhang, "Capacity Modeling of Freeway Weaving Sections," Dissertation/Thesis, Virginia Polytechnic Institute and State University, Blacksburg, Virginia, 2005.

[92] J. Lee and M. J. Cassidy, "An Empirical and Theoretical Study of Freeway Weave Bottlenecks," California Path Program, Institute of Transportation Studies, University of California, Berkeley, Berkeley, California, USA2009.

[93] G. Gomes, J. Kwon, A. Muralidharan, P. Varaiya, and R. Horowitz, "Automatic Calibration of the Fundamental Diagram and Empirical Observations on Capacity," in *88th Annual Meeting*, Washington, D.C., 2008.

[94] H. C. Frey and S. R. Patil, "Identification and Review of Sensitivity Analysis Methods," *Risk Analysis,* vol. 22, pp. 553-578, 2002.

[95] G. Gomes, A. May, and R. Horowitz, "Congested Freeway Microsimulation Model Using VISSIM," *Transportation Research Record: Journal of the Transportation Research Board,* vol. 1876, pp. 71-81, 2004.

[96] M.-H. Wang, M. J. Cassidy, P. Chan, and A. D. May, "Evaluating the capacity of freeway weaving sections," *Journal of Transportation Engineering,* vol. 119, pp. 360-384, // 1993.

[97] L. Liu, X. Li, and B. Jia, "Analysis of Capacity of Weaving Section Based on Cellular Automata Model," *Journal of Transport Information and Safety,* vol. 31, pp. 28-32, 2013.

[98] X. Wang, M. Hadiuzzaman, and T. Z. Qiu, "Analyzing Sensitivity of Freeway Capacity at a Complex Weaving Segment," presented at the 9th International Transportation Specialty Conference, Edmonton, Canada, 2012.

[99] H. Yeo, A. Skabardonis, J. Halkias, J. Colyar, and V. Alexiadis, "Oversaturated Freeway Flow Algorithm for Use in Next Generation Simulation," *Transportation Research Record: Journal of the Transportation Research Board,* vol. 2088, pp. 68-79, 12/01/ 2008.

[100] J. A. Laval and L. Leclercq, "A mechanism to describe the formation and propagation of stop-and-go waves in congested freeway traffic," *Philosophical Transactions of the Royal Society A: Mathematical, Physical and Engineering Sciences,* vol. 368, pp. 4519-4541, // 2010.

[101] R. C. Carlson, I. Papamichail, M. Papageorgiou, and A. Messmer, "Optimal Motorway Traffic Flow Control Involving Variable Speed Limits and Ramp Metering," *Transportation Science,* vol. 44, pp. 238-253, 2010/05/01 2010.

[102] G. Vigos, M. Papageorgiou, and Y. Wang, "Real-time estimation of vehicle-count within signalized links," *Transportation Research Part C:*

Emerging Technologies, vol. 16, pp. 18-35, 2// 2008.

[103] G. Gomes and R. Horowitz, "Optimal freeway ramp metering using the asymmetric cell transmission model," *Transportation Research Part C: Emerging Technologies,* vol. 14, pp. 244-262, 8// 2006.

[104] L. Zhang and D. Levinson, "Balancing efficiency and equity of ramp meters," *Journal of transportation engineering,* pp. 477-481, 2005.

[105] N. Chaudhary and C. Messer, "Freeway On-Ramp Design Criteria for Ramp Meters with Excessive Queue Detectors," *Transportation Research Record: Journal of the Transportation Research Board,* vol. 1796, pp. 80-85, 01/01/ 2002.

[106] M. Papageorgiou, E. Kosmatopoulos, I. Papamichail, and W. Yibing, "A Misapplication of the Local Ramp Metering Strategy ALINEA," *Intelligent Transportation Systems, IEEE Transactions on,* vol. 9, pp. 360-365, 2008.

[107] FHWA, *Manual on Uniform Traffic Control Devices 2009 edition*. Washington, DC, 2009.

[108] Washington State Department of Transportation. (2010). *Smarter Highways variable speed limits*. Available: http://www.wsdot.wa.gov/smarterhighways/vsl.htm

[109] Washington StateDepartment of Transportation. (2010). Available: http://www.wsdot.wa.gov/Projects/I5/activetrafficmanagement/

[110] Washington State Department of Transportation. Available: http://www.wsdot.wa.gov/projects/lkwamgt/lkwaatm/

[111] Federal Highway Administration. (2012). *Implementing Variable Speed Limits*. Available: http://www.ops.fhwa.dot.gov/publications/fhwahop08050/chap_7.htm

[112] A. Nissan and H. N. Koutsopoulosb, "Evaluation of the Impact of Advisory Variable Speed Limits on Motorway Capacity and Level of Service," *Procedia - Social and Behavioral Sciences,* vol. 16, pp. 100-109, // 2011.

[113] Minnesota Department of Transportation. (2014). *Smart Lanes*. Available: http://www.dot.state.mn.us/smartlanes/

[114] G.-L. Chang, S. Park, and J. Paracha, "Intelligent Transportation System Field Demonstration," *Transportation Research Record: Journal of the Transportation Research Board,* vol. 2243, pp. 55-66, 2011/12/01 2011.

[115] F. L. Hall and K. Agyemang-Duah, "Freeway Capacity Drop and the Definition of Capacity," *Transportation Research Record: Journal of the Transportation Research Board,* vol. 1320, pp. 91-98, 1991.

[116] L. Zhang and D. Levinson, "Some Properties of Flows at Freeway Bottlenecks," *Transportation Research Record: Journal of the Transportation Research Board,* vol. 1883, pp. 122-131, 01/01/ 2004.

[117] M. Lorenz and L. Elefteriadou, "Defining Freeway Capacity as Function of Breakdown Probability," *Transportation Research Record: Journal of the Transportation Research Board,* vol. 1776, pp. 43-51, 01/01/ 2001.

[118] J. Banks, "Part 1: Traffic Flow Theory and Characteristics: Effect of Time Gaps and Lane Flow Distributions on Freeway Bottleneck Capacity," *Transportation Research Record: Journal of the Transportation Research Board,* vol. 1965, pp. 3-11, 01/01/ 2006.

[119] Alberta Transportation Planning Branch, *Alberta Highways 1 to 986 Traffic Volume History (2005-2014)*, 2015.

[120] J. Fang, M. Hadiuzzaman, E. Yin, and T. Z. Qiu, "DynaTAM: an online algorithm for performing simultaneously optimized proactive traffic control for freeways," *Canadian Journal of Civil Engineering,* vol. 41, pp. 315-322, 2014/04/01 2014.